**SUPPORTING INFORMATION**

# Bioinspired Copper-Catalysed Nitrous Oxide Reduction with Simultaneous N-H or O-H Bond Oxidation

Bruce A. Lobo Sacchelli,[a] Suellen M. P. Onguene,[a] Ruben S. M. Almeida,[a] Alexandra M. M. Antunes,[a] Dmytro S. Nesterov,[a] Leandro H. Andrade,[b] Elisabete C. B. A. Alegria,[a,c]* Martin H. G. Prechtl,[a,d]*

[a]*Centro de Química Estrutural, Instituto Superior Técnico, Universidade de Lisboa, Av. Rovisco Pais 1, 1049-001, Lisboa, Portugal. https://cqe.tecnico.ulisboa.pt http://www.h2.bio martin.prechtl@tecnico.ulisboa.pt*

[b]*Departamento de Química Fundamental, Instituto de Química, Universidade de São Paulo, Av. Prof. Lineu Prestes, 748 – Butantã, São Paulo – SP, 05508-900, Brasil.*

[c]*Departamento de Engenharia Química, Instituto Superior de Engenharia de Lisboa, Instituto Politécnico de Lisboa, 1959-007 Lisboa, Portugal. elisabete.alegria@isel.pt*

[d] *Department of Synthesis and Analysis, Albert-Hofmann-Institute for Physiochemical Sustainability, Academy for the Advancement of Physiochemical Sustainability, Albert-Schweitzer-Str. 22, 32602 Vlotho, Germany. https://www.a-h.institute*

# Table of contents

# Figure Index

# 1 General experimental proceedings

The oxidation of benzyl alcohols was tracked through 1H nuclear magnetic resonance (NMR) analysis on a Bruker 400 MHz Avance II NMR spectrometer with a 5 mm BBO probe (d1 time = 1s). Deuterated $CDCl_3$ was used as the solvent, and cyclohexane (20 µL, 0.184 mmol) served as an internal standard. For comprehensive analysis, all reactions underwent GC-MS analysis on a Clarus 600 (GC-MS) equipped with a Zebron ZB-5 (Phenomenex) column measuring 30 m × 0.25 mm × 0.25 µm. The applied method involved a 14-minute temperature program: 2 minutes at 80 °C, followed by a ramp of 10°C/min. to 120 °C, holding for 0 minutes, further ramping at 30°C/min. to 300 °C, and then maintaining at 300 °C for 2 minutes. High-resolution mass spectrometry with electrospray ionization (HRMS-ESI) flow injection analyses (FIA) were performed on a Bruker Impact II quadrupole time-of-flight mass spectrometer equipped with an ESI source (Bruker Daltoniks, Bremen, Germany), using sodium formate solution as internal standard and acetonitrile as eluent. All measurements were performed on positive ion mode in the m/z 50–2,000 range, in the full scan or auto-MS/MS modes. The acquired data were processed by DataAnalysis 4.1 software (Bruker Daltoniks). Calibration was performed using high-precision calibration mode (HPC). All theoretical masses and simulated spectra were calculated with Compass IsotopePattern (Bruker) or XCalibur FreeStyle (Thermo Scientific). The deuterated $CDCl_3$, benzylamines and benzyl alcohols were purchased from Tokyo Chemical Industry (TCI, Japan) and used without additional purification. The oxygen, nitrogen and nitrous oxide cylinders were obtained from Air Liquide. Silica (200 mesh) were used for column chromatography and monitored with TLC. Residual air elimination in the reaction vessel proceeds through freeze-pump-cycles prior to gas phase exchange. For details on theoretical calculations see under section 6.

## 1.1. Catalyst stock solution ([(bipy)Cu(NMI)(MeCN)]I)[1]

In a round bottom flask, CuI (0.212 mmol, 40.4 mg) was dissolved in 20 ml of acetonitrile. Afterwards, 2,2'-bipyridine (0.212 mmol, 33.1 mg) and NMI (0.44 mmol, 35.0 µL) were added. The reaction mixture was stirred for 30 minutes at room temperature resulting in the formation of a dark green solution which was used directly for the oxidation reactions.

In some cases the solution was also prepared in a lower concentration (see tables). 1 mL of stock solution was diluted in 4 mL of acetonitrile yielding a solution with CuI (0.0424 mmol), 2,2'-bipyridine (0.0424 mmol) and NMI (0.088 mmol). The reaction mixture was stirred for 30 minutes at room temperature resulting in the formation of a lighter green solution.

# 2 Aminals from primary and secondary amines

## 2.1 Optimisation for benzylamine oxidation in the presence of methanol

In a 25 mL *tube equipped with high-vacuum Teflon valve*, TEMPO (16.7 mg, 0.11 mmol or 8.4 mg, 0.055 mmol) was added along with 5 mL of the stock solution. Following this, methanol (89 µL, 2.2 mmol) and benzylamine (120 µL, 1.1 mmol) were introduced. The mixture was stirred under $N_2O$. 100 mL of $N_2O$ was condensed into the tube at -196°C.The flask was then heated to the desired temperature range (30-90 °C) for a specified duration (2-20 hours).

After heating, the reaction mixture was allowed to cool to room temperature, and then carefully opened to release the solubilized gas. The reaction mixture was subsequently transferred to a round-bottom flask, and acetonitrile was evaporated. Following evaporation, an internal standard of cyclohexane (20 µL, 0.184 mmol) and 50 µL of $CDCl_3$ were added to the

solution. A portion (40 µL) of this mixture, along with 500 µL of $CDCl_3$, was then transferred to an NMR tube for $^1H$ NMR analysis. Results, refer Scheme 1 of the manuscript.

Note: for the NMR characterisation under Section 2.2 a sample was filtered over a plug of silica (short column) to separate the copper catalyst from the product. During the filtration the column with the product mixture has been washed with ethanol to recover the product from the column. The residue signal of ethanol appeared since ethanol was not fully evaporated together with acetonitrile at reduced pressure previous to the NMR analysis in Section 2.2.

## 2.2 Aminal characterization

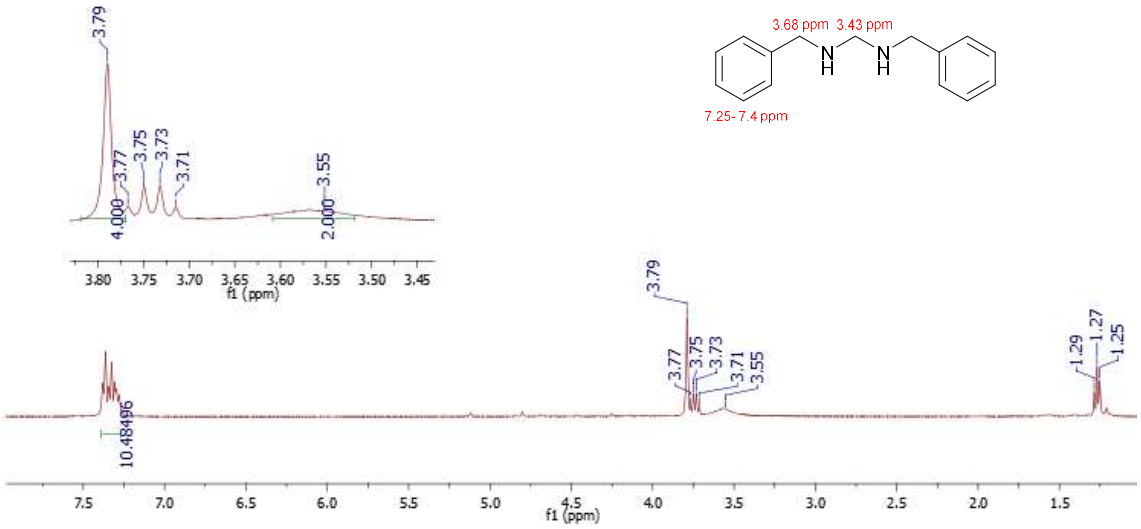


Figure 1. $^{1}$H NMR of *N,N'*-dibenzylmethanediamine. Signals of ethanol in 3.74 ppm (q, 2H) and 1.27 ppm (t, 3H) from purification (see Note in Section 2.1).

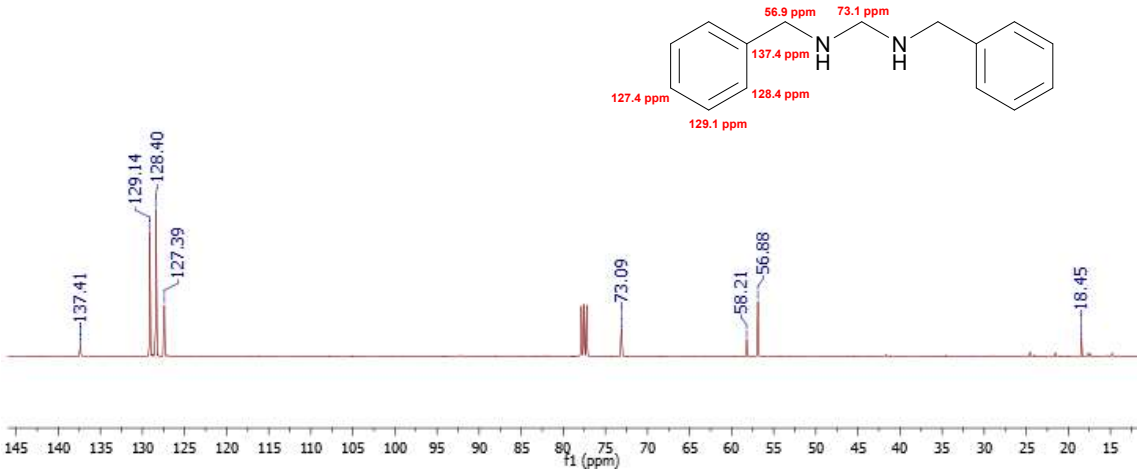


Figure 2. $^{13}$C NMR of *N,N'*-dibenzylmethanediamine. Signals of ethanol in 58.21 and 18.45 ppm from purification (see Note inSection 2.1).

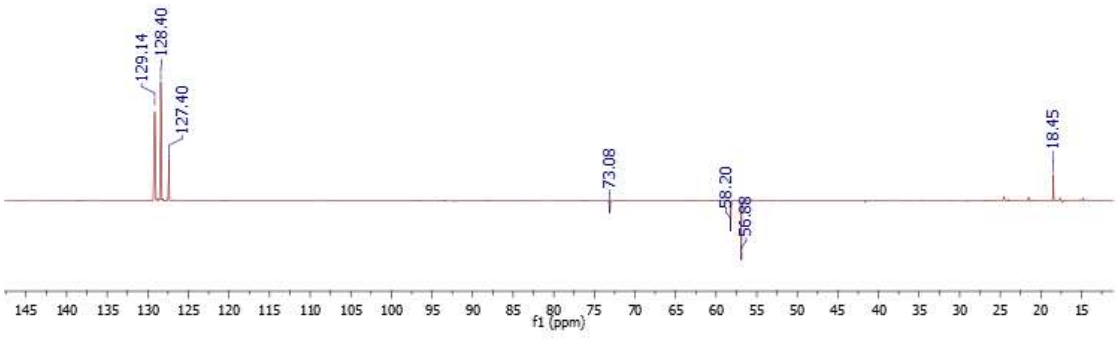


Figure 3. Dept-135 of *N,N'*-dibenzylmethanediamine. Signals of ethanol in 58.21 and 18.45 ppm from purification (see Note in Section 2.1)..

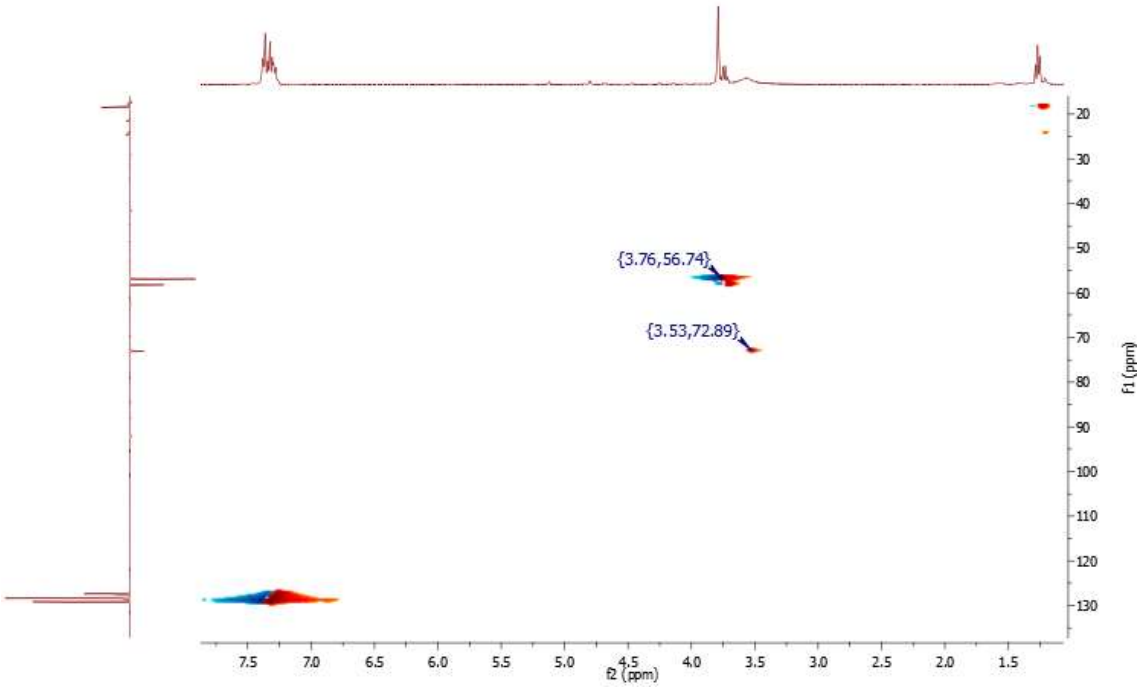


Figure 4. HSQC of *N,N'*-dibenzylmethanediamine. Signals of ethanol ($^{13}$C NMR: 58.21 and 18.45 ppm/ $^{1}$H NMR: 3.74 and 1.27 ppm) from purification (see Note inSection 2.1)..

## 2.3 Selected $^{1}$H NMR spectra and MS spectrograms for Scheme 1

**Entry 1**

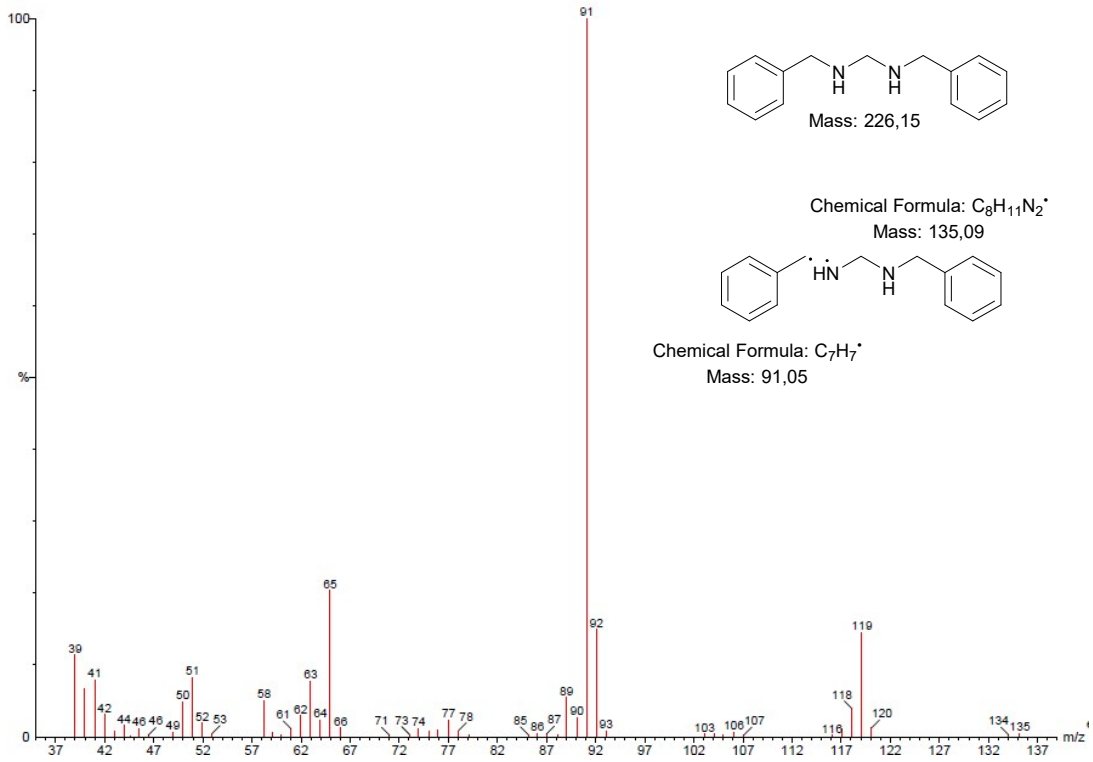


Figure 5. **MS** of *N,N'*-dibenzylmethanediamine.

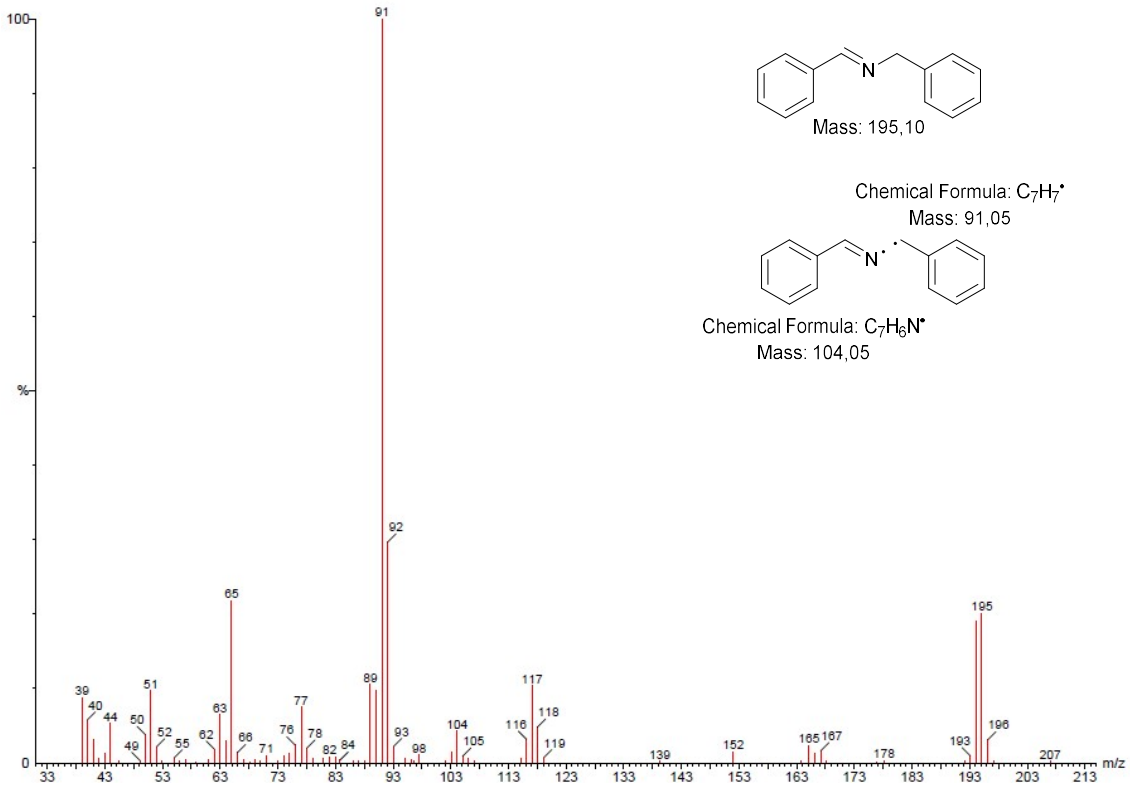


Figure 6. **MS** of *N*-benzyl-1-phenylmethanimine.

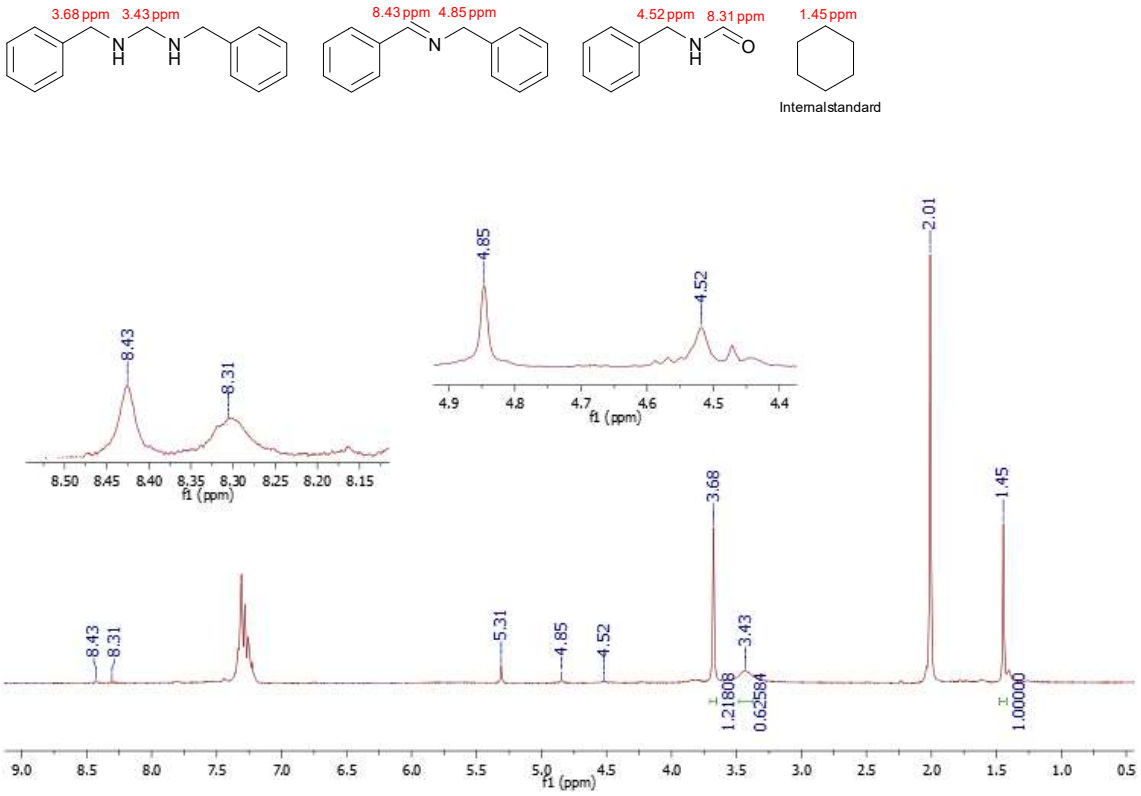


Figure 7. **$^{1}$H NMR of entry 1**. 5.31 ppm: DCM, 2.01 ppm: acetonitrile.

**Scheme 1 (60°C)**

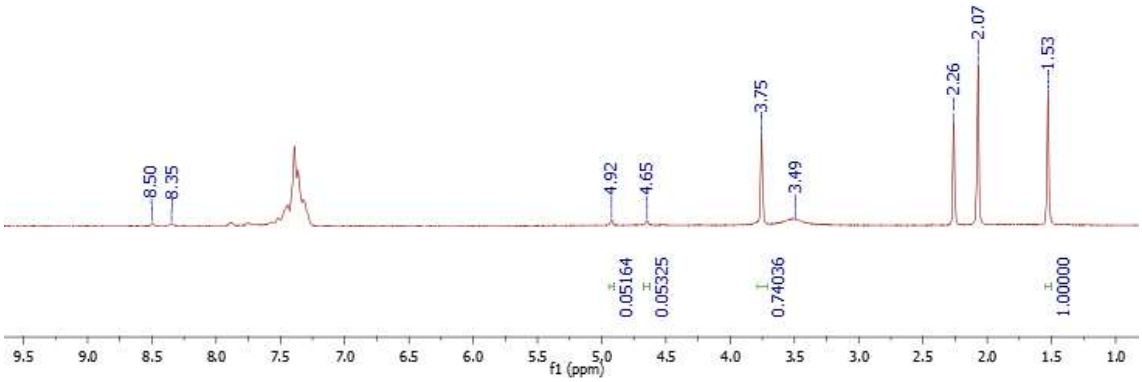


Figure 8. $^{1}$H NMR of Scheme 1***(60°C)***. 2.26 ppm: acetone..

**Scheme 1 (90°C)**

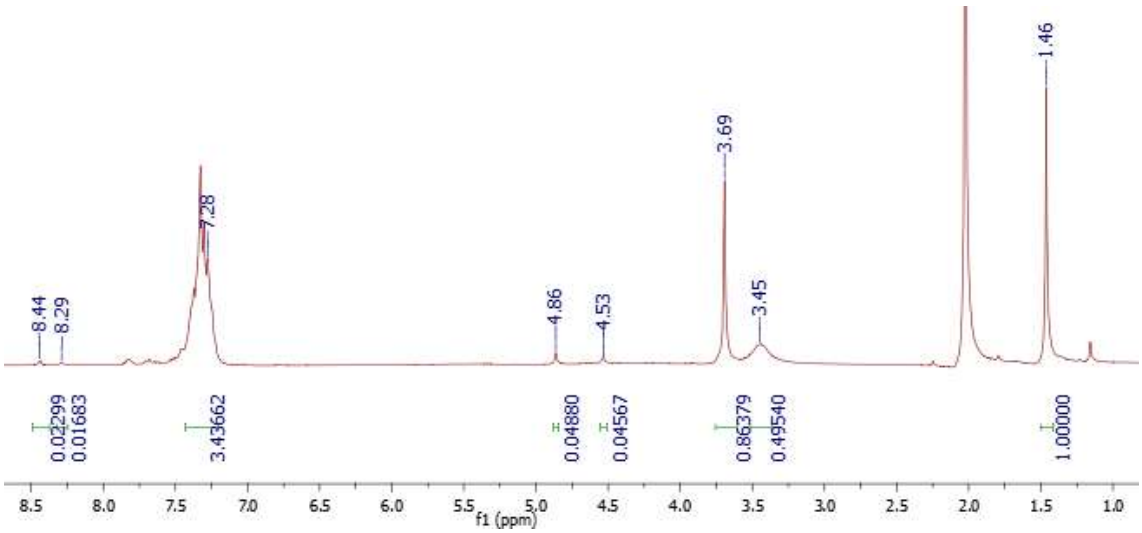


Figure 9. $^{1}$H NMR of Scheme 1 ***(90°C)***. 2.03 ppm: acetonitrile

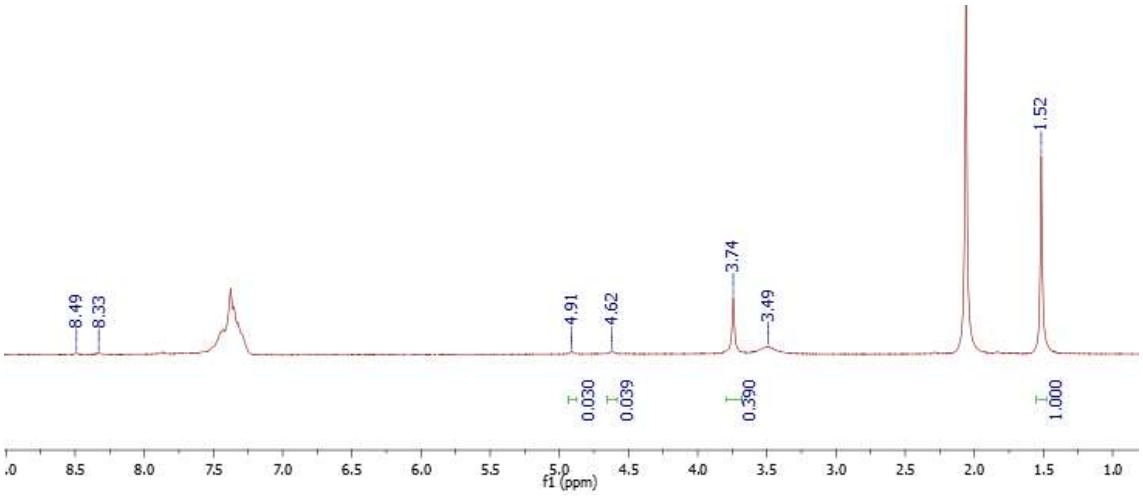


Figure 10.[1]H NMR of Scheme 1 ***(30°C)***. 2.03 ppm: acetonitrile

## 2.4 Experiment conduced with $CD_3OD$

An experiment was conducted to demonstrate that C1-unit originates from methanol. Following the standard experimental protocol above, $CH_3OH$ was substituted by $CD_3OD$, the NMR results are presented.

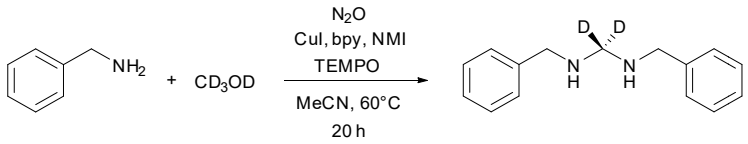


In a 25 mL *tube equipped with high-vacuum Teflon valve*, TEMPO (16.7 mg, 0.11 mmol) was added along with 5 mL of the diluted stock solution. After that deuterated methanol (89 µL, 2.2 mmol) and benzylamine (120 µL, 1.1 mmol) were introduced. The mixture was stirred under $N_2O$. 100 mL of $N_2O$ was condensed into the tube at -196°C.The flask was then heated to 60 °C for 20 hours.

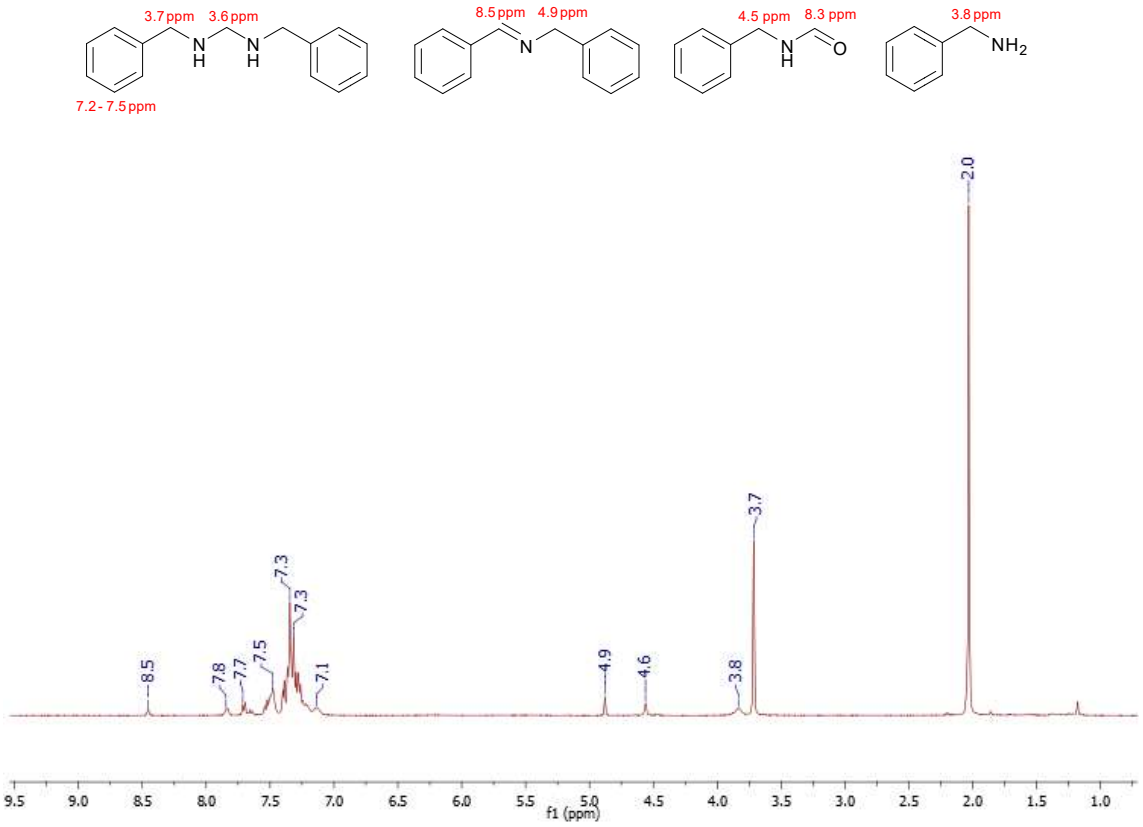


Figure 11. $^1$H NMR analysis for the $CD_3OD$ experiment. 2.0 ppm: acetonitrile.

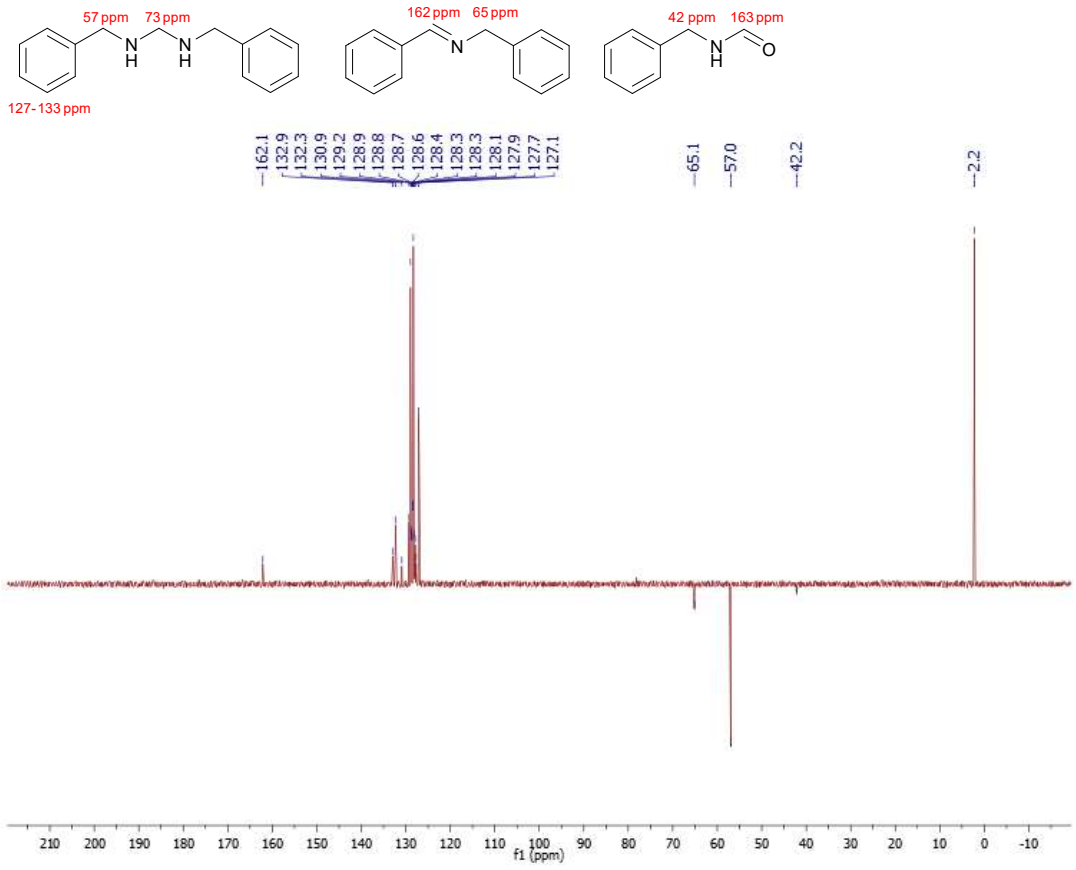


Figure 12. Dept-135 experiment for the reaction with $CD_3OD$.

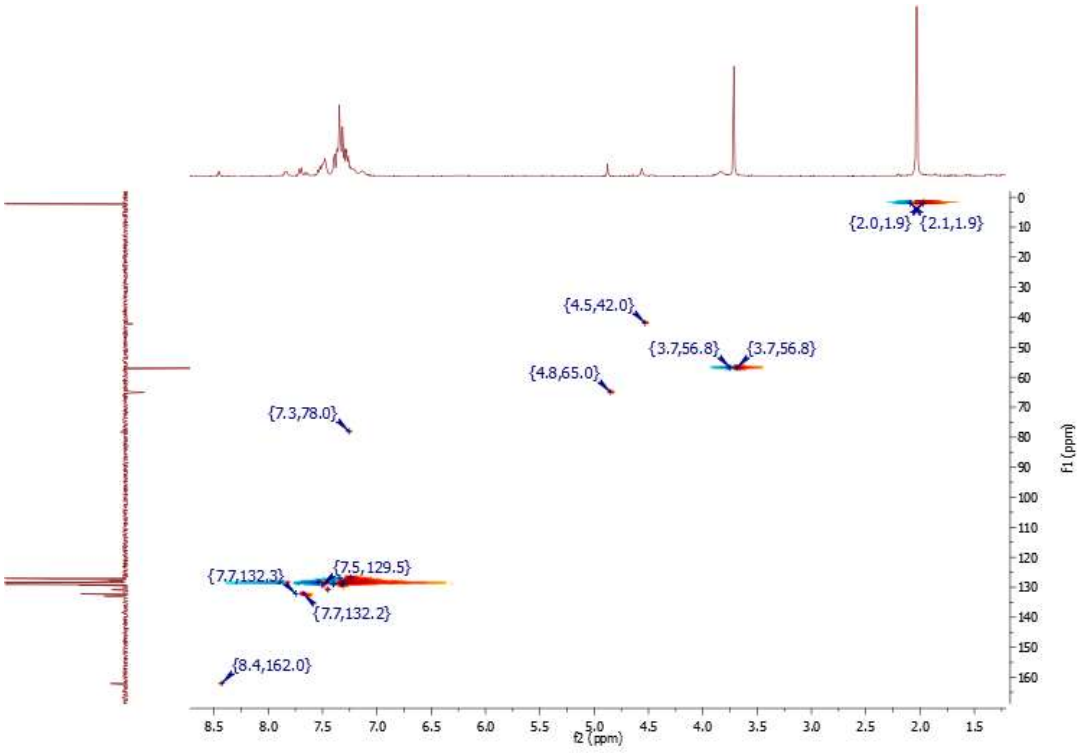


Figure 13. HSQC experiment for the reaction with $CD_3OD$.

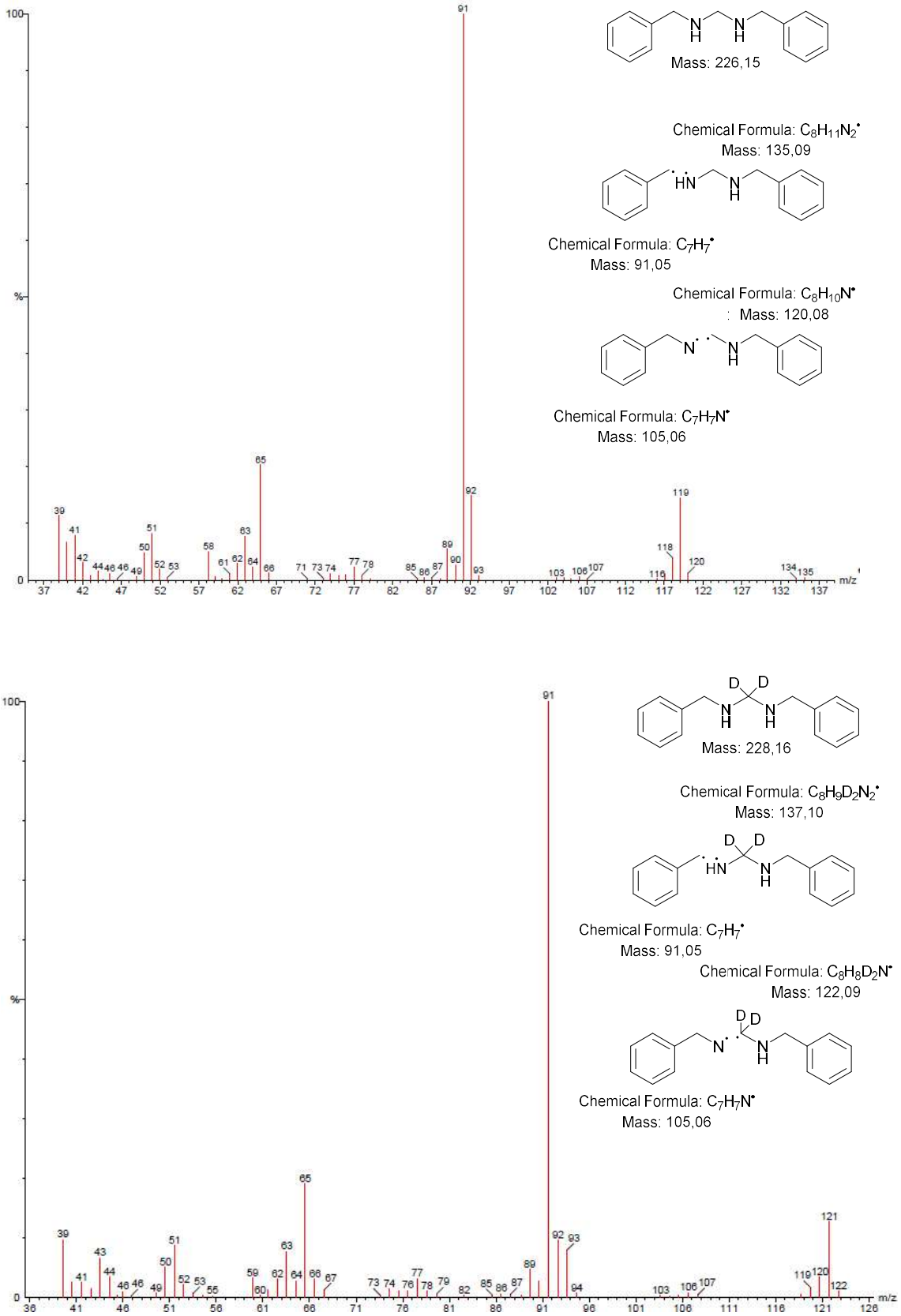


Figure 14. Comparison of the mass spectrograms of the reactions $CH_3OH$ (top) and $CD_3OD$ (bottom). The isotope-shift is visible for the fragments $C_8H_{10}N$ (m/z: 120 (calc); 119 (measured) and $C_8H_8D_2N$ (m/z: 122 (calc); 121 (measured) respectively.

## 2.5 General procedure for the substrate scope for aminal formation

In a 25 mL *tube equipped with high-vacuum Teflon valve*, TEMPO (16.7 mg, 0.11 mmol) was added along with 5 mL of the diluted stock solution (0.0424 mmol of CuI, 0.0424 mmol of 2,2'-bipyridine and 0.088 mmol of NMI). Following this, methanol (89 µL, 2.2 mmol) and benzylamine (120 µL, 1.1 mmol) were introduced. The mixture was stirred under $N_2O$. 100 mL of $N_2O$ was condensed into the tube at -196°C. The flask was then heated to the 90 °C for 2 hours.

After heating, the reaction mixture was allowed to cool to room temperature, and then carefully opened to release the solubilized gas. The reaction mixture was subsequently transferred to a round-bottom flask, and acetonitrile was evaporated. Following evaporation, an internal standard of cyclohexane (20 µL, 0.184 mmol) and 50 µL of $CDCl_3$ were added to the solution. A portion (40 µL) of this mixture, along with 500 µL of $CDCl_3$, was then transferred to an NMR tube for $^1H$ NMR analysis. Results, refer Table 1 of the manuscript.

**Entry 2 - piperidine**

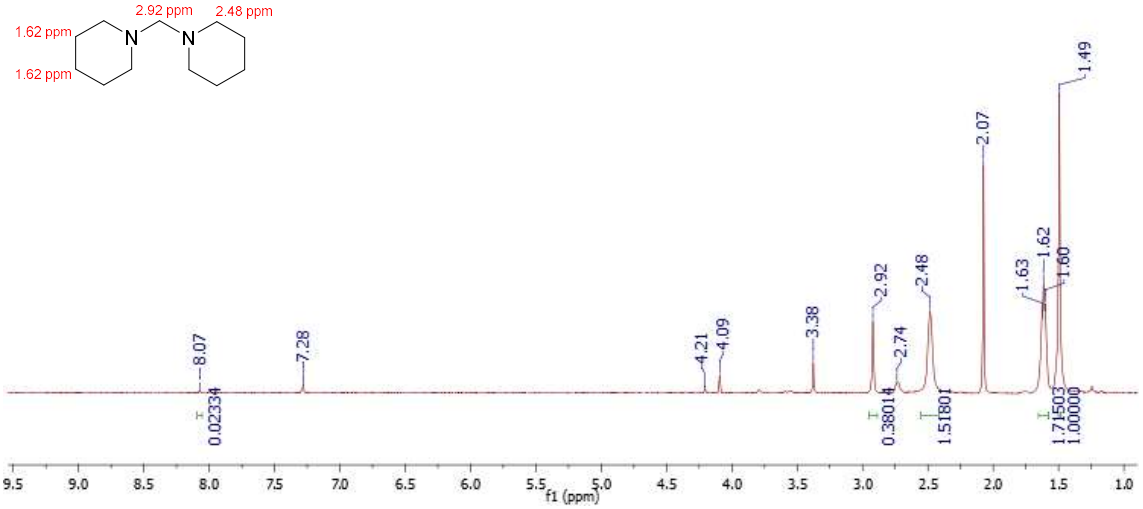


Figure 15. $^{1}$H NMR analysis of piperidine aminal formation.

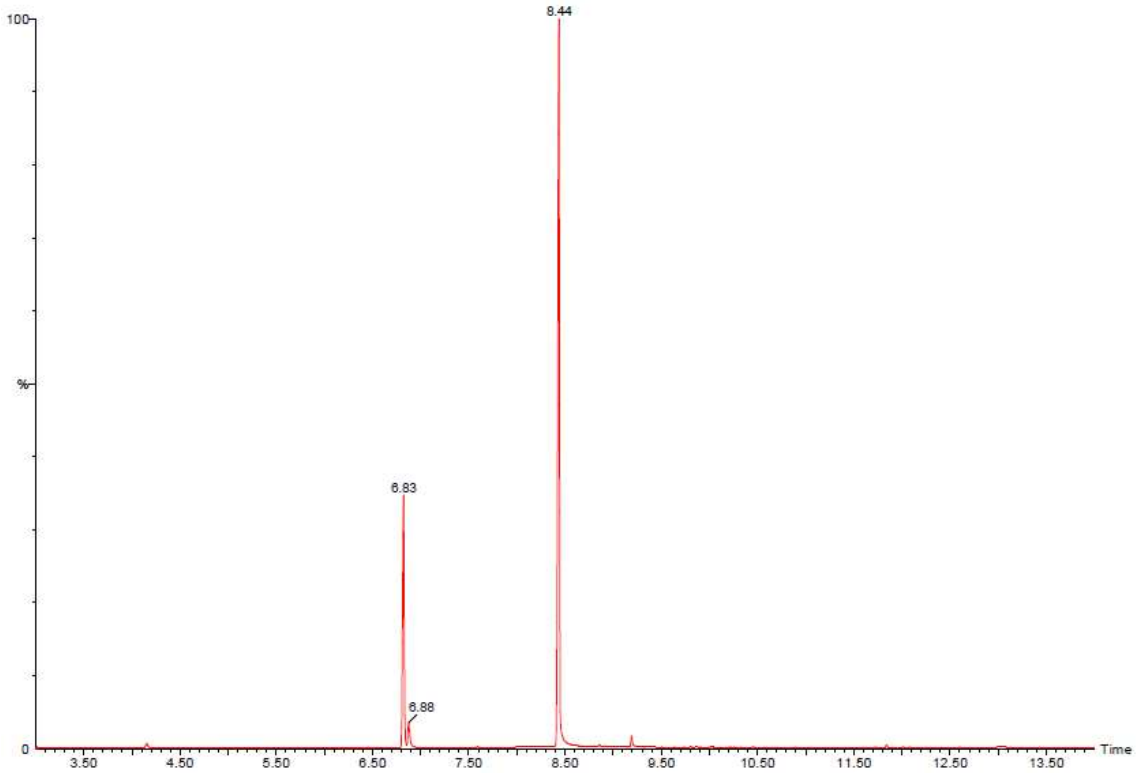


Figure 16. GC-MS analysis of piperidine aminal formation. 6.83 min.: TEMPO, 6.88 min.: *N*-formylpiperidine and 8.44 min.: dipiperidinomethane.

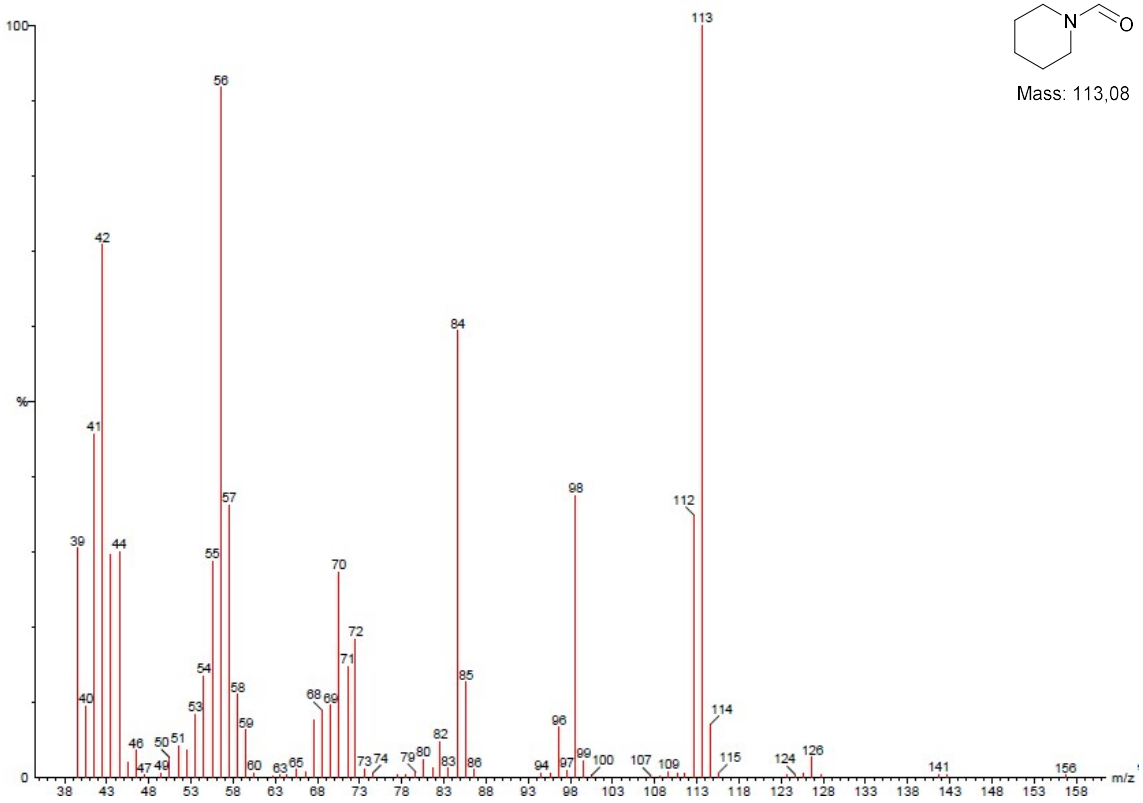


Figure 17. MS of *N*-formylpiperidine.

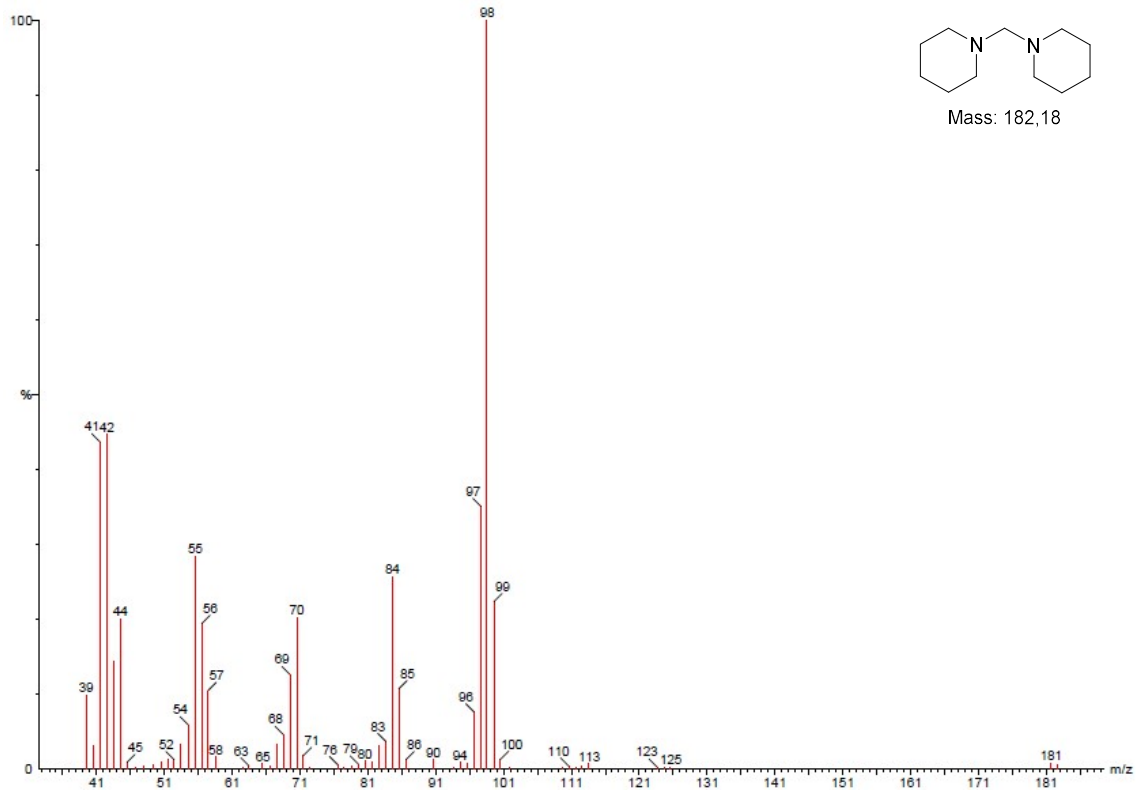


Figure 18. MS of dipiperidinomethane.

## Entry 3 – 2,4-dimethoxybenzylamine

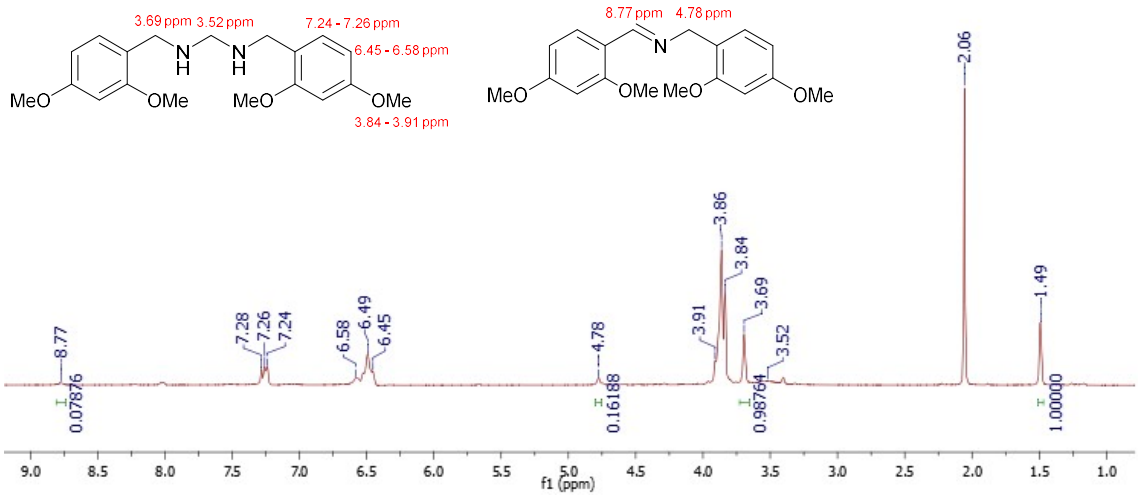


Figure 19. $^{1}$H NMR analysis of 2,4-dimenthoxybenzylamine aminal formation

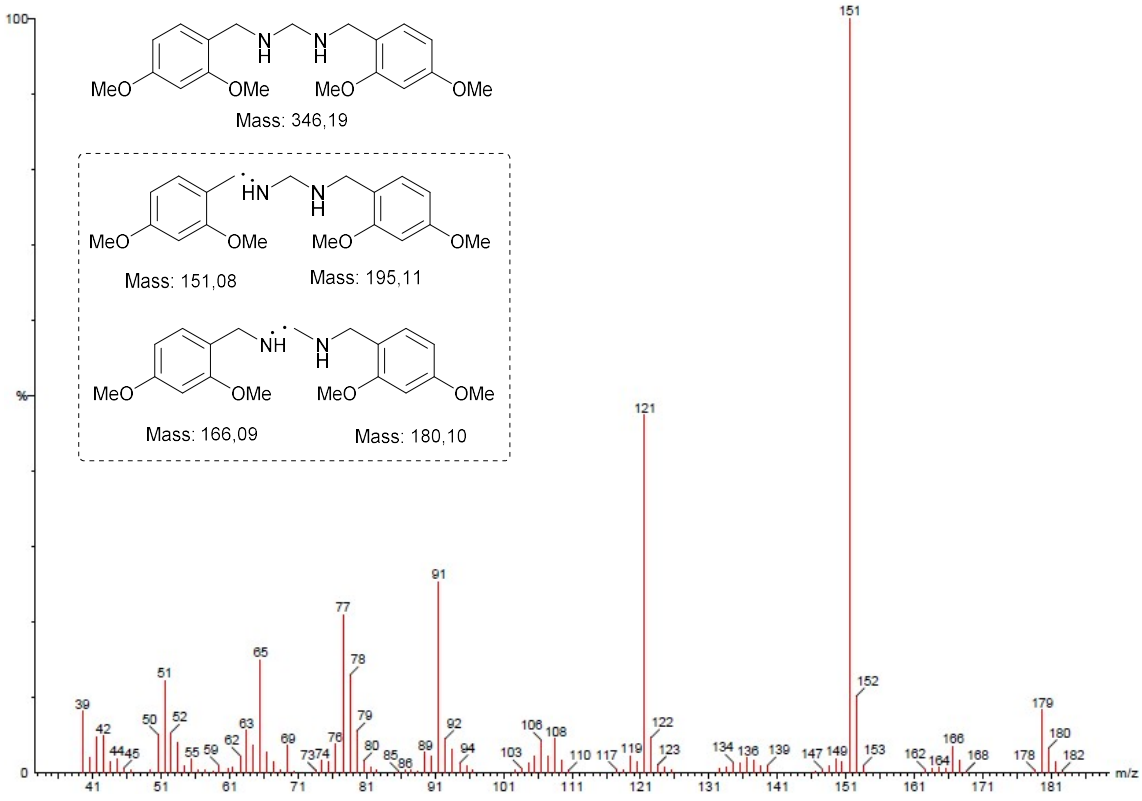


Figure 20. MS of *N,N'*-bis(2,4-dimethoxybenzyl)methanediamine.

## Entry 4 – 4-chlorobenzylamine

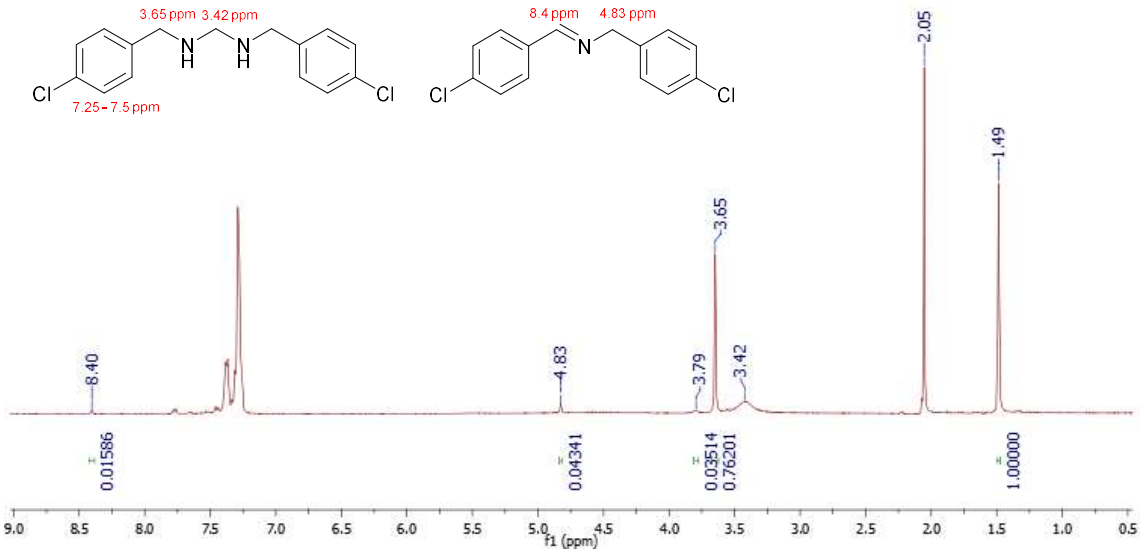


Figure 21. $^{1}$H NMR analysis of 4-chlorobenzylamine aminal formation.

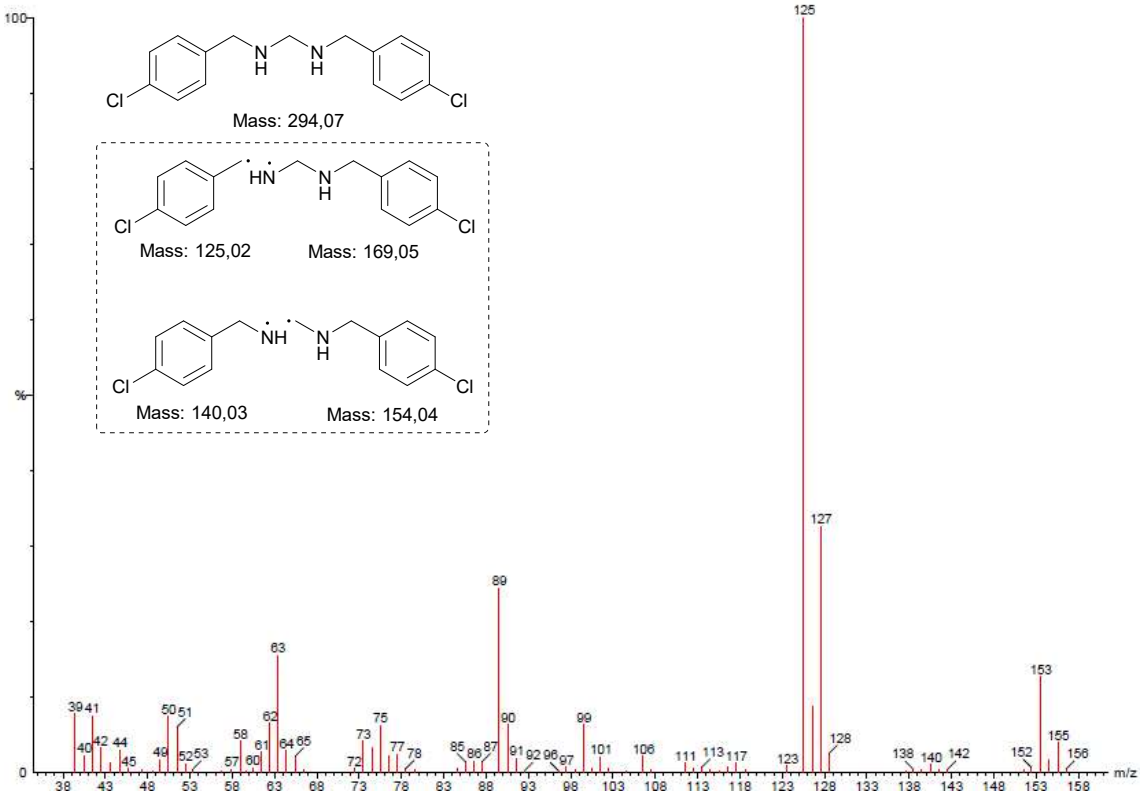


Figure 22. MS of *N,N'*-bis(4-chloro)methanediamine.

## Entry 5 – 4-methylbenzylamine

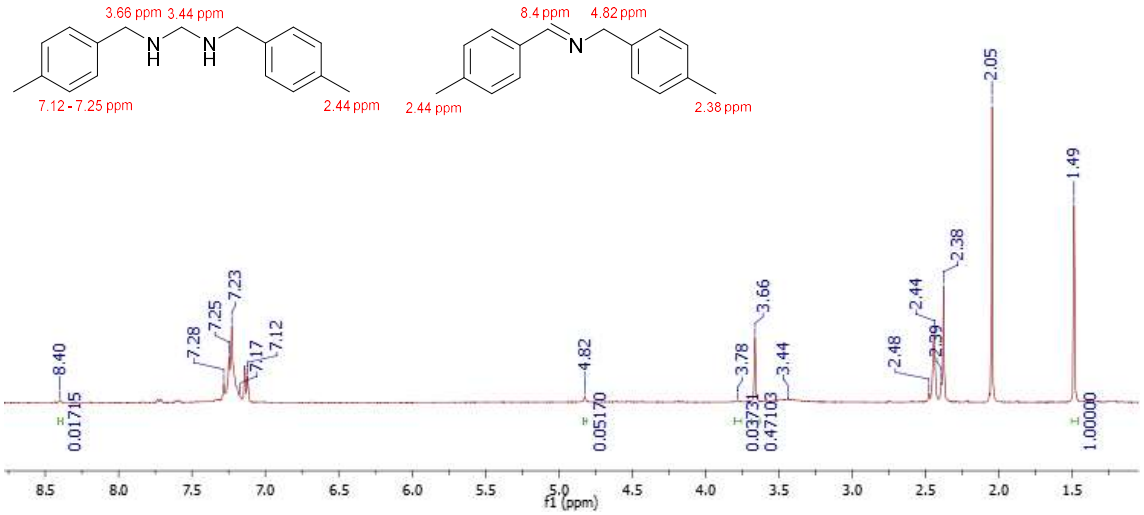


Figure 23. $^{1}$H NMR analysis of 4-methylbenzylamine aminal formation.

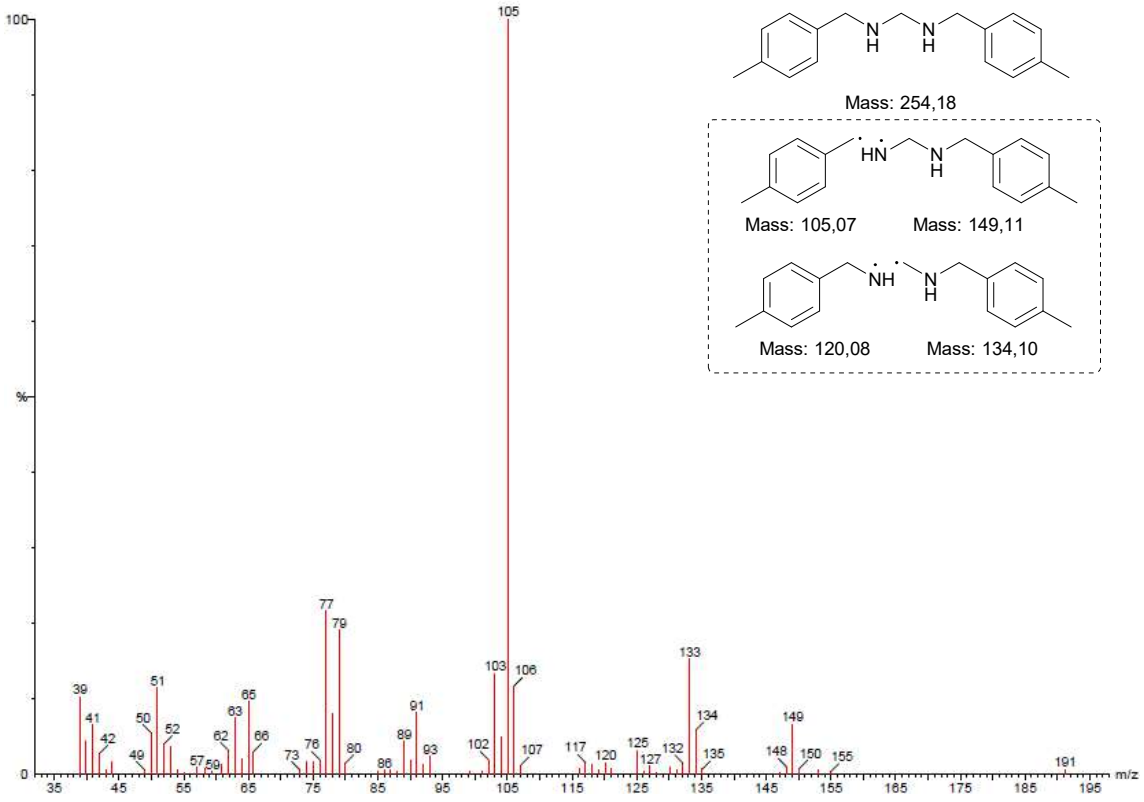


Figure 24. MS of *N,N'*-bis(4-methyl)methanediamine.

## Entry 6 – 4-trifluoromethylbenzylamine

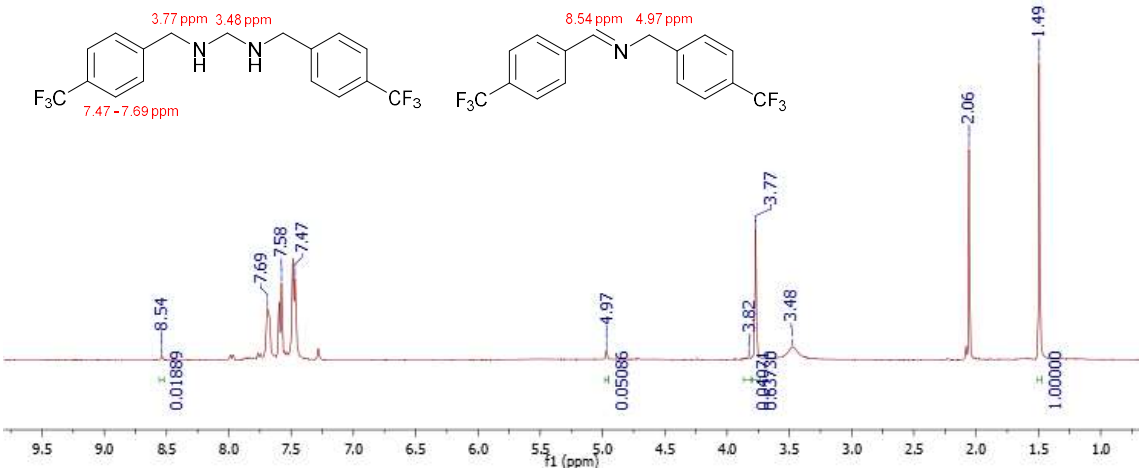


Figure 25. $^{1}$H NMR analysis of 4-trifluoromethylbenzylamine aminal formation.

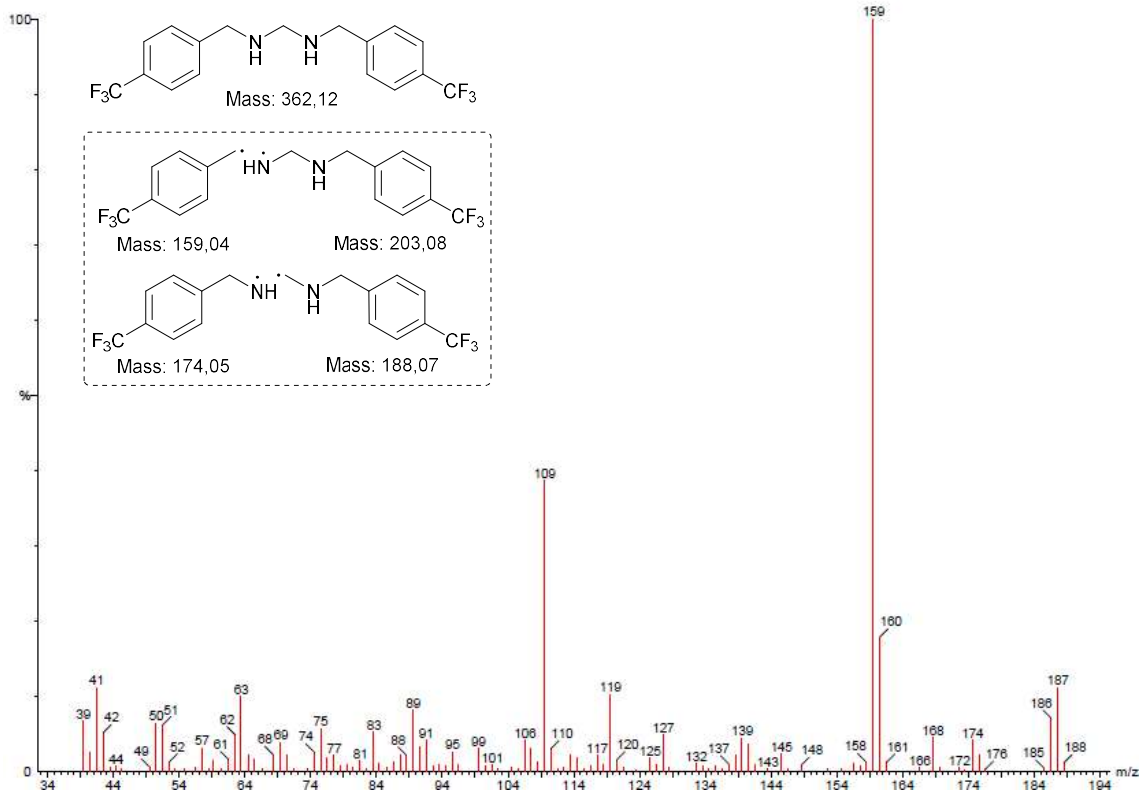


Figure 26. MS of *N,N'*-bis(4-trifluoromethyl)methanediamine.

## Entry 7 – 2-chlorobenzylamine

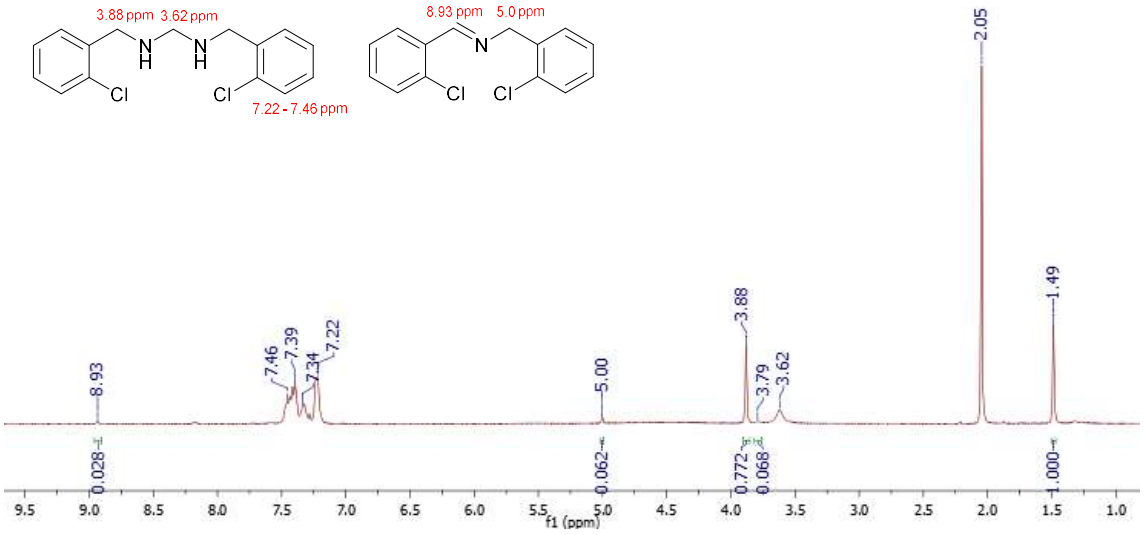


Figure 27.[1]H NMR analysis of 2-chlorobenzylamine aminal formation.

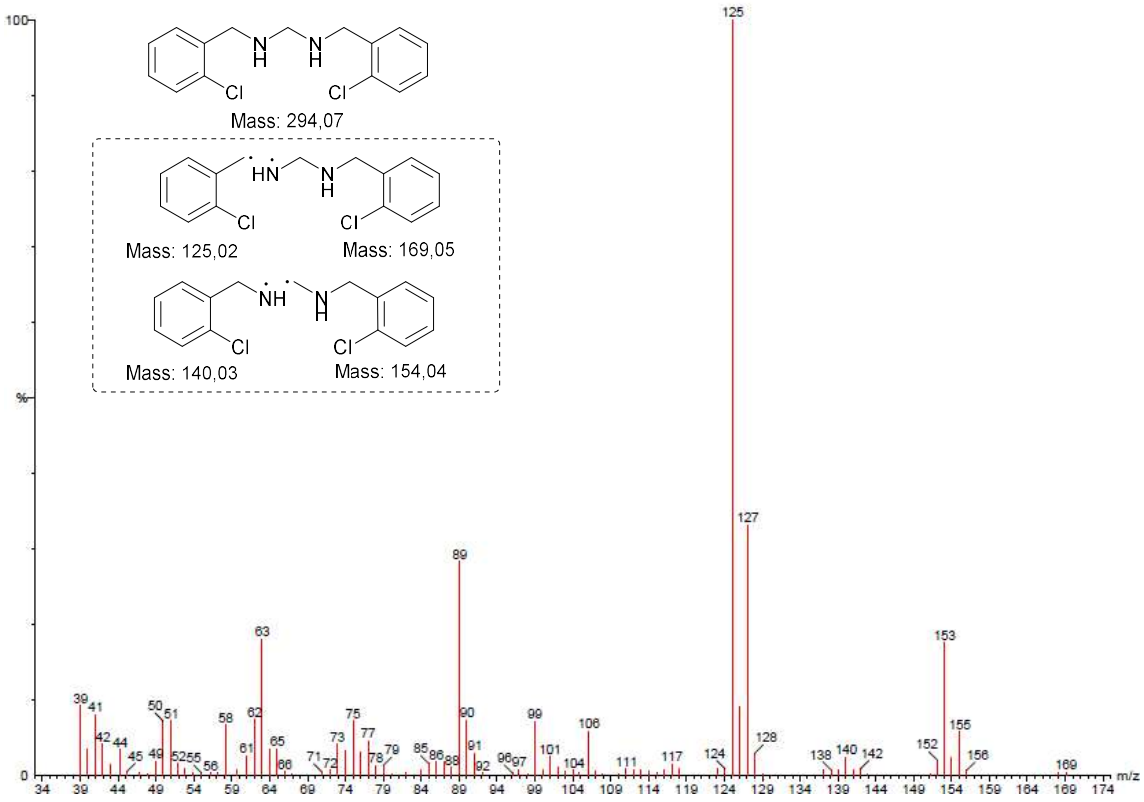


Figure 28. MS of *N,N'*-bis(2-chloro)methanediamine.

## Entry 8 – 3-bromobenzylamine

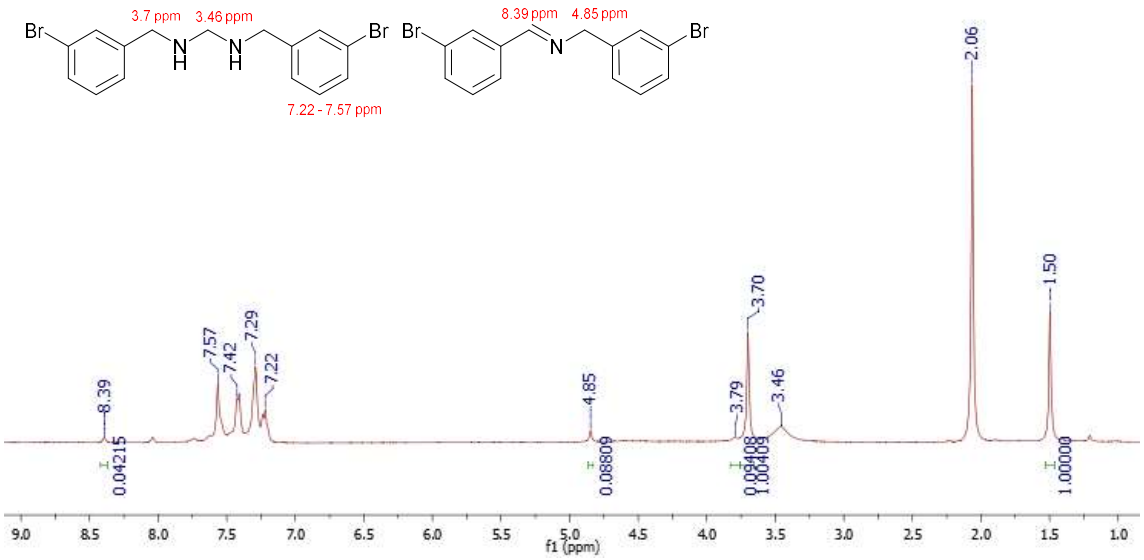


Figure 29. $^{1}$H NMR analysis of 3-bromobenzylamine aminal formation.

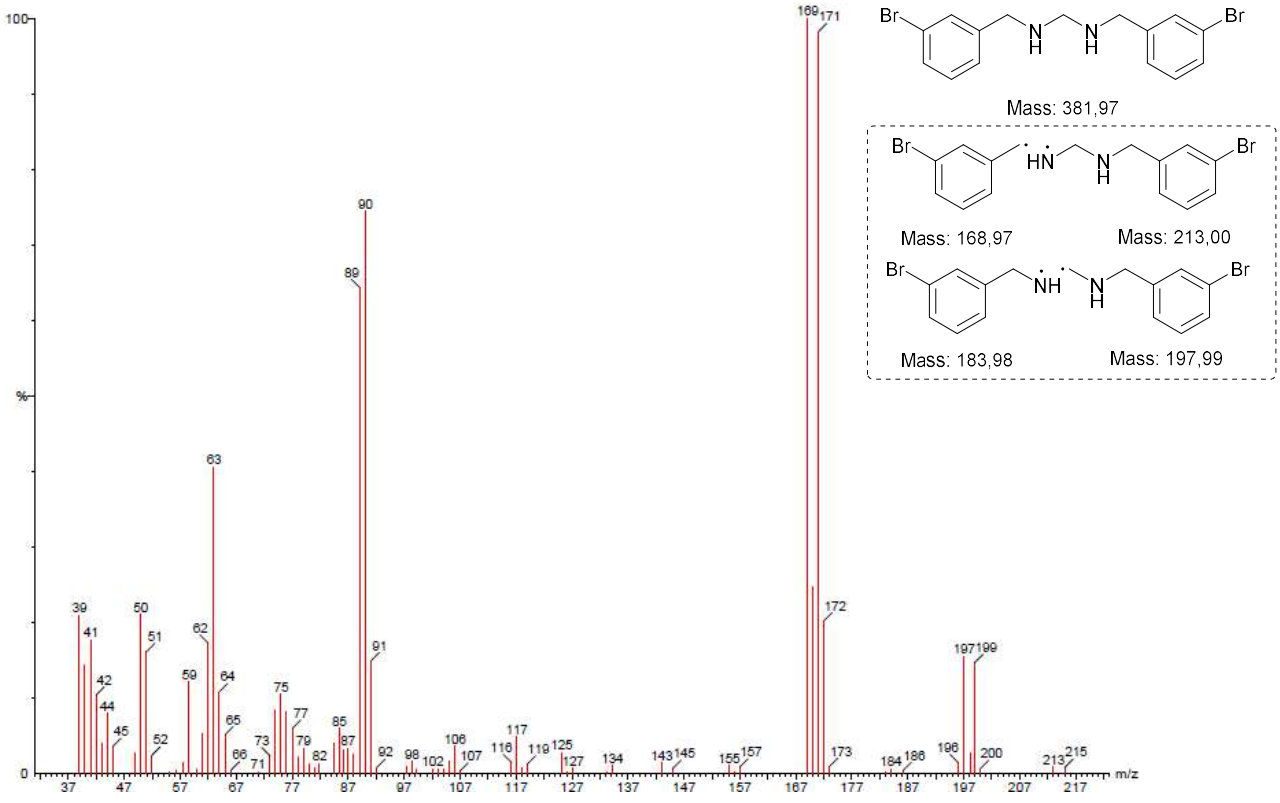


Figure 30. MS of *N,N'*-bis(3-bromo)methanediamine.

## Entry 9 – 4-tertbutylbenzylamine

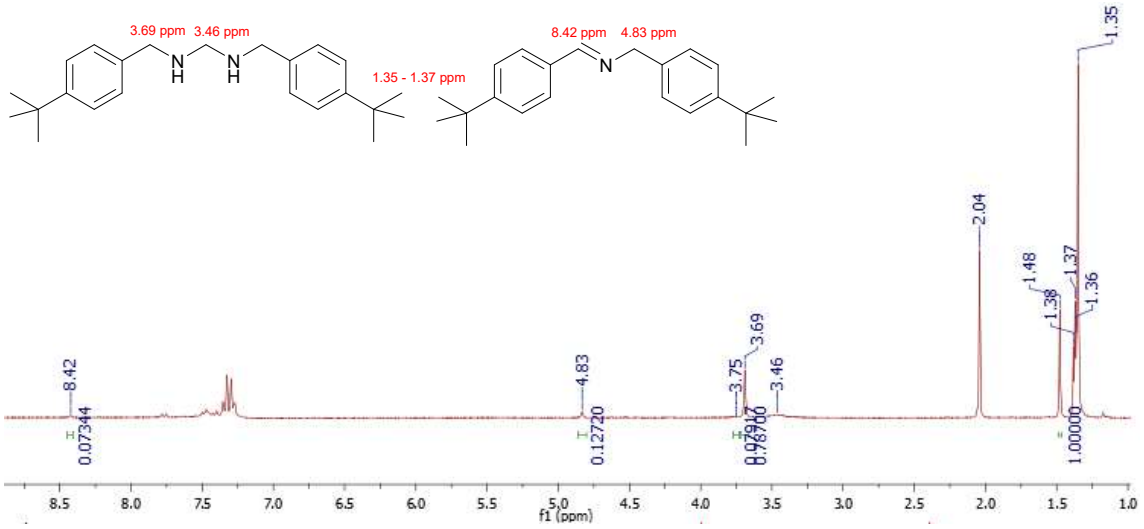


Figure 31. $^{1}$H NMR analysis of 4-tertbutylbenzylamine aminal formation.

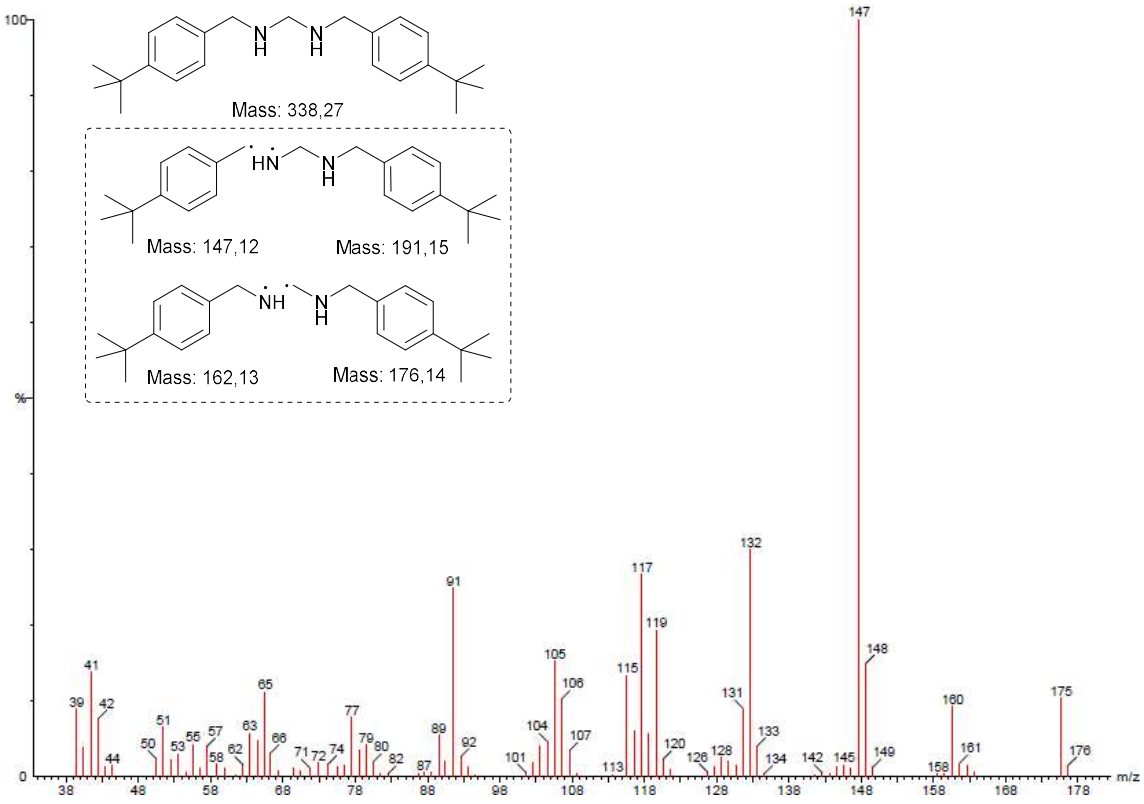


Figure 32. MS of *N,N'*-bis(4-tertbutyl)methanediamine.

**Isolation of compound 2a *N,N'*-dibenzylmethanediamine**

After the reaction period, the tube was cooled to room temperature, and the reaction solution was filtered through silica to remove the copper catalyst. The silica was washed with DCM (3 x 3 mL). MeCN and DCM in the filtered solution were removed by evaporation. The concentrated crude product was solubilized in $CHCl_3$ and purified by column chromatography on silica gel (from pure $CHCl_3$ to $CHCl_3$: MeOH 19:1). After evaporating the eluent, the solid was weighed and analyzed by $^{1}H$ and $^{13}C$ NMR in $CDCl_3$.

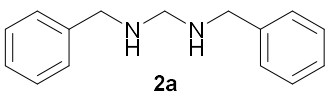

2a

***N,N'*-dibenzylmethanediamine:** light yellow oil, Rf= 0.74 ($CHCl_3$: MeOH, 19:1), 86% yield.

**$^{1}H$ NMR** (300 MHz, $CDCl_3$) δ 7.36-7.24 (m, 10H), 3.74 (s, 4H), 3.49 (s, 2H). **$^{13}C$ NMR** (300 MHz, $CDCl_3$) δ 138.4, 128.9, 128.6, 127.0, 73.8, 57.1 ppm.

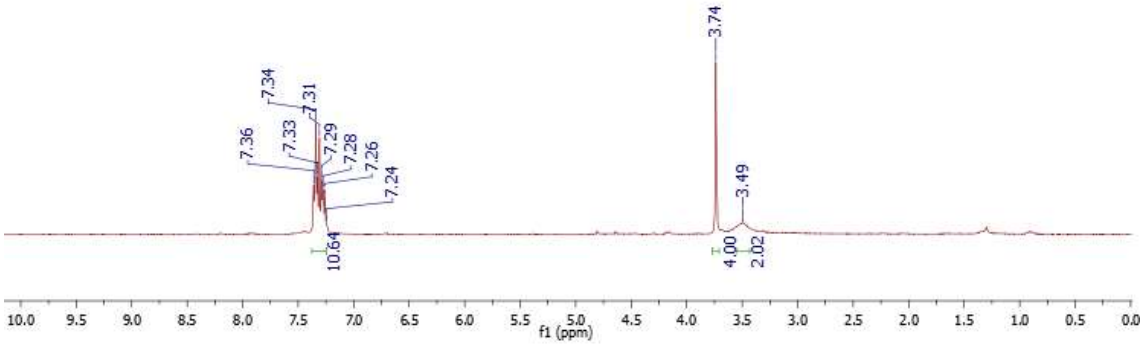


Figure 33.$^{1}H$ NMR analysis of isolated compound **2a**.

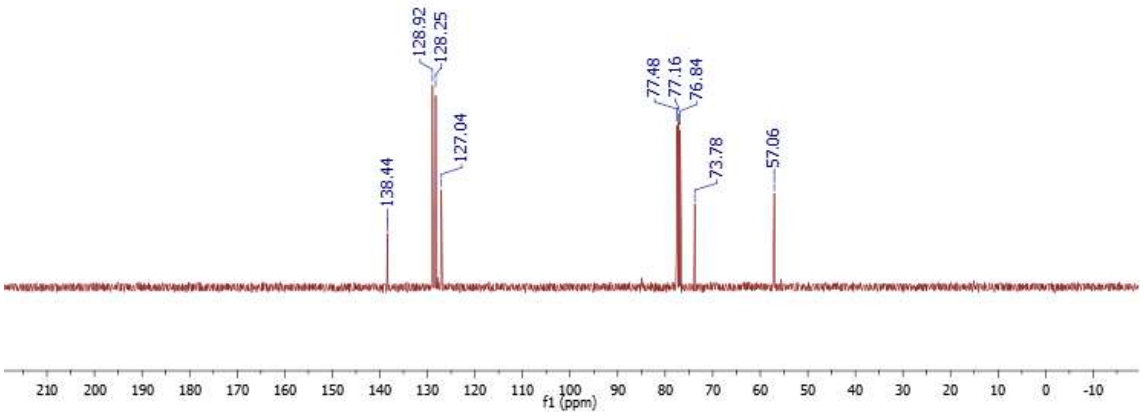


Figure 34.$^{13}C$ NMR analysis of isolated compound **2a**.

**Isolation of compounds 2e and 2i**

After the reaction period, the tubes were cooled to room temperature and then refrigerated at -32°C for 16 hours. After this time, a precipitated white solid was observed. The reactions were then filtered, and the solid was washed with cold acetonitrile (3 x 1 mL). The filter was washed with DCM to ensure that no compound was lost. After evaporation of DCM the solid was weighed and analyzed by $^{1}H$ and $^{13}C$ NMR with $CDCl_3$.

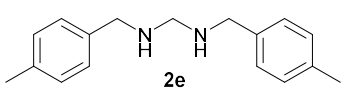

2e

***N,N'*-bis(4-methylbenzyl)methanediamine:** white solid, 56% yield.

**$^{1}H$ NMR** (300 MHz, $CDCl_3$) δ 7.22 (d, *J*= 7.6, 4H), 7.11 (d, *J*= 7.6, 4H), 3.64 (s, 4H), 3.42 (s, 2H), 2.36 (s, 6H). **$^{13}C$ NMR** (300 MHz, $CDCl_3$) δ 136.5, 135.4, 128.9, 73.7, 56.8, 21.1 ppm.

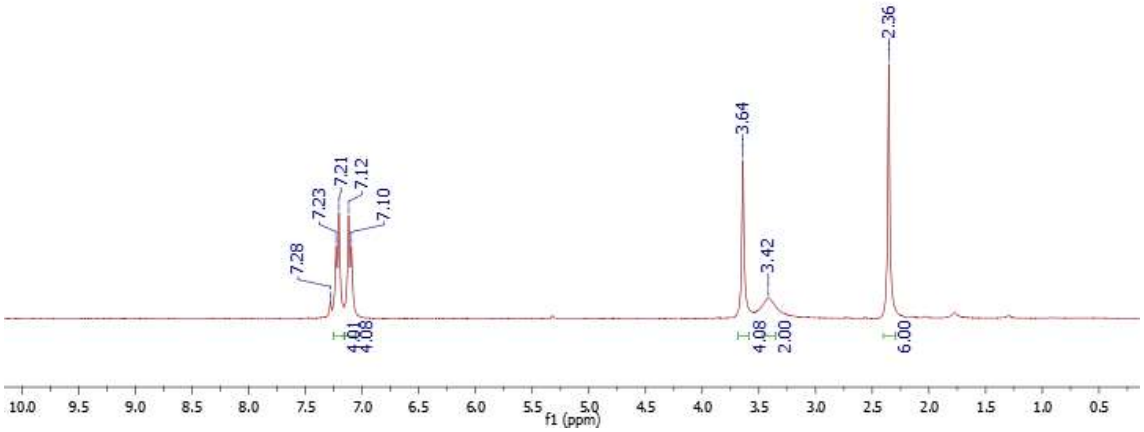


Figure 35. $^{1}H$ NMR analysis of isolated compound **2e**.

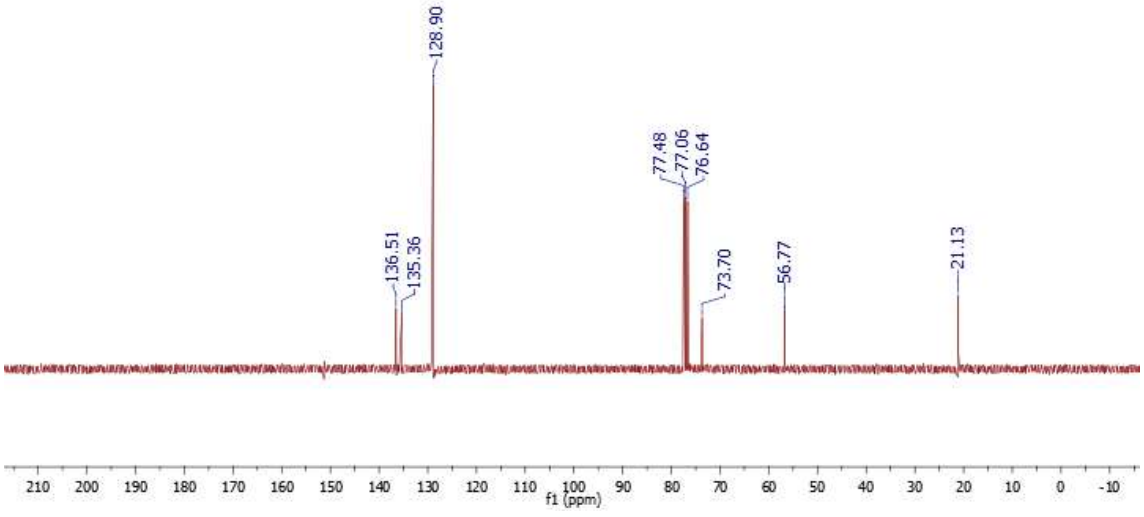


Figure 36. $^{13}C$ NMR analysis of isolated compound **2e**.

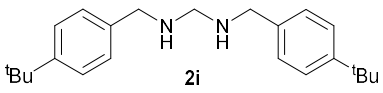

2i

***N,N'*-bis(4-(*tert*-butyl)benzyl)methanediamine:** white solid, 60% yield.

**$^{1}$H NMR** (300 MHz, $CDCl_3$) δ 7.40 (d, *J*= 7.9, 4H), 7.35 (d, *J*= 7.9, 4H), 3.76 (s, 4H), 3.53 (s, 2H), 1.41 (s, 18H). **$^{13}$C NMR** (300 MHz, $CDCl_3$) δ 149.9, 135.6, 128.7, 125.1, 74.0, 56.8, 34.5, 31.5 ppm.

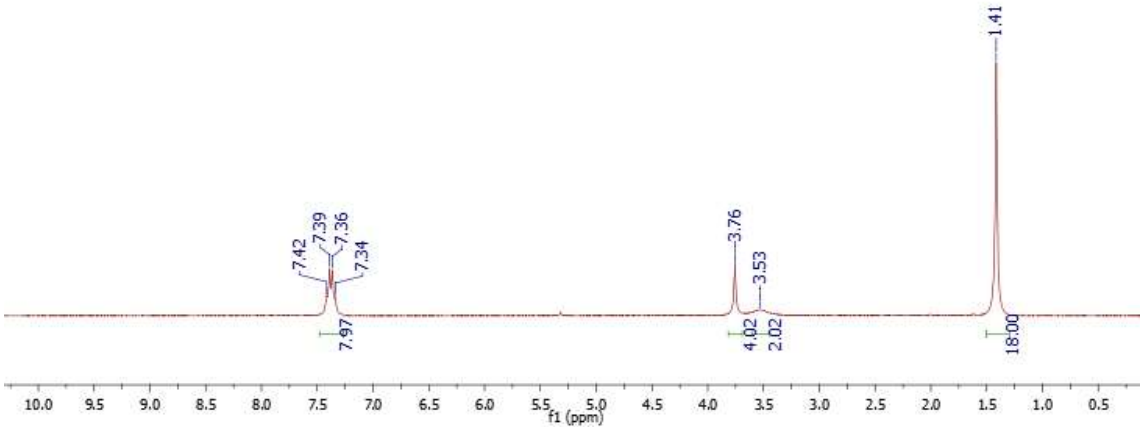


Figure 37. $^{1}$H NMR analysis of isolated compound **2i**.

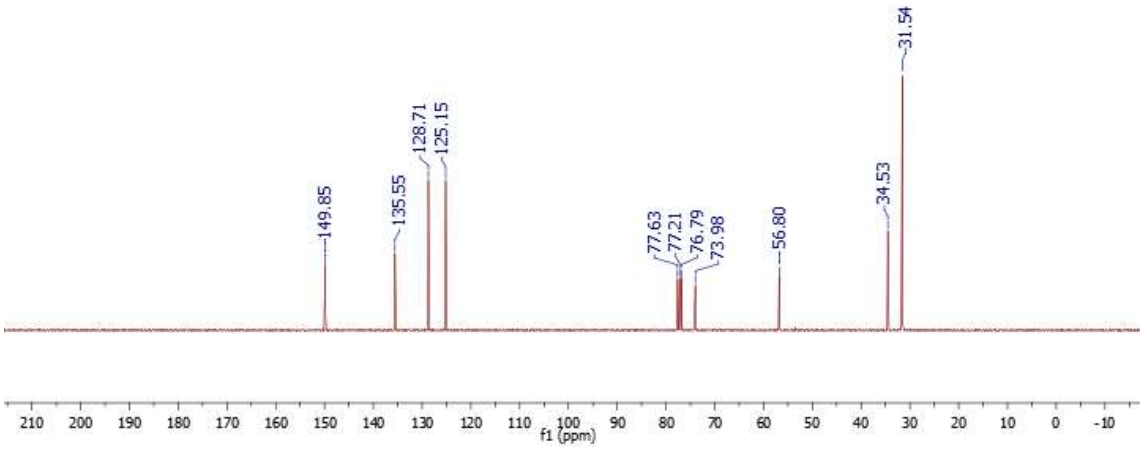


Figure 38. $^{13}$C NMR analysis of isolated compound **2i**.

# 3 Benzylamine oxidation with nitrous oxide

## 3.1 General procedure for the oxidation of benzylamines with copper and $N_2O$

In a 25 mL *tube equipped with high-vacuum Teflon valve*, TEMPO (16.7 mg, 0.11 mmol) was added with 5 mL of the diluted stock solution (0.0424 mmol of CuI, 0.0424 mmol of 2,2'-bipyridine and 0.088 mmol of NMI). Following this, benzylamines (1.1 mmol) were introduced. The mixture was stirred under $N_2O$. 100 mL of $N_2O$ was condensed into the tube at -196°C. The flask was then heated to 90 °C over a period of 4 hours.

After heating, the reaction mixture was allowed to cool to room temperature, and then carefully opened to release the solubilized gas. The reaction mixture was subsequently transferred to a round-bottom flask, and acetonitrile was evaporated. Following evaporation, an internal standard of cyclohexane (20 µL, 0.184 mmol) and 50 µL of $CDCl_3$ were added to the solution. A portion (40 µL) of this mixture, along with 500 µL of $CDCl_3$, was then transferred to an NMR tube for $^1H$ NMR analysis. Results, refer Table 2 of the manuscript.

## 3.2 Selected MS data for qualitative analysis of imine formation

Table 2, Entry 1

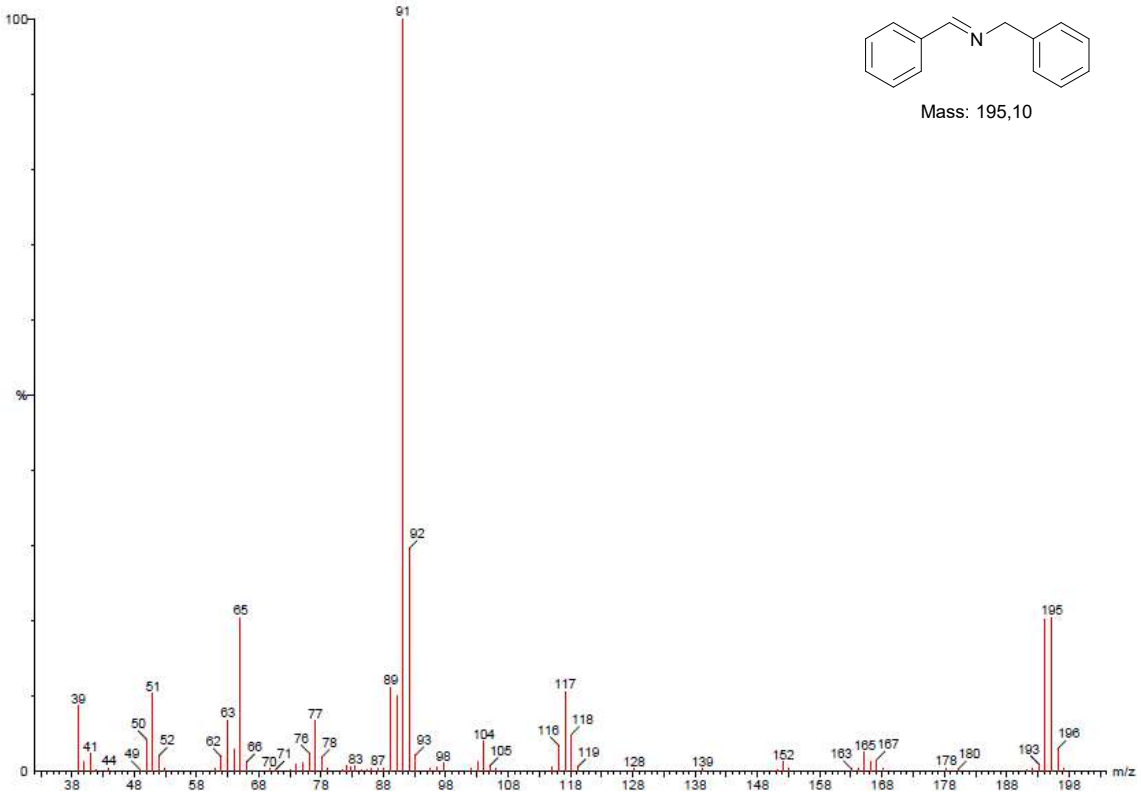


Figure 39. **MS** of *N*-benzyl-1-phenylmethanimine.

Table 2, Entry 2

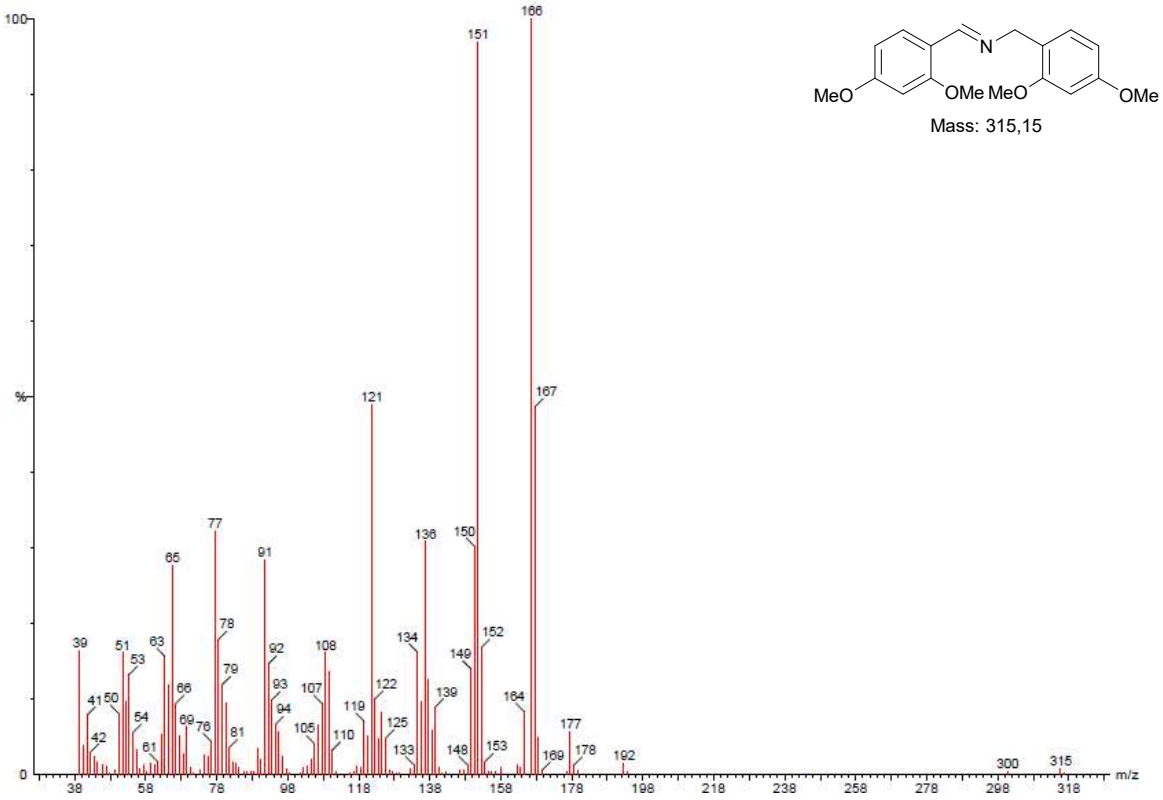


Figure 40. **MS** of *N*-(2,4-dimethoxybenzyl)-1-(2,4-dimethoxyphenyl)methanimine.

Table 2, Entry 3

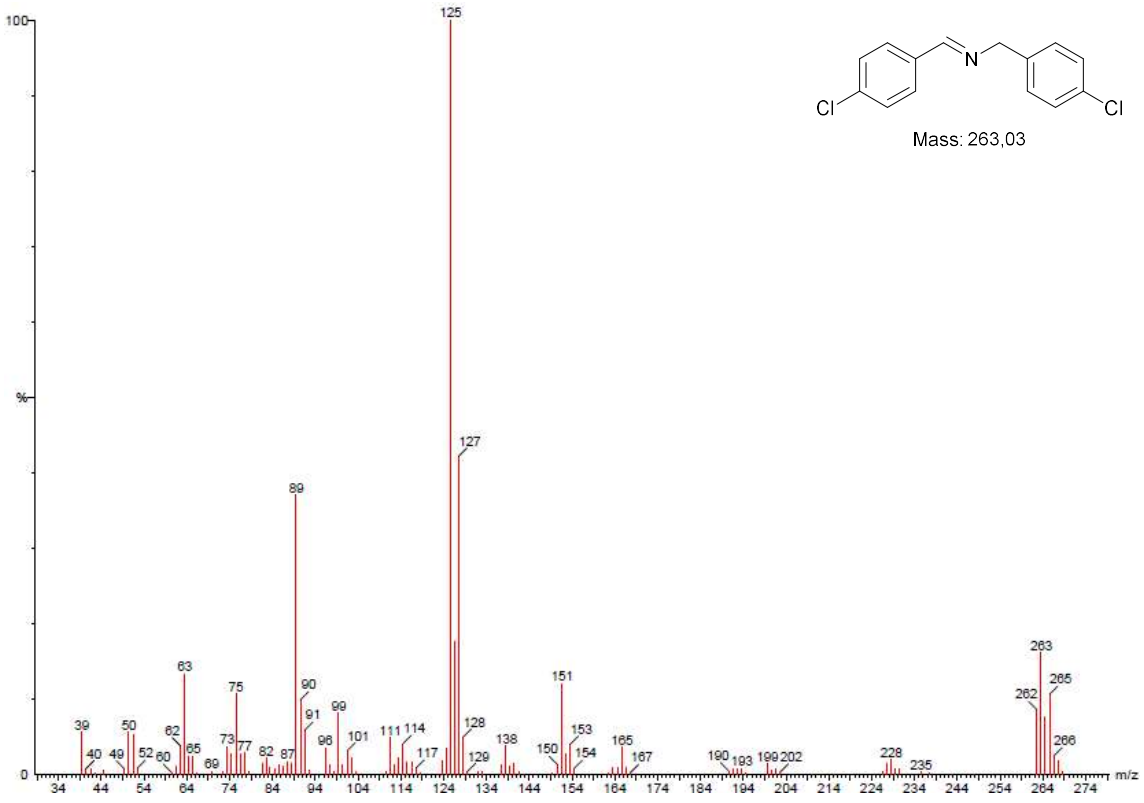


Figure 41. MS of *N*-(4-chlorobenzyl)-1-(4-chlorophenyl)methanimine.

Table 2, Entry 4

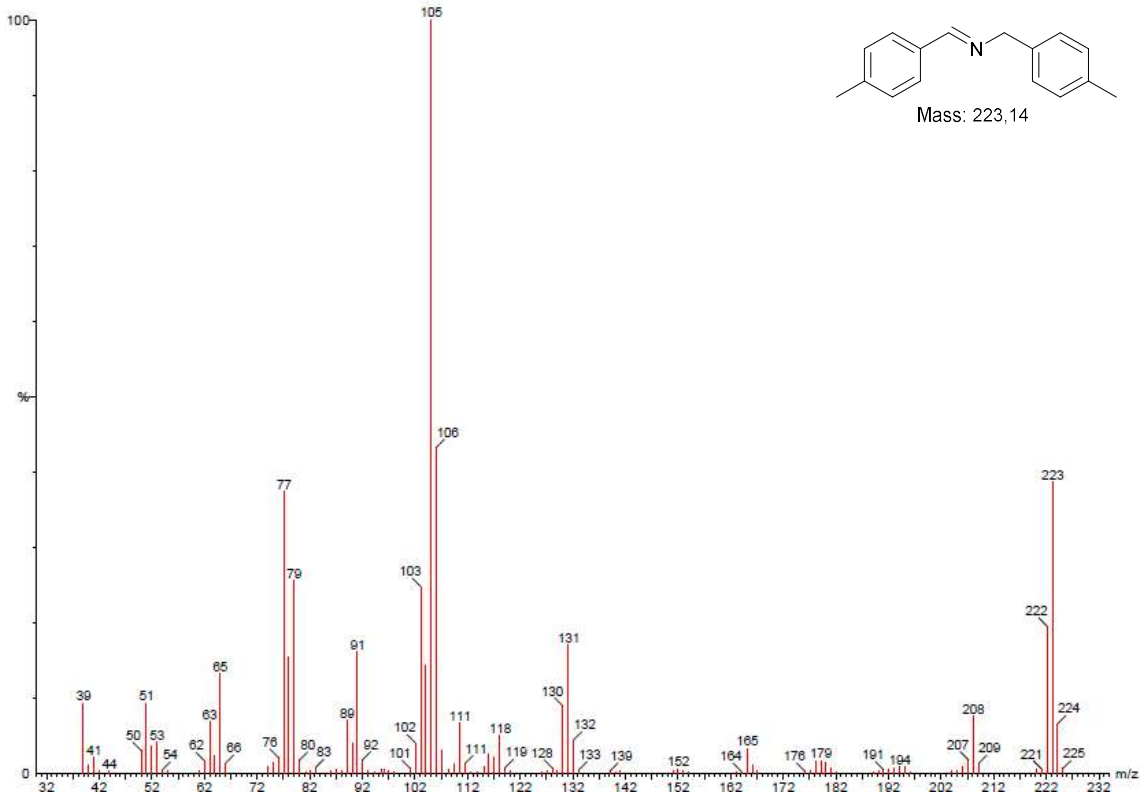


Figure 42. **MS** of *N*-(4-methylbenzyl)-1-(*p*-tolyl)methanimine.

Table 2, Entry 5

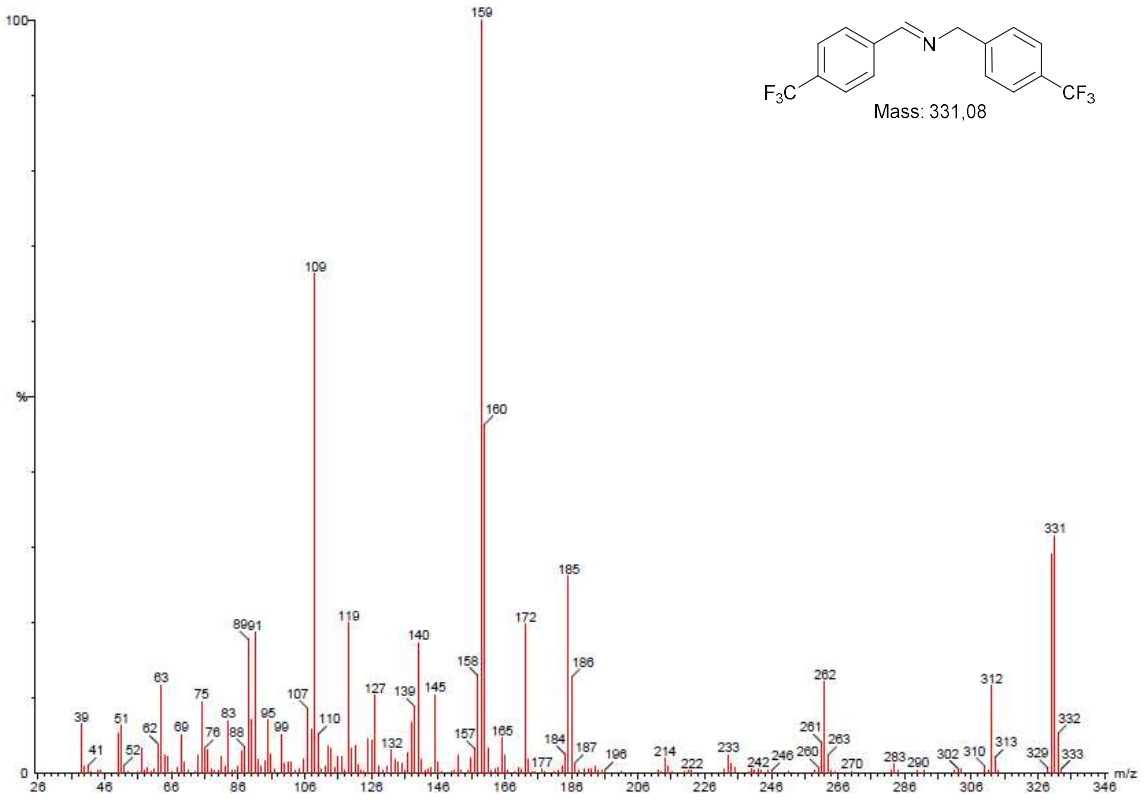


Figure 43. **MS** of *N*-(4-(trifluoromethyl)benzyl)-1-(4-(trifluoromethyl)phenyl)methanimine.

Tabl2, Entry 6

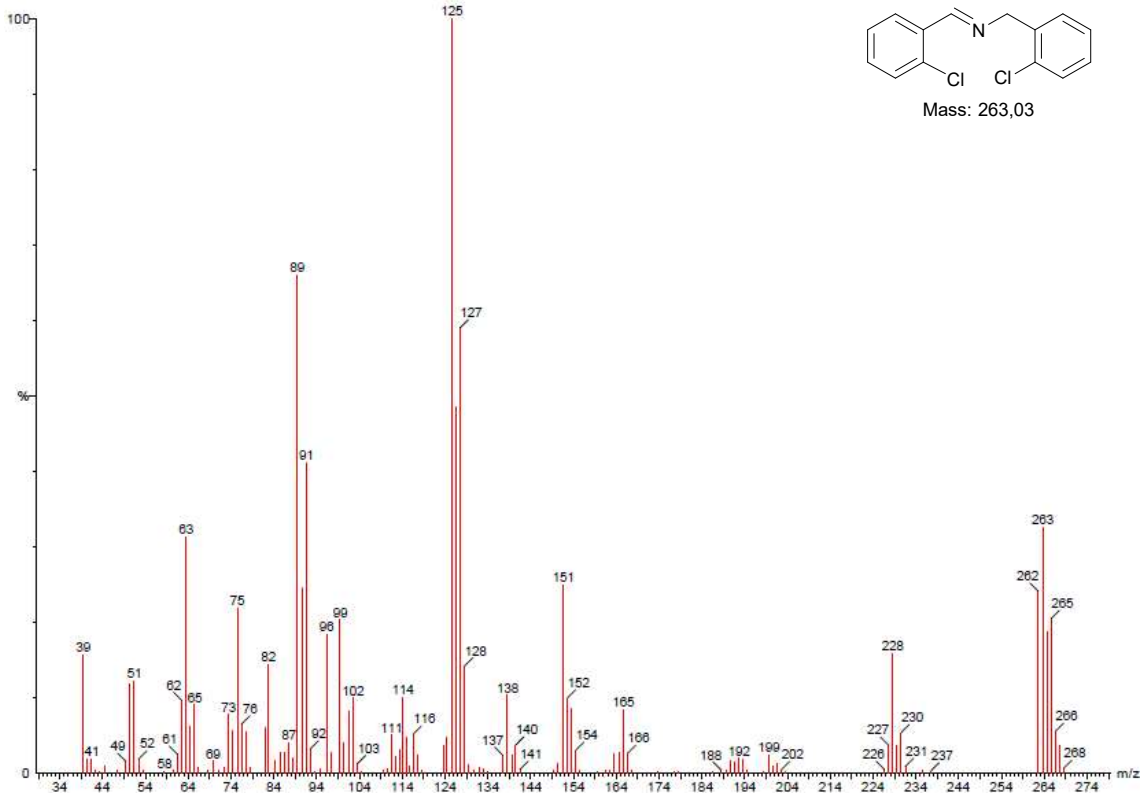


Figure 44. **MS** of *N*-(2-chlorobenzyl)-1-(2-chlorophenyl)methanimine.

Table 2, Entry 7

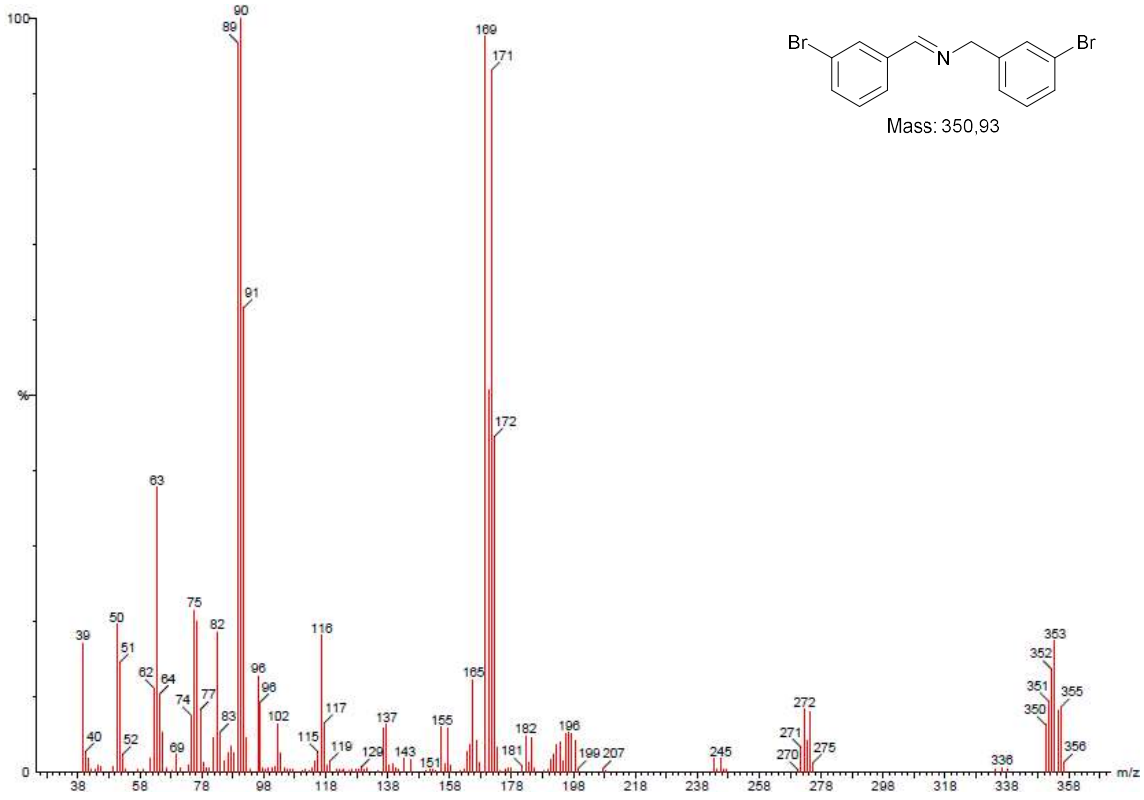


Figure 45. *N*-(3-bromobenzyl)-1-(3-bromophenyl)methanimine.

Table 2, Entry 8

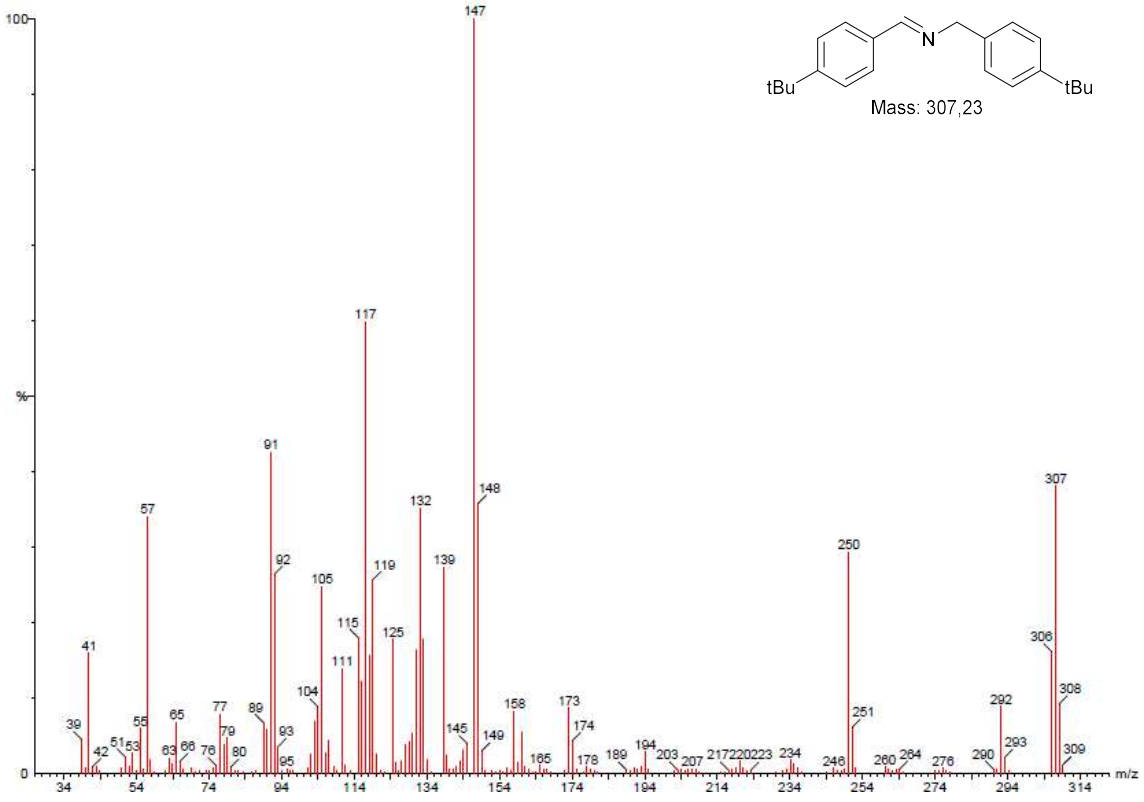


Figure 46. **MS** of *N*-(4-(tert-butyl)benzyl)-1-(4-(tert-butyl)phenyl)methanimine.

## 3.3 $^{1}$H-NMR spectrum for quantitative analysis of benzylamines oxidation

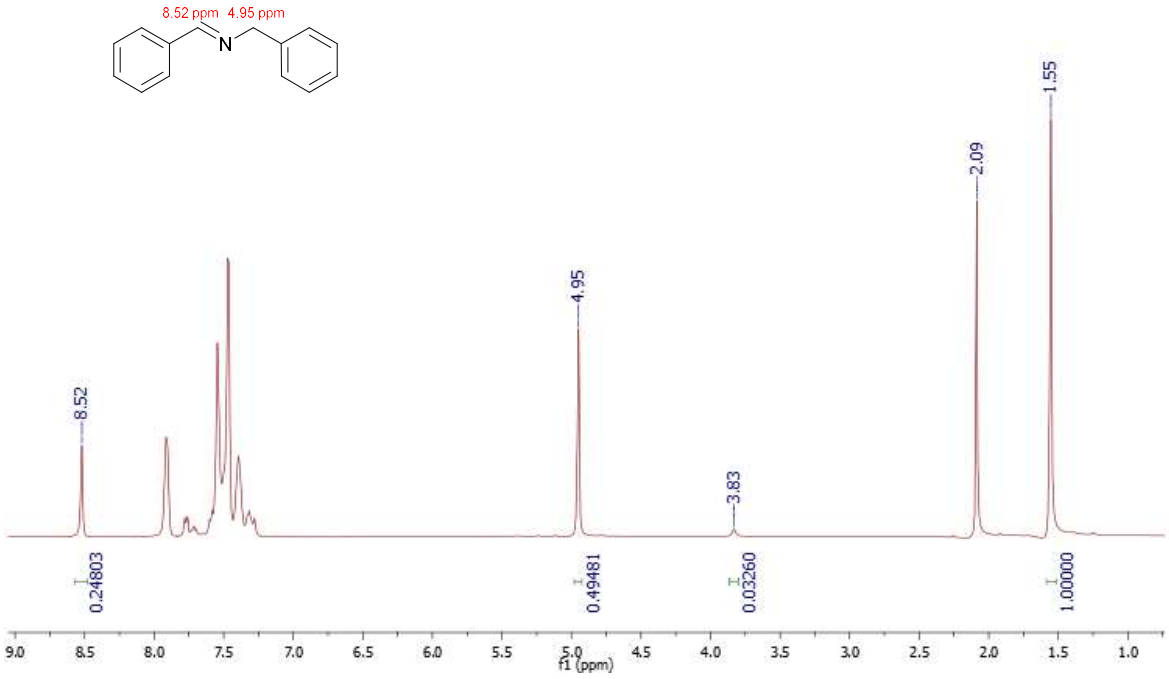


Figure 47. **$^{1}$H NMR of entry 1 .**. 2.09 ppm: acetonitrile, 3.83 ppm: benzylamine.

### Entry 2 – 2,4-dimethoxybenzylamine

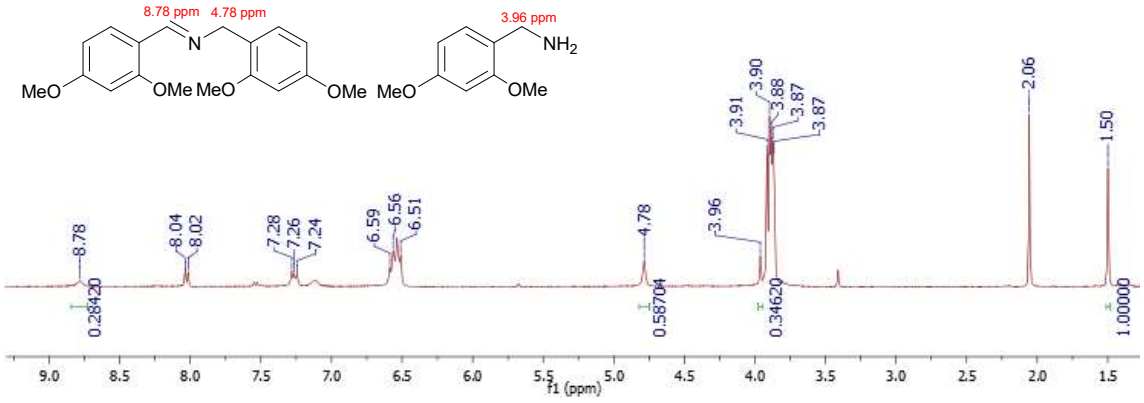


Figure 48. $^{1}$H NMR of entry 2. 1.5 ppm: cyclohexane,.2.06 ppm: acetonitrile, 3.96 ppm: 2,4-dimethoxybenzylamine.

## Entry 3 – 4-chlorobenzylamine

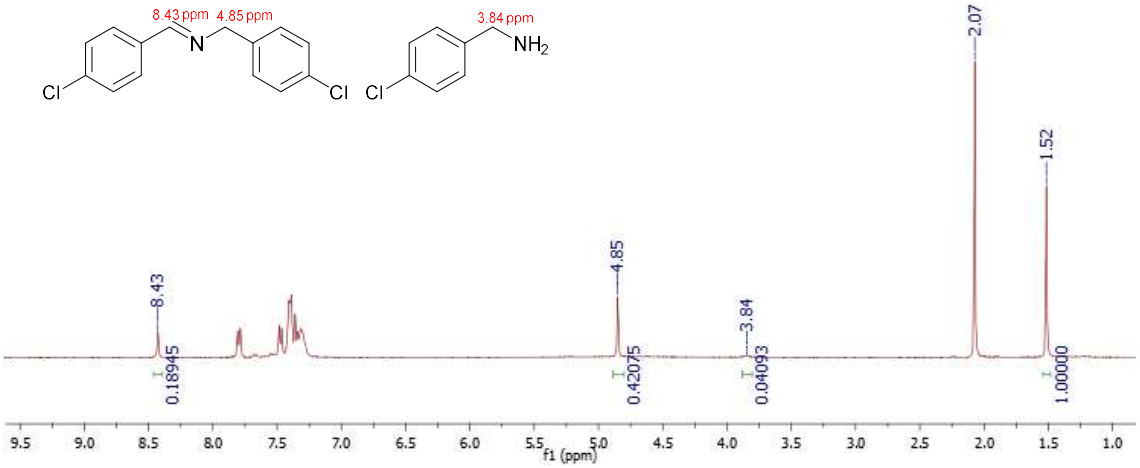


Figure 49. $^{1}$H NMR of entry 3. 1.52 ppm: cyclohexane,.2.07 ppm: acetonitrile, 3.84 ppm: 4-chlorobenzylamine.

## Entry 4 – 4-methylbenzylamine

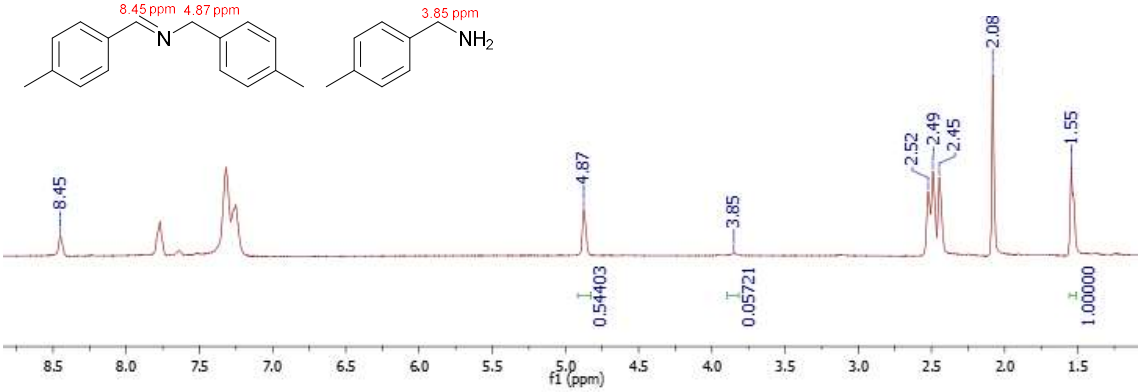


Figure 50. $^{1}$H NMR of entry 4. 1.55 ppm: cyclohexane,.2.08 ppm: acetonitrile, 3.85 ppm: 4-methylbenzylamine.

## Entry 5 – 4-trifluomethylbenzylamine

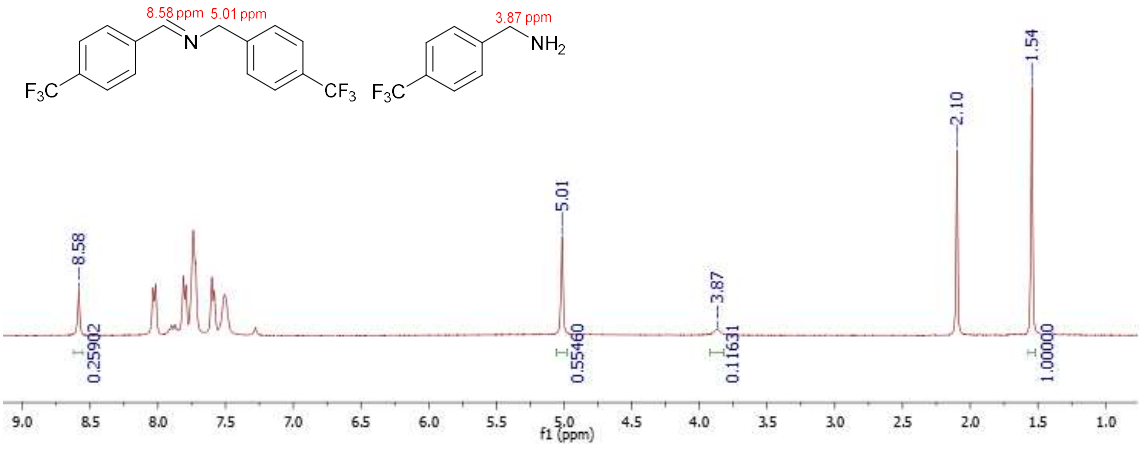


Figure 51. $^{1}$H NMR of entry 5. 1.54 ppm: cyclohexane,.2.10 ppm: acetonitrile, 3.87 ppm: 4-trifluoromethylbenzylamine.

## Entry 6 – 2-chloromethylbenzylamine

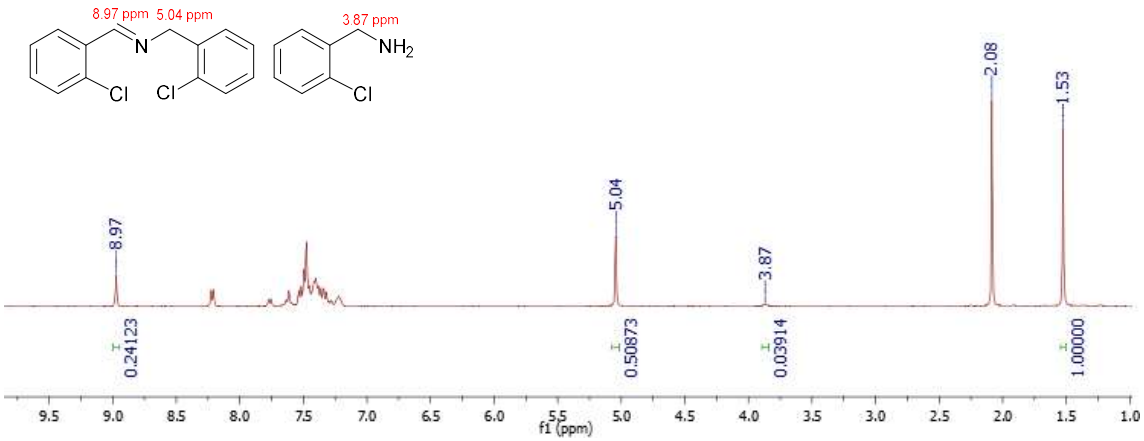


Figure 52. $^{1}$H NMR of entry 6. 1.53 ppm: cyclohexane,.2.08 ppm: acetonitrile, 3.87 ppm: 2-chlorobenzylamine.

## Entry 7 – 3-bromobenzylamine

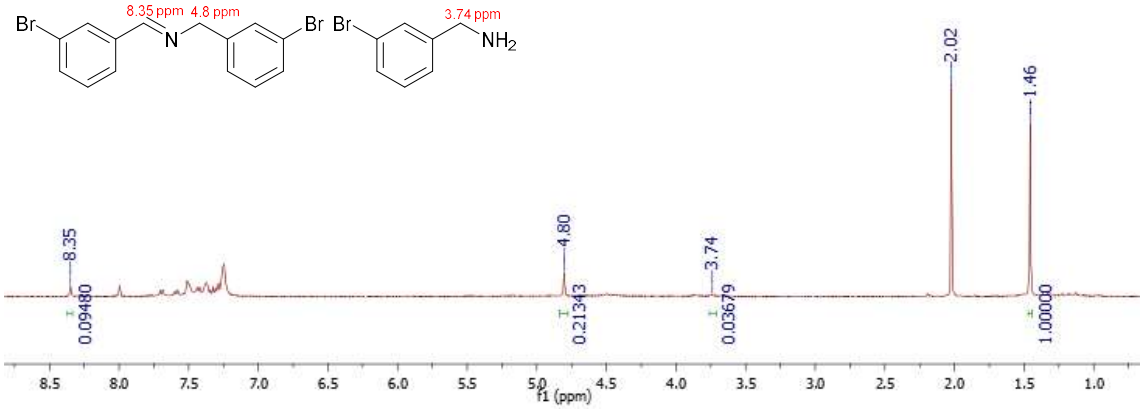


Figure 53. $^{1}$H NMR of entry 7. 1.46 ppm: cyclohexane,.2.02 ppm: acetonitrile, 3.74 ppm: 3-bromobenzylamine.

## Entry 8 – 4-tertbutylbenzylamine

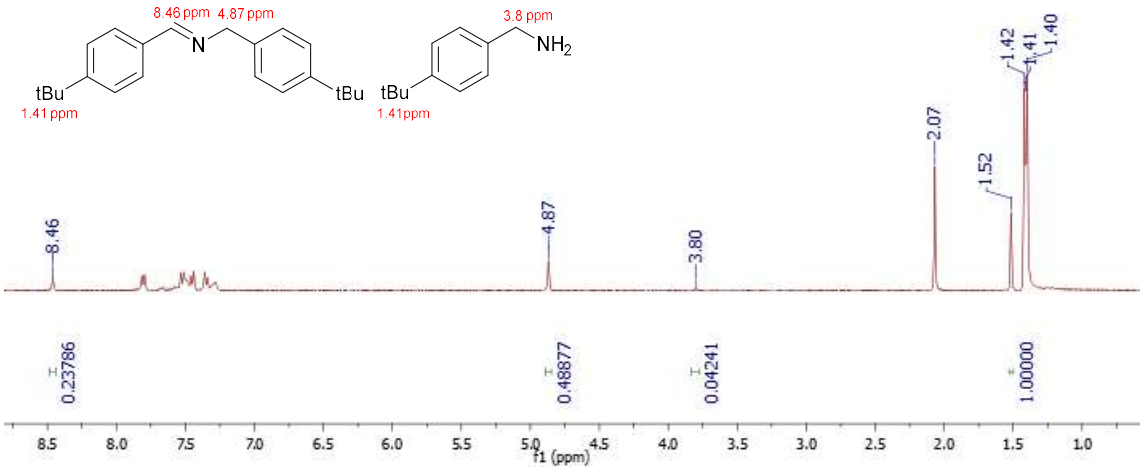


*Figure 54. $^{1}$H NMR of entry 8. 1.52 ppm: cyclohexane,.2.07 ppm: acetonitrile, 3.8 ppm: 4-tertbutylbenzylamine.*

# 4. Benzyl alcohol oxidation with nitrous oxide (Table 3)

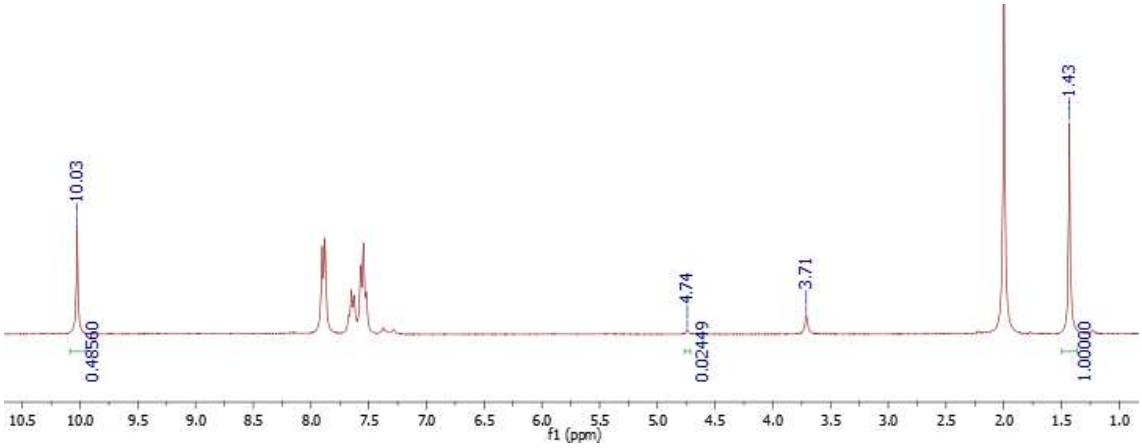


Figure 55. $^{1}$H NMR of **5a** benzyl alcohol oxidation to the corresponding aldehyde. 1.43 ppm: cyclohexane (internal standard), 2 ppm: acetonitrile, 3.7 ppm: NMI, 4.7 ppm: benzyl alcohol, 10.0 ppm: aldehyde proton.

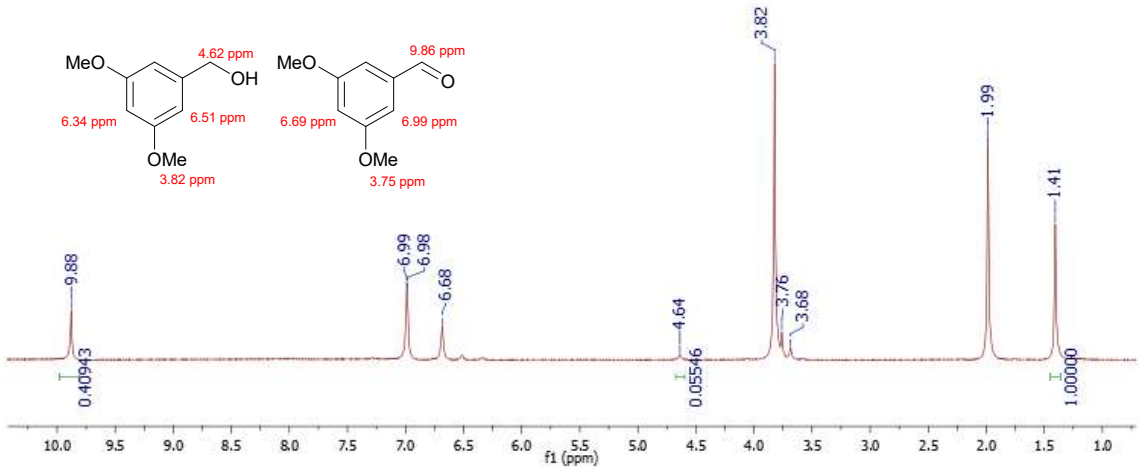


Figure 56. $^{1}$H NMR of **5b** 3,5-dimethoxybenzyl alcohol oxidation to the corresponding aldehyde. 1.41 ppm: cyclohexane (internal standard), 2 ppm: acetonitrile, 3.7 ppm: NMI, 4.64 ppm: benzyl alcohol, 9.88 ppm: aldehyde proton.

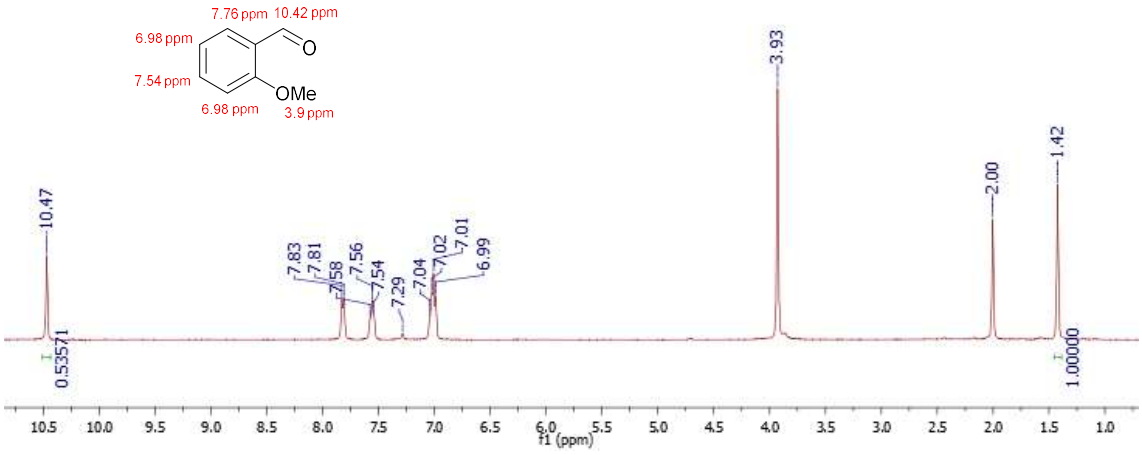


Figure 57. $^{1}$H NMR of **5c** 2-methoxybenzyl alcohol oxidation to the corresponding aldehyde. 1.42 ppm: cyclohexane (internal standard), 2 ppm: acetonitrile, 3.7 ppm: NMI, 4.74 ppm: benzyl alcohol, 10.47 ppm: aldehyde proton.

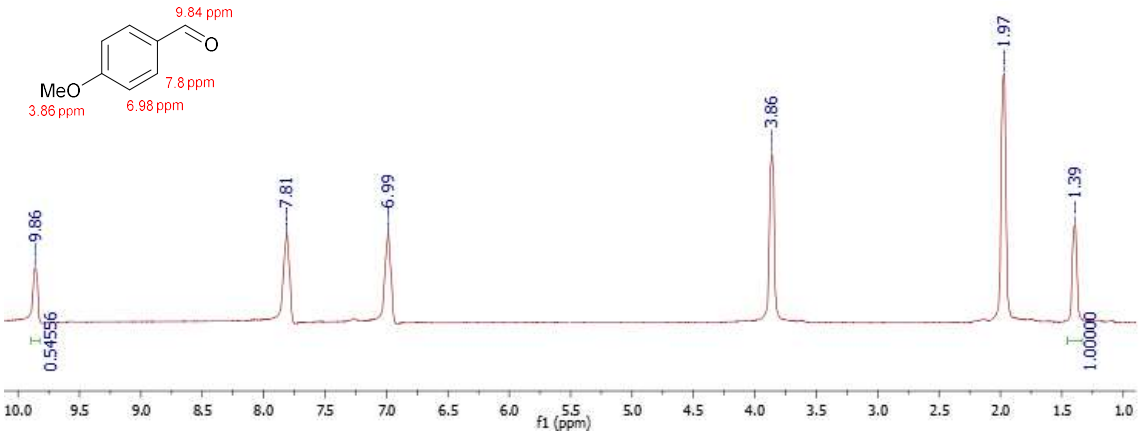


Figure 58. $^{1}$H NMR of **5d** 4-methoxybenzyl alcohol oxidation to the corresponding aldehyde. 1.39 ppm: cyclohexane (internal standard), 2 ppm: acetonitrile, 3.7 ppm: NMI, 9.86 ppm: aldehyde proton.

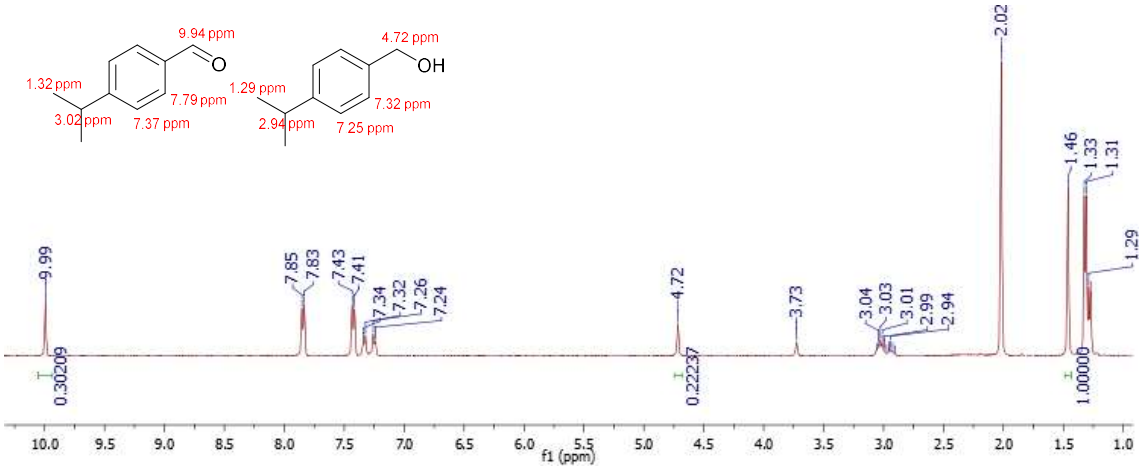


Figure 59. $^{1}$H NMR of **5e** 4-isopropylbenzyl alcohol oxidation to the corresponding aldehyde. 1.46 ppm: cyclohexane (internal standard), 2 ppm: acetonitrile, 3.7 ppm: NMI, 4.72 ppm: benzyl alcohol, 9.99 ppm: aldehyde proton.

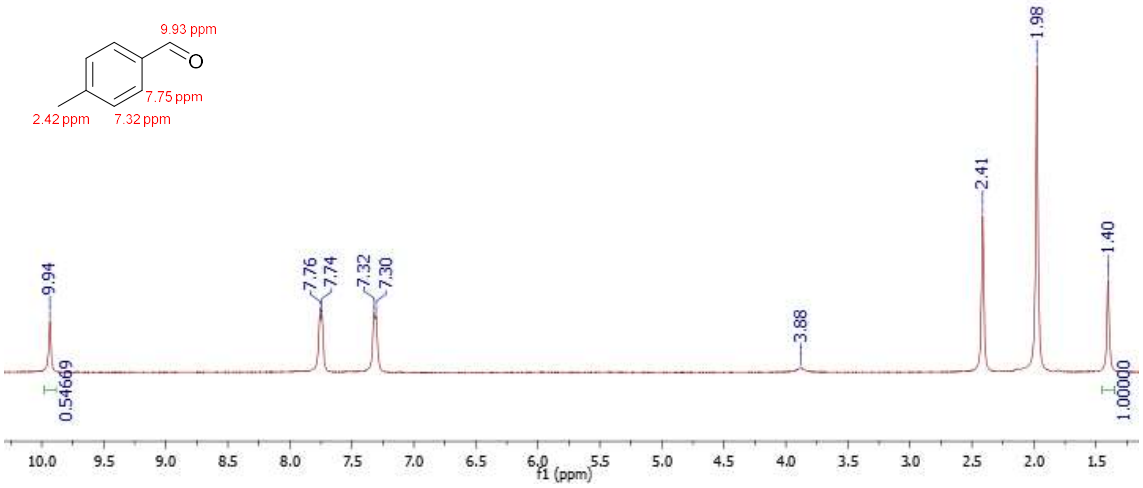


Figure 60. $^{1}$H NMR of **5f** 4-methybenzyl alcohol oxidation to the corresponding aldehyde. 1.40 ppm: cyclohexane (internal standard), 2 ppm: acetonitrile, 3.8 ppm: NMI, 9.94 ppm: aldehyde proton.

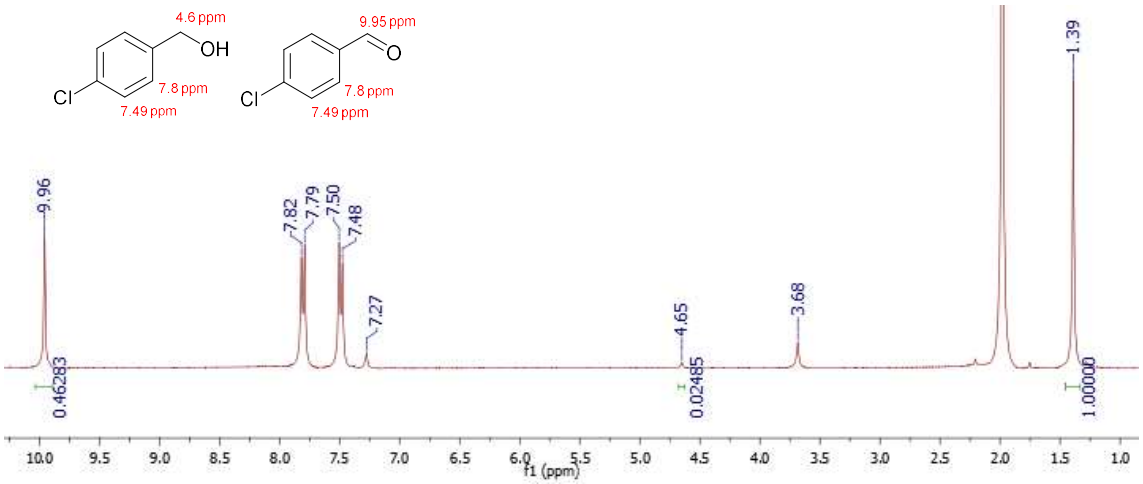


Figure 61. $^{1}$H NMR of **5g** 4-chlorobenzyl alcohol oxidation to the corresponding aldehyde. 1.39 ppm: cyclohexane (internal standard), 2 ppm: acetonitrile, 3.7 ppm: NMI, 4.65 ppm: benzyl alcohol, 9.96 ppm: aldehyde proton.

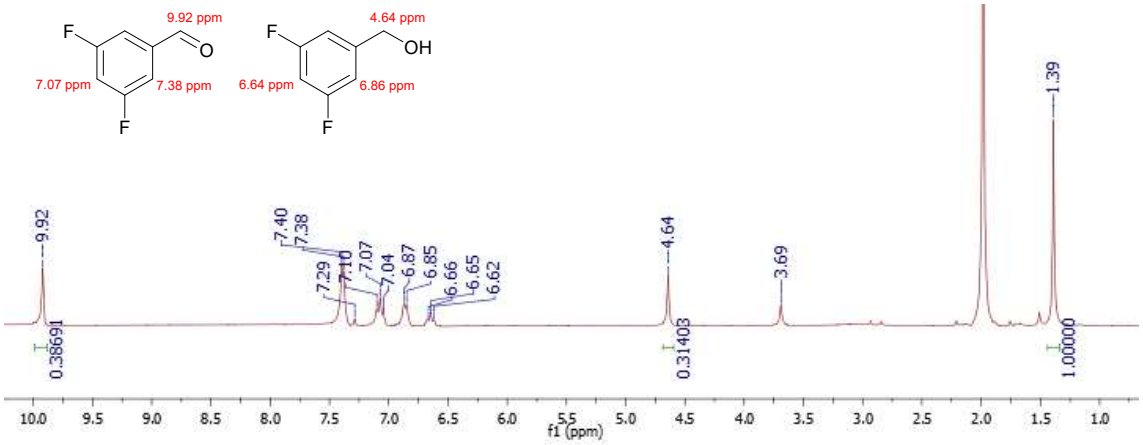


Figure 62. $^{1}$H NMR of **5h** 3,5-difluorobenzyl alcohol oxidation to the corresponding aldehyde. 1.39 ppm: cyclohexane (internal standard), 2 ppm: acetonitrile, 3.7 ppm: NMI, 4.64 ppm: benzyl alcohol, 9.92 ppm: aldehyde proton.

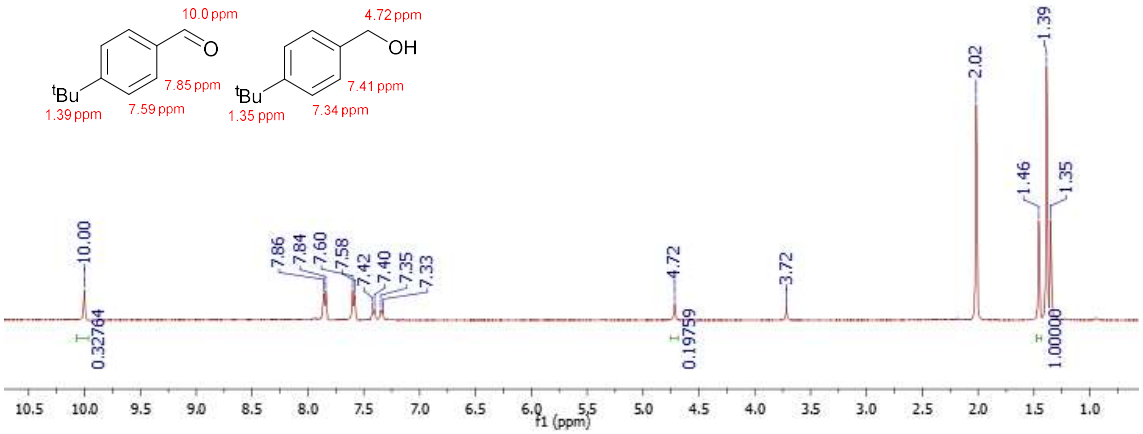


Figure 63. $^{1}$H NMR of **5i** 4-tert.-butylbenzyl alcohol oxidation to the corresponding aldehyde. 1.39 ppm: cyclohexane (internal standard), 2 ppm: acetonitrile, 3.7 ppm: NMI, 4.72 ppm: benzyl alcohol, 10.00 ppm: aldehyde proton.

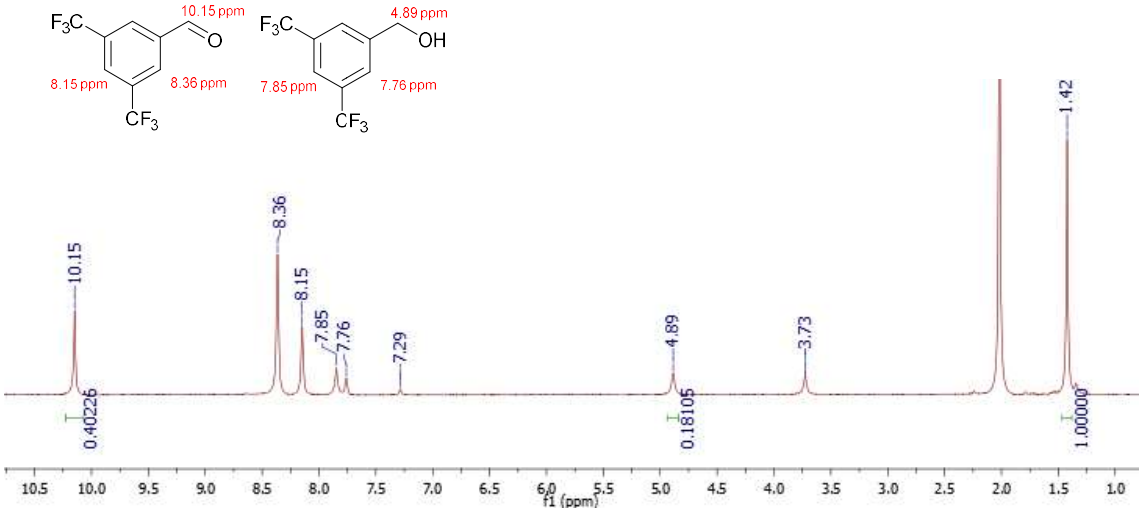


Figure 64. $^{1}$H NMR of **5j** 3,5-bis(trifluoromethyl)benzyl alcohol oxidation to the corresponding aldehyde. 1.39 ppm: cyclohexane (internal standard), 2 ppm: acetonitrile, 3.7 ppm: NMI, 4.89 ppm: benzyl alcohol, 10.15 ppm: aldehyde proton.

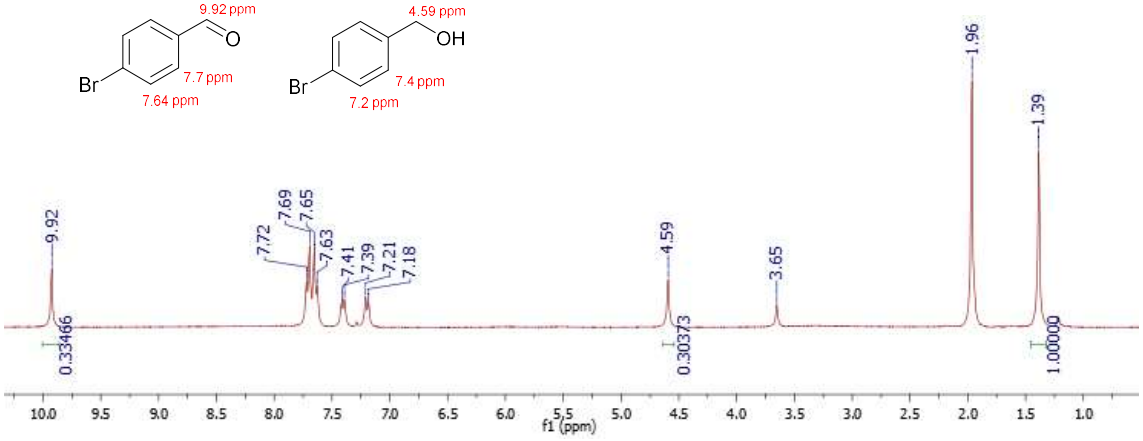


Figure 65. $^{1}$H NMR of **5k** 4-bromobenzyl alcohol oxidation to the corresponding aldehyde. 1.39 ppm: cyclohexane (internal standard), 1.96 ppm: acetonitrile, 3.65 ppm: NMI, 4.59 ppm: benzyl alcohol, 9.92 ppm: aldehyde proton.

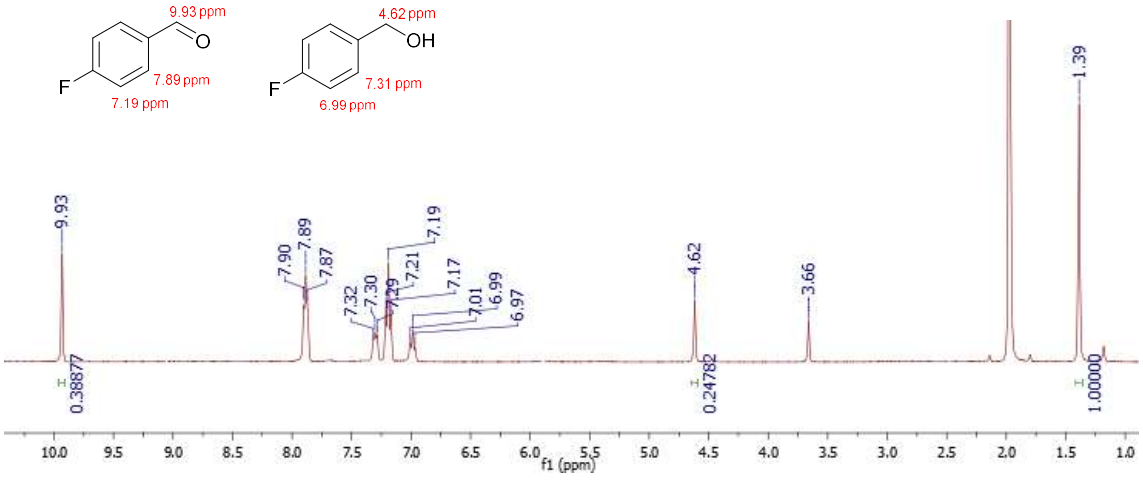


Figure 66. $^{1}$H NMR of **5l** 4-fluorrobenzyl alcohol oxidation to the corresponding aldehyde. 1.39 ppm: cyclohexane (internal standard), 2 ppm: acetonitrile, 3.66 ppm: NMI, 4.62 ppm: benzyl alcohol, 9.93 ppm: aldehyde proton.

# 5. ESI-MS spectrograms of the oxidative aminal formation

The aliquots for the ESI-MS analyses were taken from freshly prepared reactions according the protocol above (vide supra) with methanol or deuterated methanol and piperidine as amine components. The reactions were heated to 90°C for one hour. An aliquot of the reaction mixture was diluted in acetonitrile (2 mL), and an aliquot of this solution was further diluted in 2 mL of acetonitrile. In addition, we analysed samples of the catalyst precursors, ligands and subtstrates. (Values in ppm in brackets relates to errors between measurement and simulation)

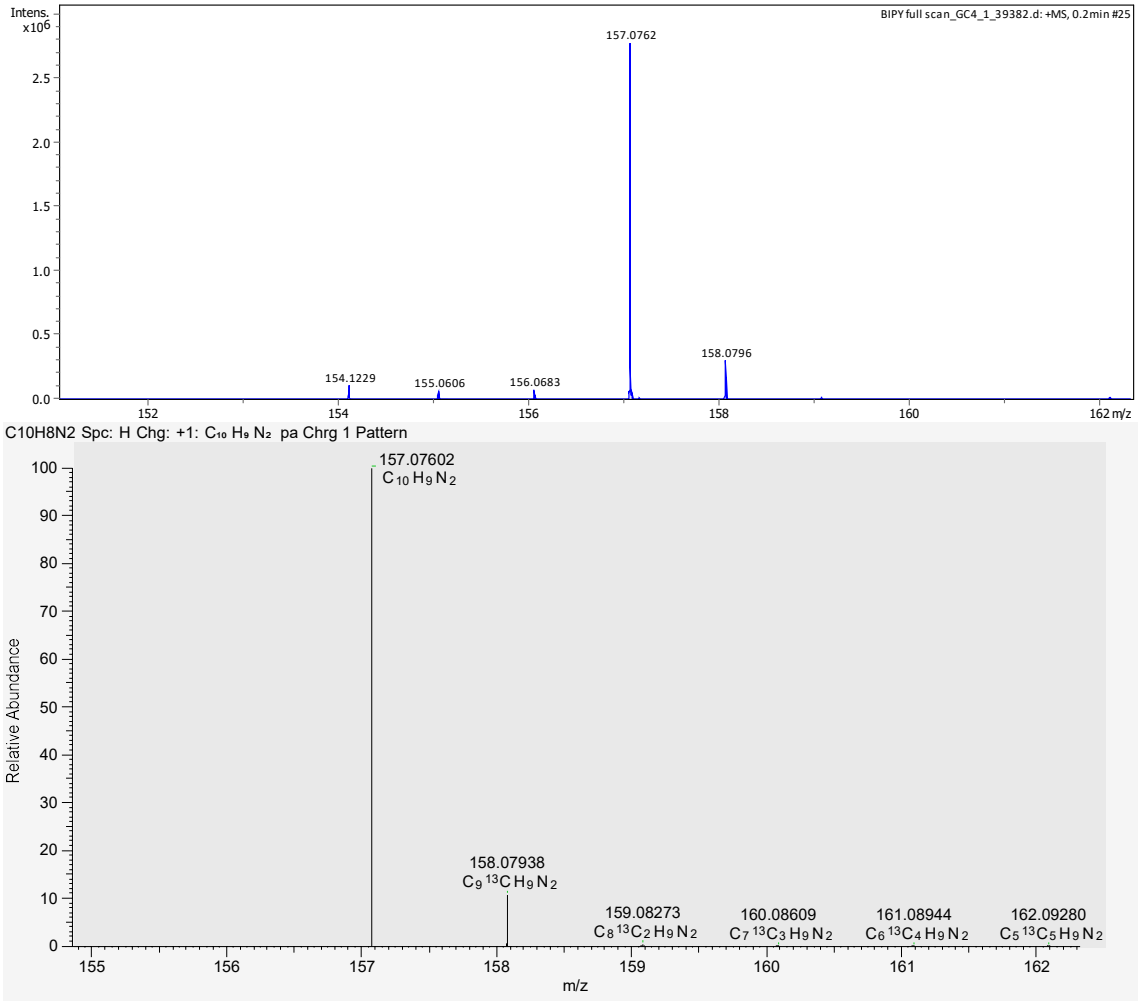


Figure 67: Bipyridine ($C_{10}H_8N_2$, bipy) ligand HR-MS (top) and simulation (bottom), **[M+H]$^+$** m/z 157.0762 (-1.3 ppm)

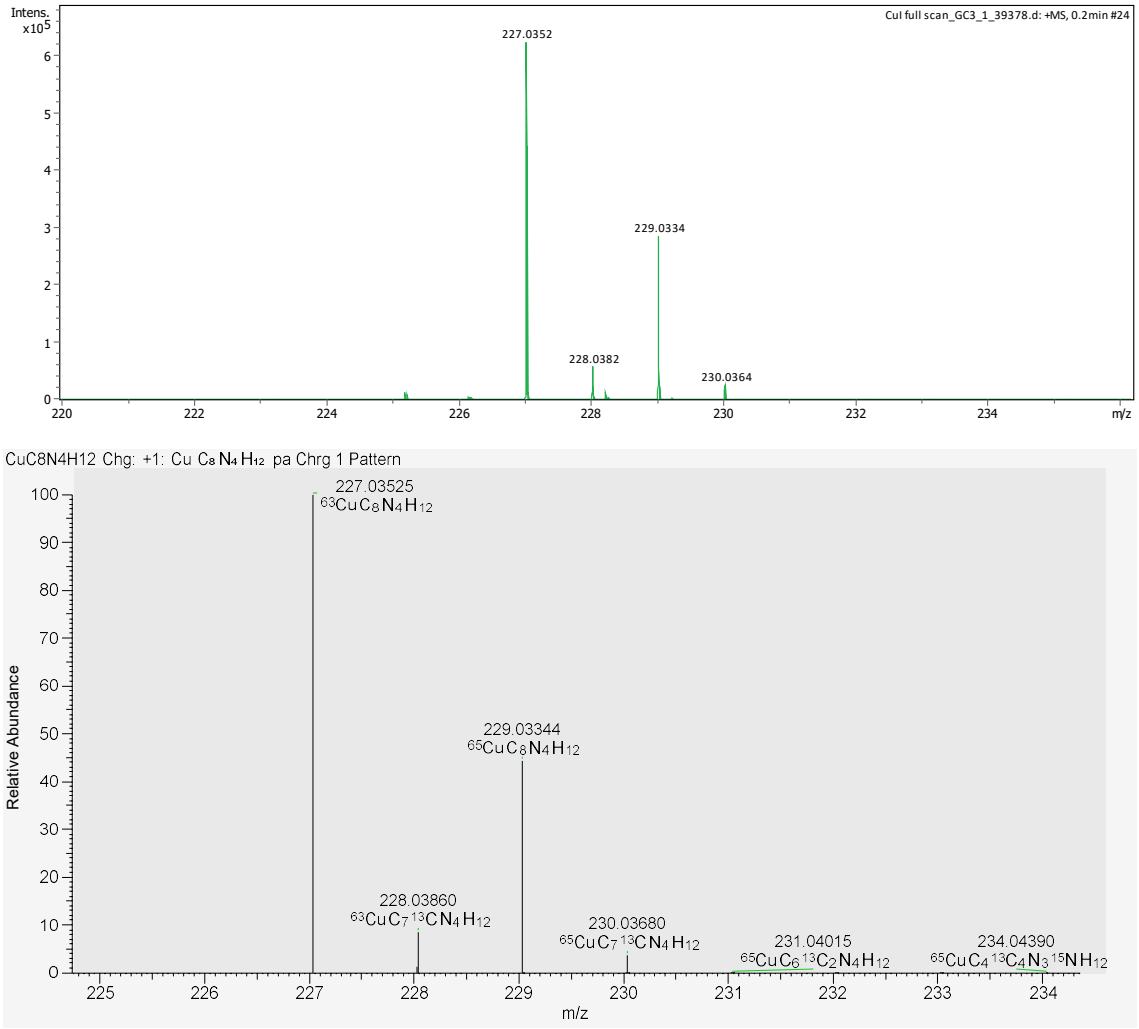


Figure 68 $[Cu(CH_3CN)4]^+$ formed from CuI by dissolution in MeCN, HR-MS (top) and simulation (bottom), **[M]**$^+$ m/z 227.0352 (0 ppm)

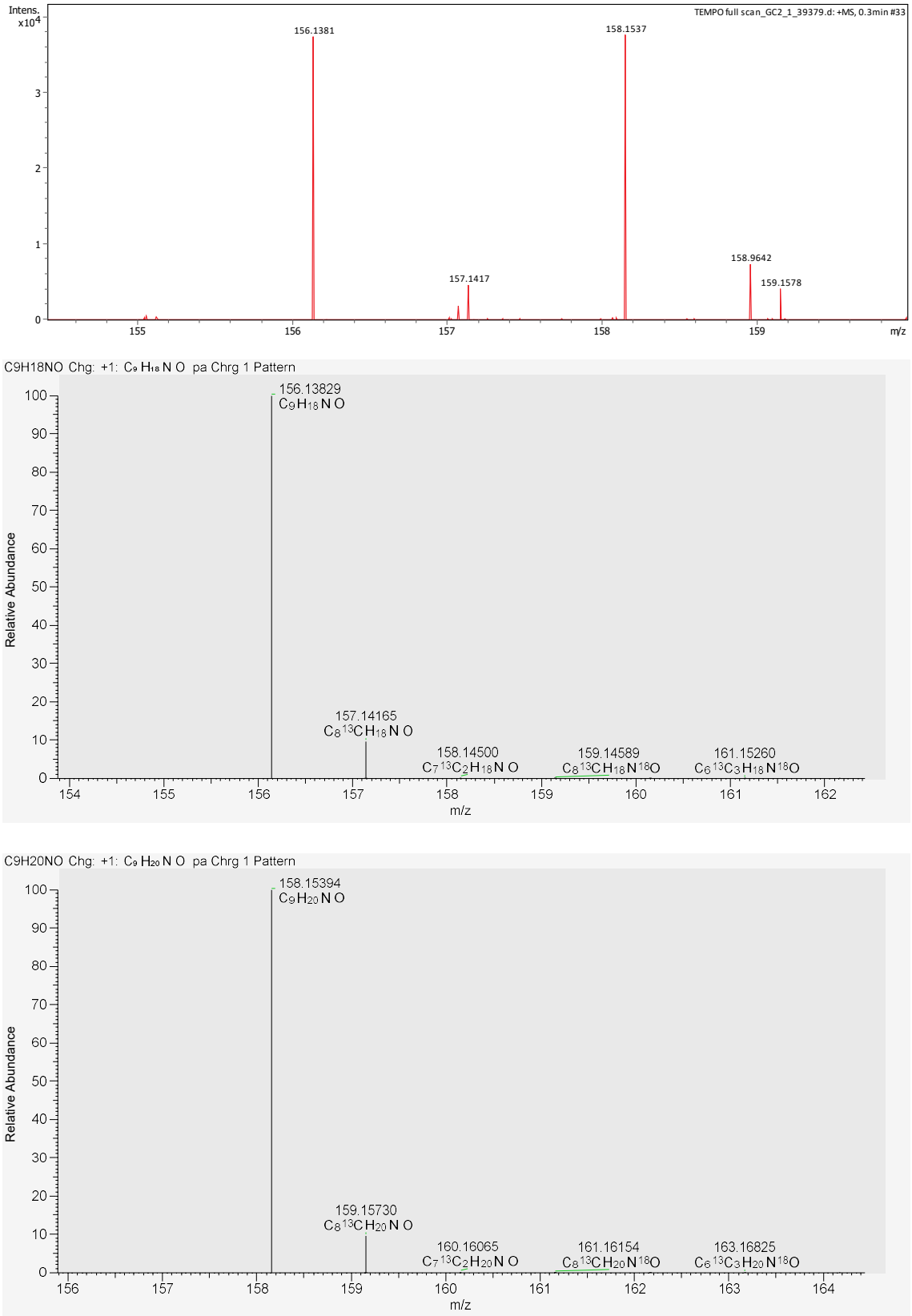


Figure 69 TEMPO (HR-MS (top) and simulation (middle and bottom), **[M]**$^{+}$ m/z 156.1381 (-1.3 ppm) and **[M+H]**$^{+}$ m/z 158.1537 (-1.3 ppm)

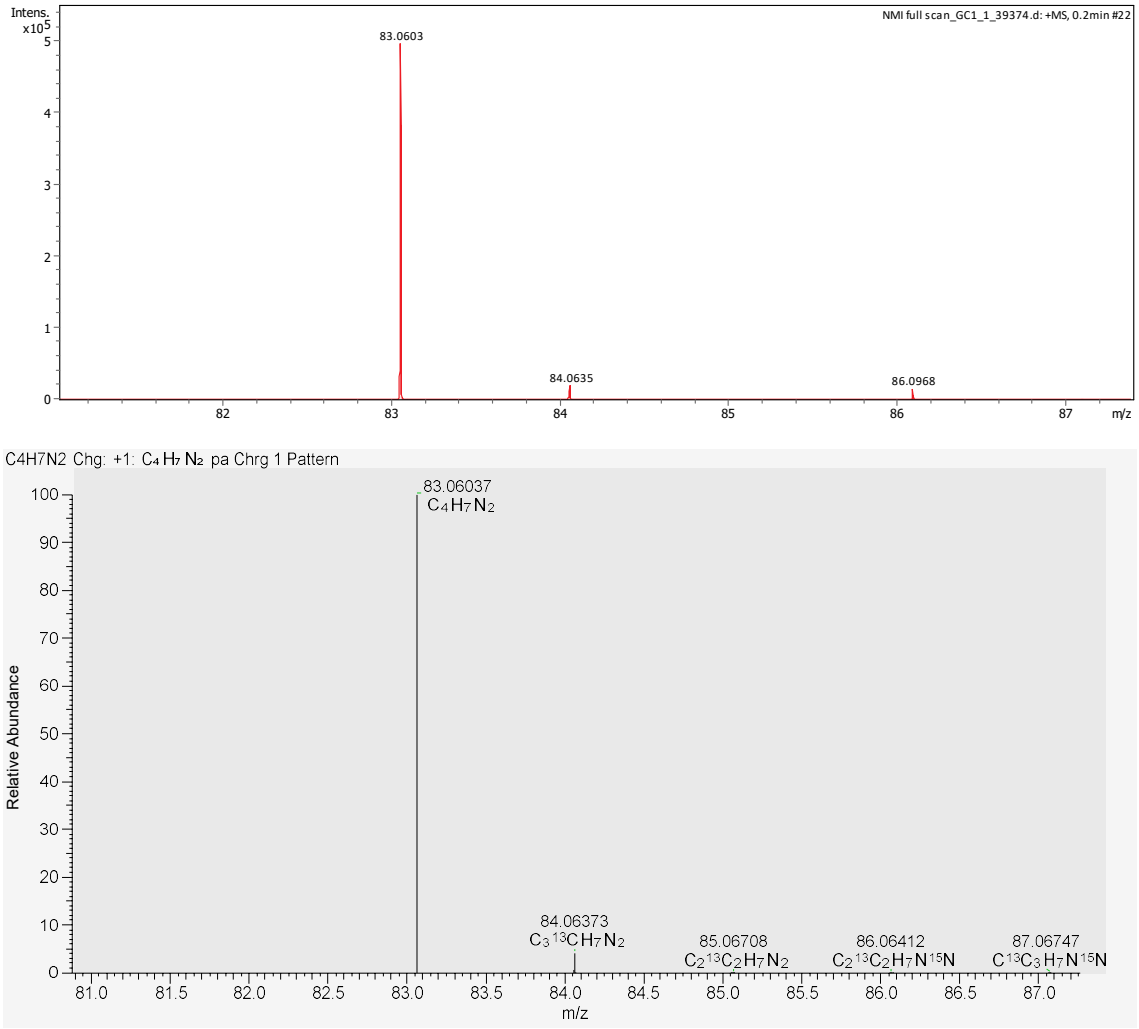


Figure 70 N-Methylimidazole ($C_4H_7N_2$) ligand HR-MS (top) and simulation (bottom), **[M+H]$^+$** m/z 83.0604 (-1.2 ppm)

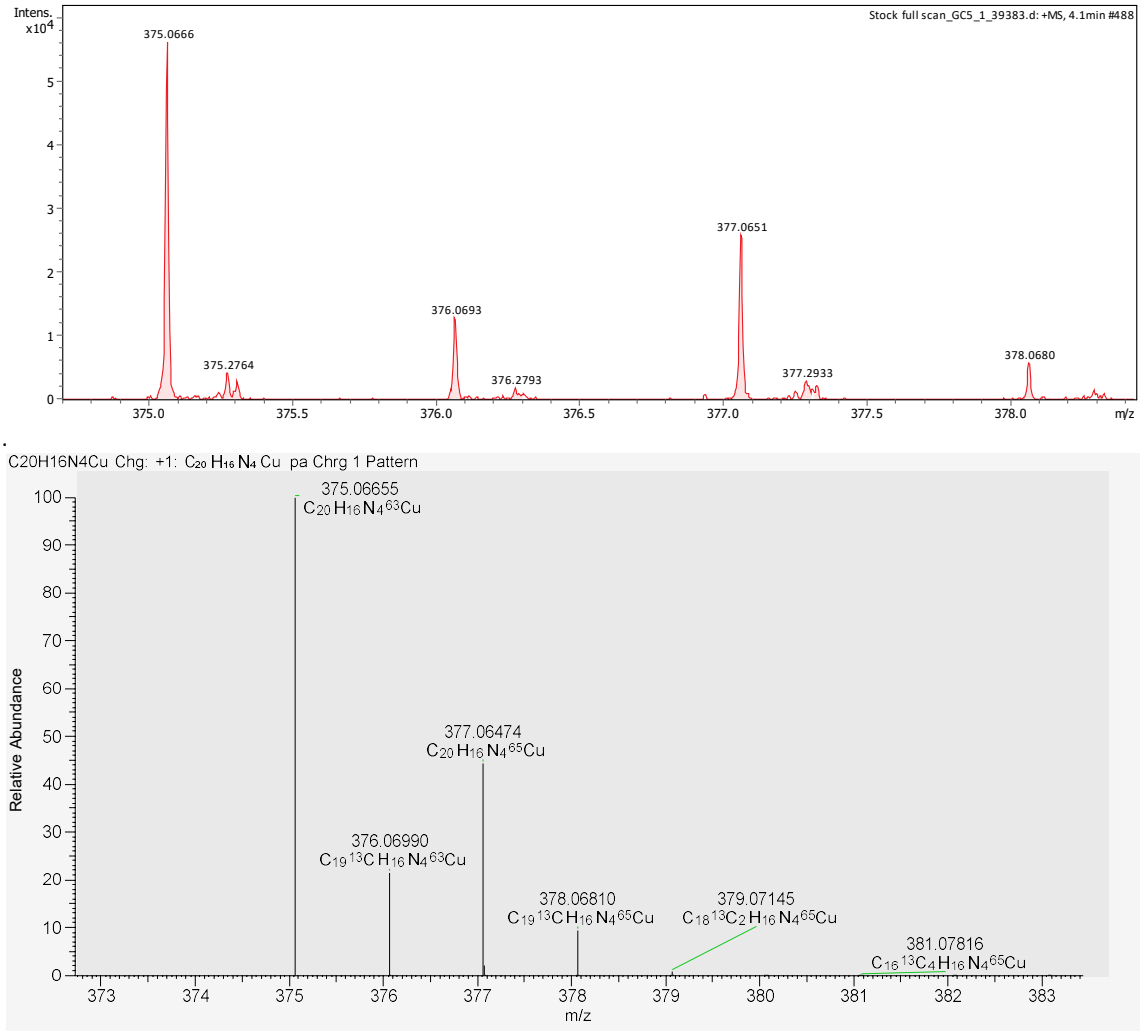


Figure 71 Copper catalyst stock solution, $[Cu(bipy)_2]^+$ formed from CuI and bipy by dissolution in MeCN, HR-MS (top) and simulation (bottom), **[M]**$^+$ m/z 375.06655 (-0.3 ppm)

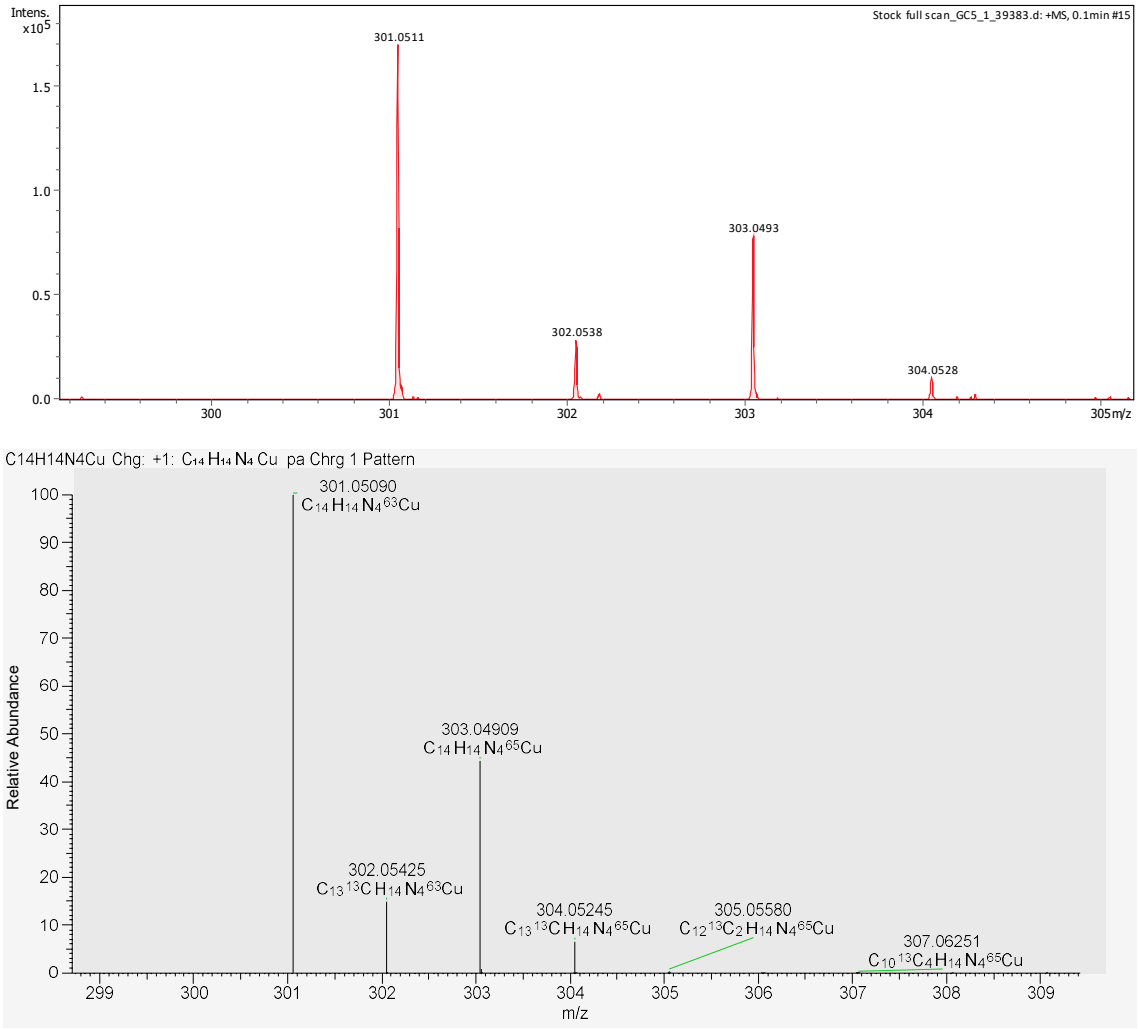


Figure 72 Copper catalyst stock solution, $[Cu(bipy)(MeCN)_2]^+$ formed from CuI and bipy by dissolution in MeCN, HR-MS (top) and simulation (bottom), **[M]**$^+$ m/z 301.0509 (-1.0 ppm)

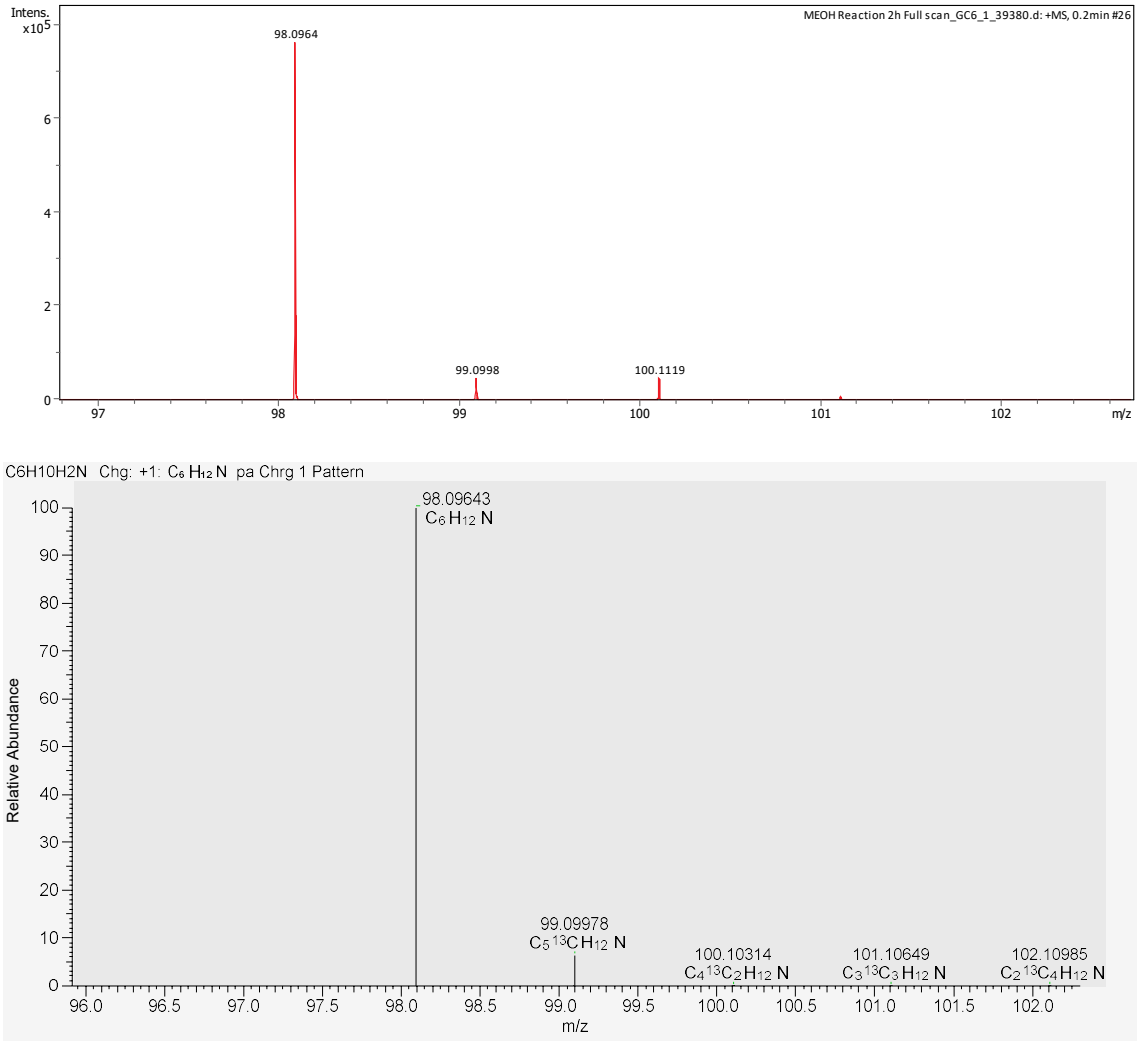


Figure 73 Iminium cation formed from piperidine ($C_5H_{10}N^+=CH_2$) in presence of methanol, **[M]$^+$** m/z 98.0964 (-5.1 ppm)

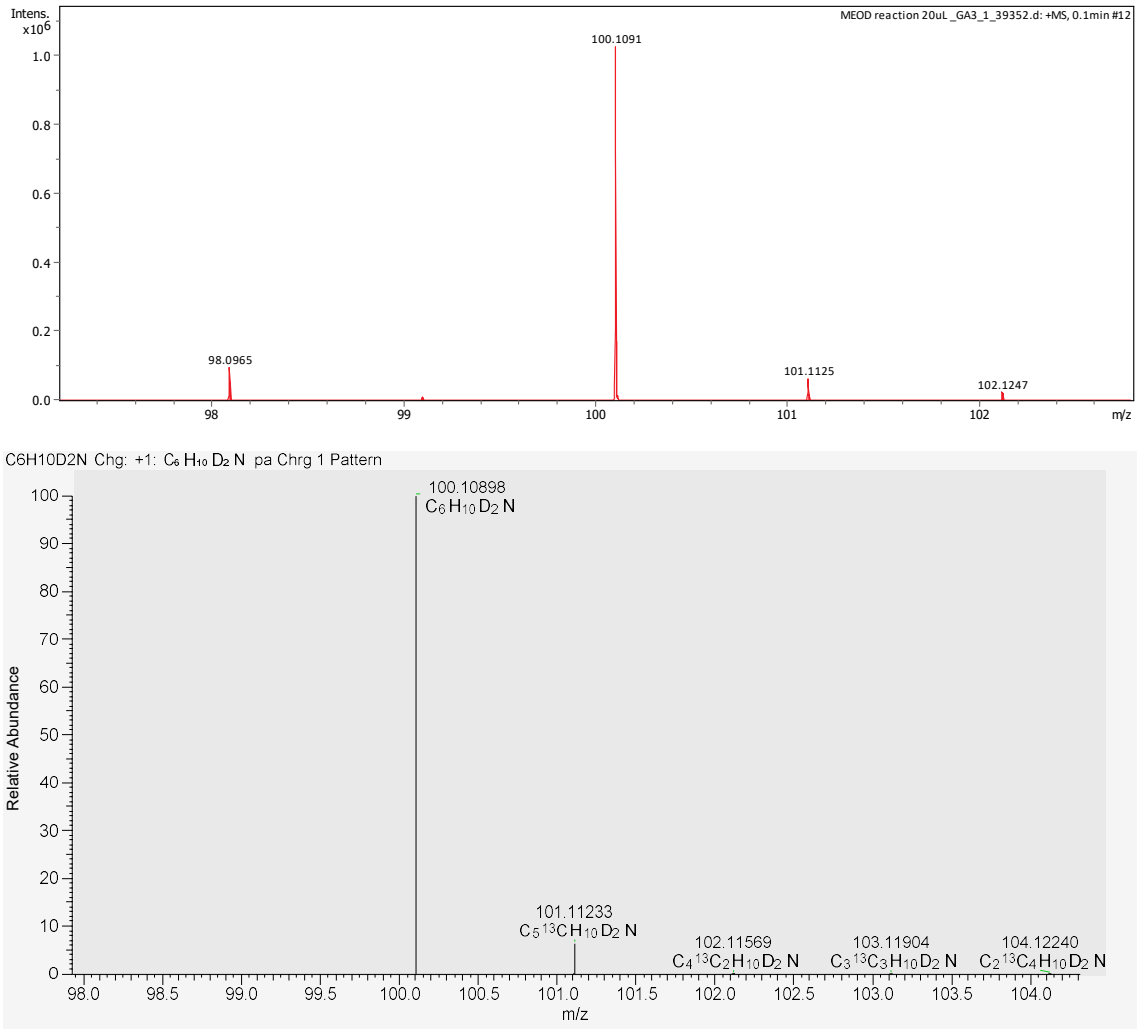


Figure 74 Iminium cation formed from piperidine ($C_5H_{10}N^+=CD_2$) in presence of deuterated methanol $CD_3OD$, **[M]**$^+$ m/z 98.0964 (-5.1 ppm, non-deuterated) and **[M]**$^+$ m/z 100.1091 (+1.0 ppm, deuterated)

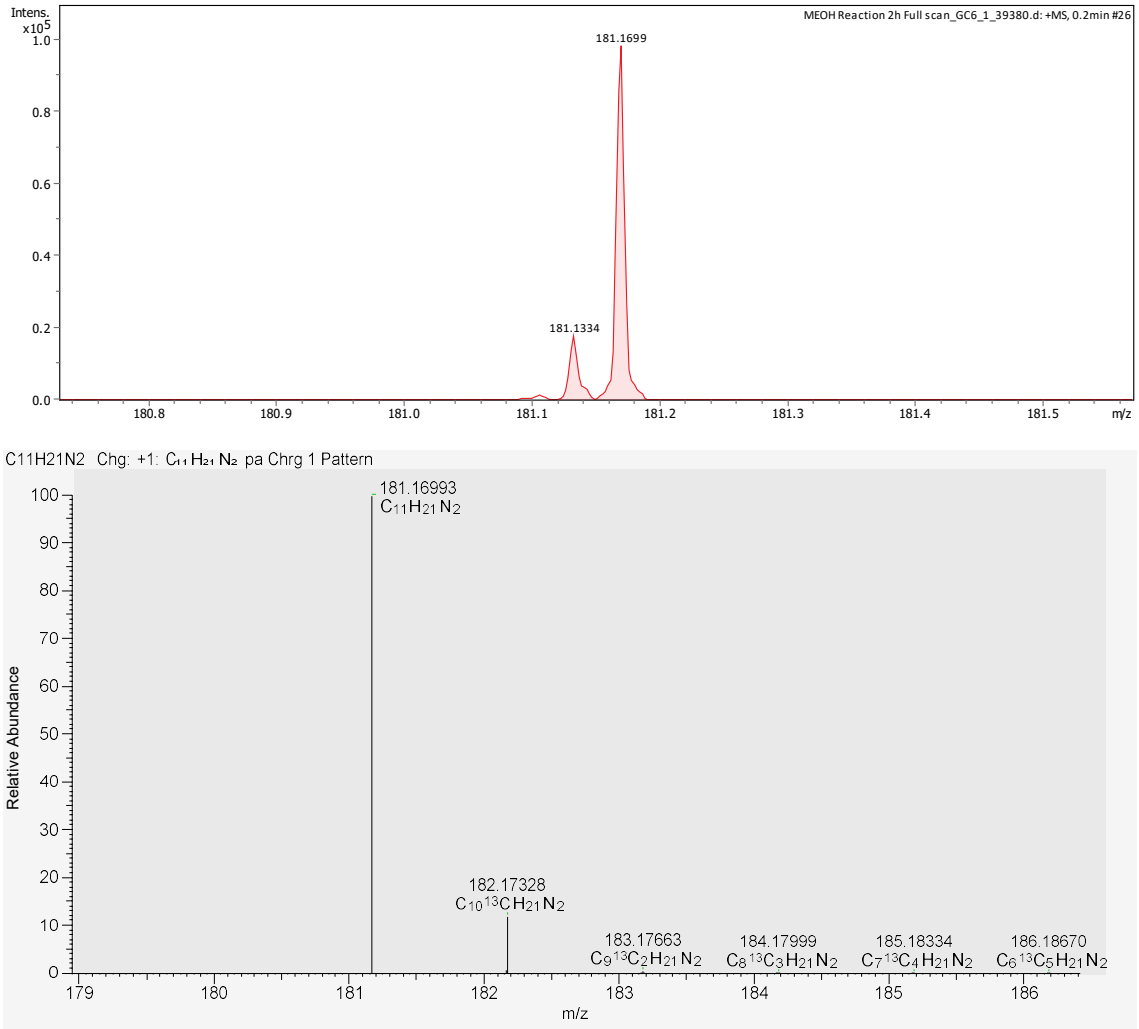


Figure 75 Aminal formed from piperidine ($(C_5H_{10}N)_2CH_2$) in presence of methanol, **[M-H]**$^+$ m/z **[M]**$^+$ m/z 181.1699 (0 ppm)

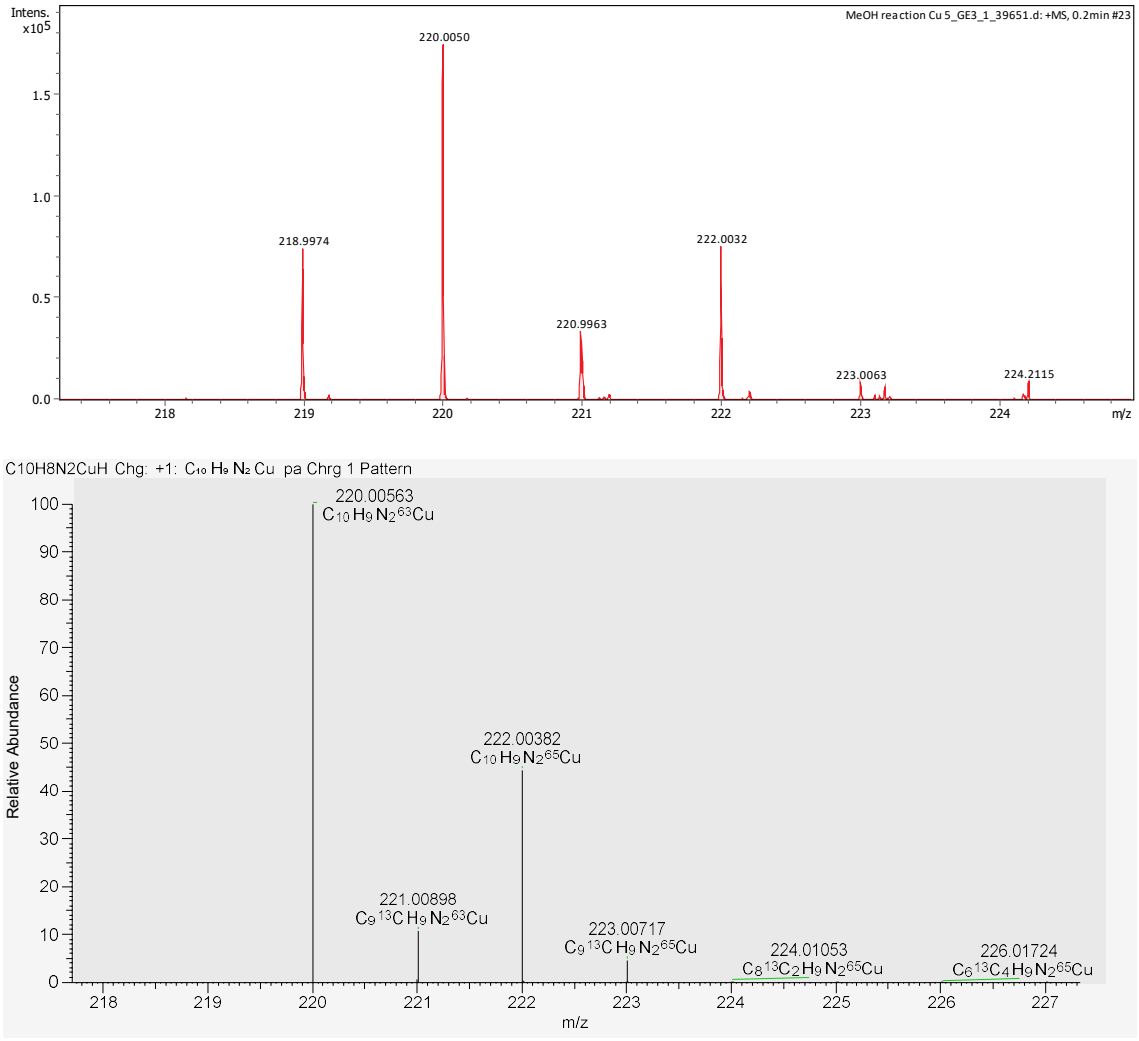


Figure 76 $[Cu(bipy)H]^+$ determined in the reaction mixture, HR-MS (top) and simulation (bottom), $[M]^+$ m/z 220.0050 (-2.7 ppm)

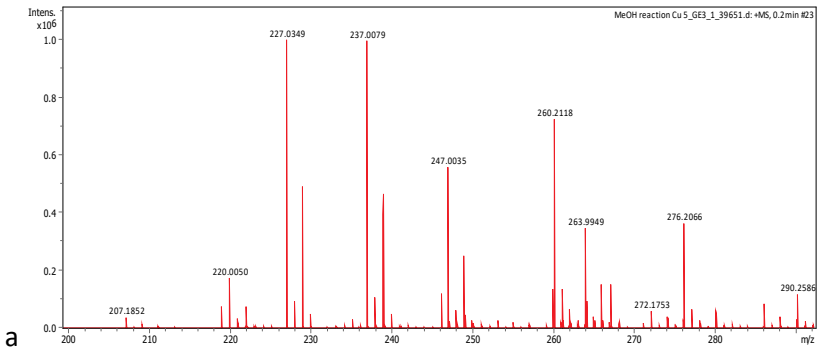


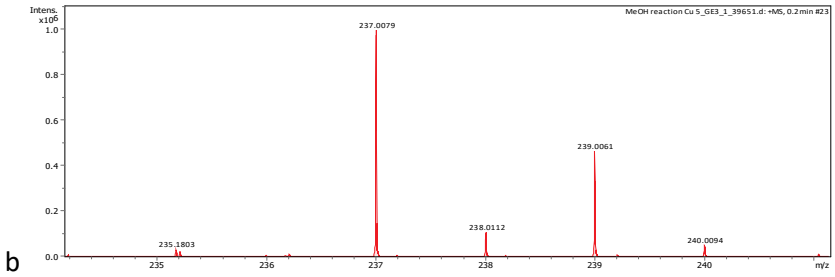


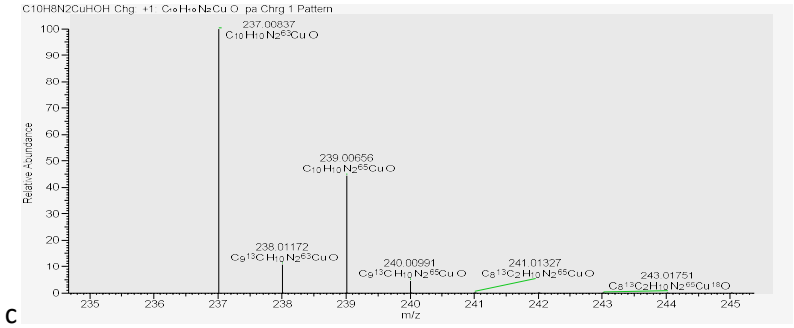


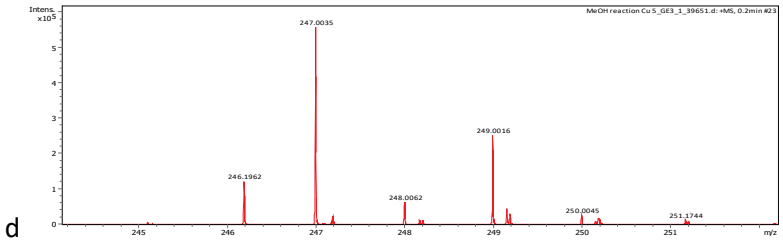


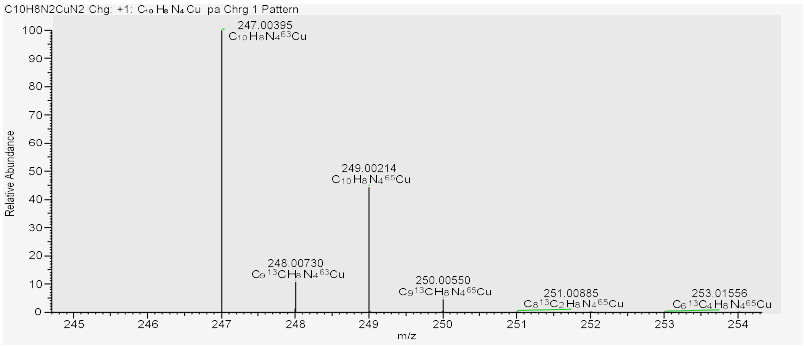


Figure 77 Low-weight copper species detectable in the reaction mixture (a: overview), $[bipyCuH]^+$ ($[M]^+$ m/z 220.0050 (-2.7 ppm; simulation see above), $[bipyCu(MeCN)_2]^+$ ($[M]^+$ m/z 227.0349 (-1.8 ppm, simulation see MS under stock solution), b+c) $[bipyCu(H_2O)]^+$ ($[M]^+$ m/z 237.0084 (measured and simulated), d+e) $[bipyCuN_2]^+$ ($[M]^+$ m/z 247.00395 (measured and simulated); $[M]^+$ m/z 263.9949 (related copper species).

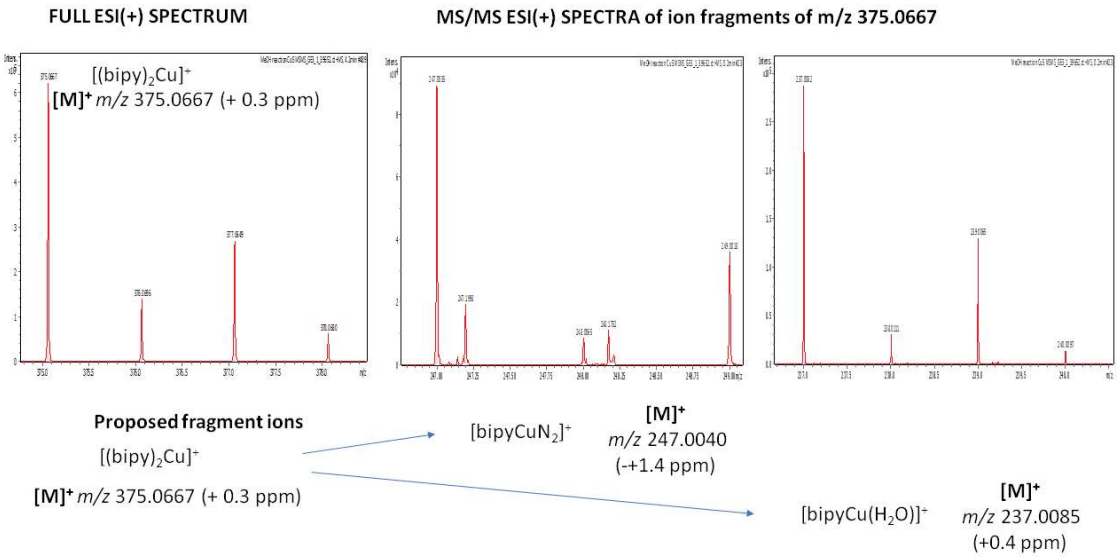


Figure 78 Fragmentation of $[(bipy)_2Cu]^+$ to $[bipyCu(H_2O)]^+$ and $[bipyCuN_2]^+$ under MS/MS conditions.

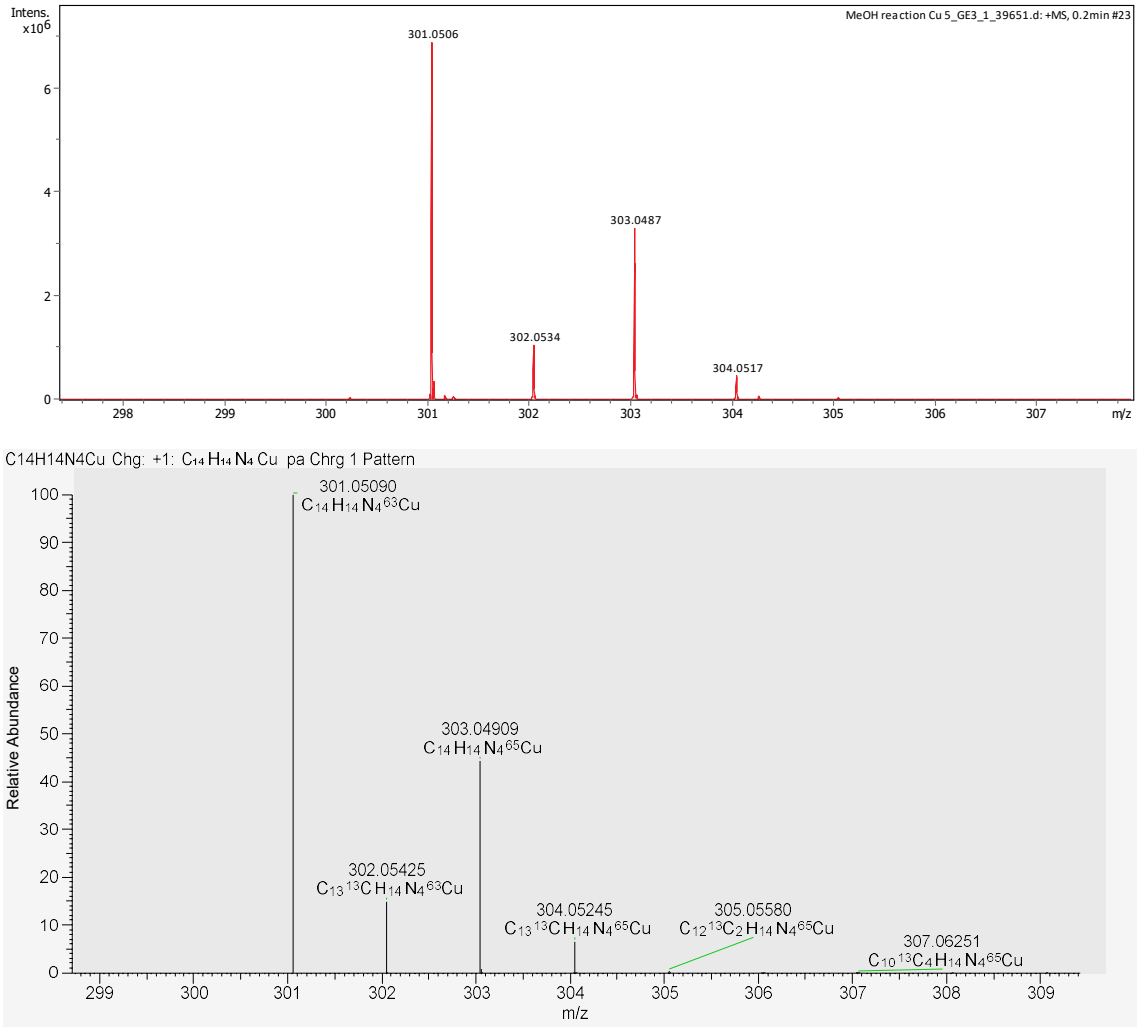


Figure 79 $[Cu(bipy)(MeCN)_2]^+$ determined in the reaction mixture, HR-MS (top) and simulation (bottom), **[M]**$^+$ m/z 301.0509 (-2.6 ppm)

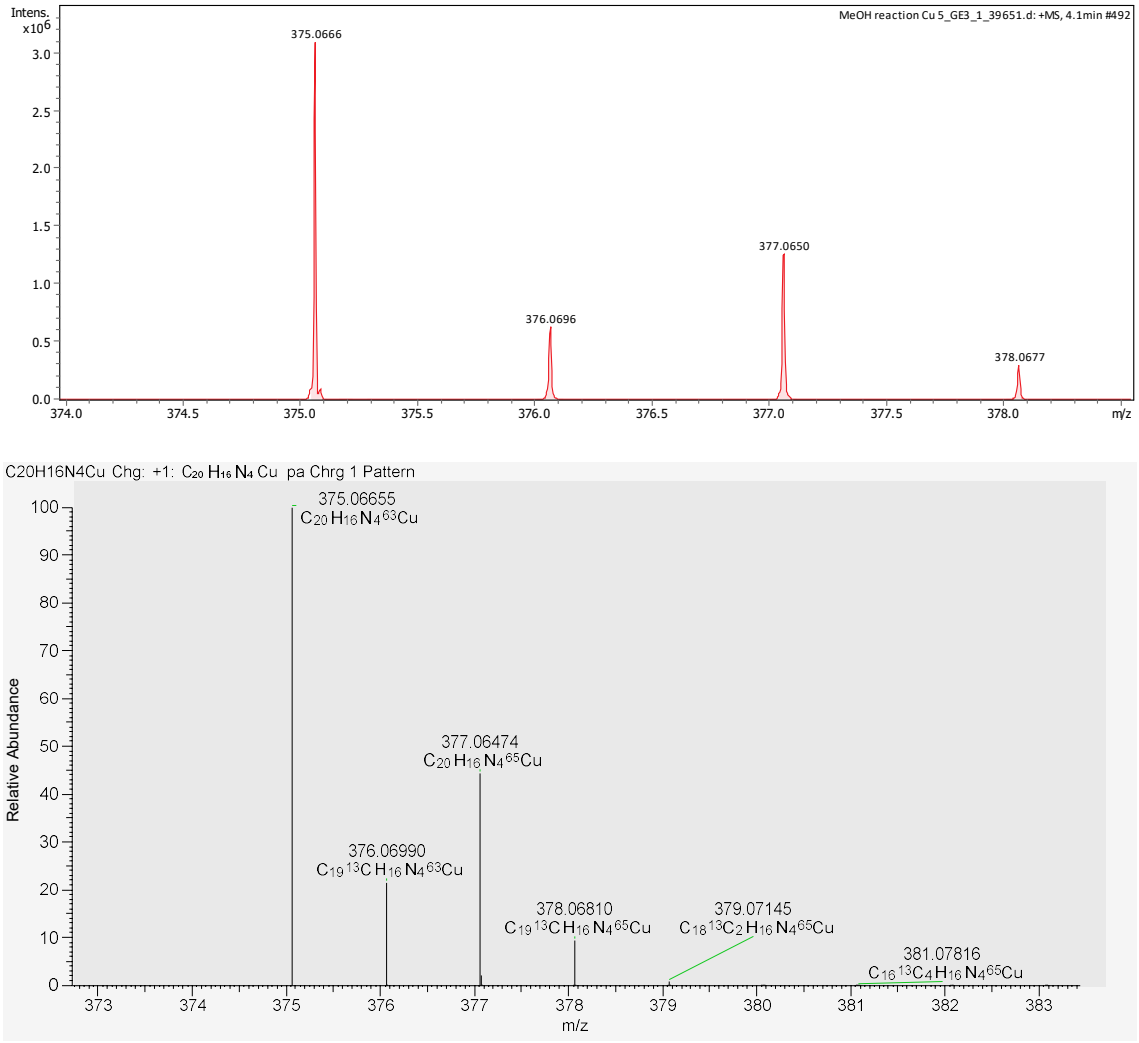


Figure 80 $[Cu(bipy)_2]^+$ determined in the reaction mixture, HR-MS (top) and simulation (bottom), **[M]**$^+$ m/z 375.06655 (+0.3 ppm)

# 6. Theoretical calculations

The ORCA 5.0.4 software package was used for all calculations.[2] Unless stated otherwise, the calculations were performed using B3LYP functional[3, 4] with the def2-SVP and def2-TZVP basis sets[5] for non-metal and metal atoms, respectively (for geometries and frequencies) or the def2-TZVPP basis set[5] for all atoms (final single point energies). Dispersion correction was introduced through the *D4* keyword (Grimme's atom-pairwise approach).[6] The *AutoAux* keyword[7] was used to generate auxiliary basis sets in all cases. SCF geometry optimization convergence criteria were set by the *VeryTightSCF* and *TightOPT* keywords. Transition states were found using either nudged elastic band (NEB).[8] The correctness of the transition state optimisation was confirmed by the presence of a single imaginary frequency. The minimum energy crossing points (MECPs)[9] for intersection of triplet and singlet surfaces were located using the *SurfCrossOpt* keyword. The solvent (acetonitrile) effects were accounted for by means of the conductor-like polarisable continuum model (C-PCM).[10] The correction Δ*G* term of 1.89 kcal $mol^{-1}$ was added to the final Gibbs energies of single molecules to convert 1 atm to 1 M standard states.[11] Molecular structures of intermediates and transition states were draws using CYLview20 program.[12] The visualisation of spin density was made using the Avogadro 1.2 program.[13] Cartesian coordinates of the DFT optimised structures are given in the form or XYZ files. The numbering of intermediates adopts the following scheme: $^{m}$**TN-X**, where m = multiplicity, T = type (**R** for reactant, **I** for intermediate, **TS** for transition state, **MECP** for MECP point and **P** for product), N = number of the intermediate in the current reaction pathway, X = index of the pathway.

**Benchmark analysis of $N_2O$ dissociation**

The $N_2O$ molecule has a linear configuration and a closed-shell state, where p-electrons of nitrogen and oxygen atoms occupy σ- and π-molecular orbitals. Spin-forbidden dissociation of $N_2O$ molecule to $N_2$ and triplet oxygen atom O ($^3$P) requires the activation energy around 60 kcal $mol^{-1}$ and proceeds through the minimum energy crossing point (MECP) where the overall multiplicity changes from singlet to triplet one.[14] Thus, modelling of $N_2O$ oxidative activity requires finding the geometries corresponding to intersection of single and triplet potential energy surfaces. As the first step, we calculated the $N_2O$ dissociation pathway with the purpose of comparing our results with the literature data. Optimization of the $N_2O$ geometry at the B3LYP/def2-TZVPP level involving the implicit solvation model (C-PCM, acetonitrile) gave *d*(N–N) and *d*(N–O) distances of 1.119 and 1.182 Å, respectively, with ideally linear ∠(N–N–O)

angle (Fig. 81). The respective $^{1\text{-}3}$**MECP1-A** structure features both elongated distances *d*(N–N) and *d*(N–O) of 1.215 and 1.275 Å and angular structure where ∠(N–N–O) of 117.46°. The free Gibbs energies calculated for singlet and triplet states of $^{1\text{-}3}$**MECP1-A** point constitute 63.2 and 63.5 kcal mol$^{-1}$ relative to the starting relaxed single $N_2O$ structure. These values are in excellent agreement with that found earlier.[14] Relaxing the $^{1\text{-}3}$**MECP1-A** structure on the triplet surface does not afford notable changes to the structure, as evidenced by slight change of Gibbs energy down to 62.8 kcal mol$^{-1}$. Further decomposition of the $^3\{N_2\cdots O\}$ assembly into $^1N_2$ and $^3O$ leads to the drop of the Gibbs energy down to 34.6 kcal mol$^{-1}$, which is comparable to 41.2 kcal mol$^{-1}$ reported for the system $^1N_2$ + $^3O$.[14] The difference from the literature data is due to the different methods as well as the inclusion of solvation model herein. As the calculations using def2-TZVPP are computationally costly and cannot be applied for the analysis of catalytically active species under our conditions, we verified if the lighter method, namely B3LYP/def2-SVP for geometries and frequencies accompanied with B3LYP/def2-TZVPP for single point energy corrections, can give satisfactory results. Recalculation of the $N_2O$ dissociation pathway at this level resulted in MECP energies of 63.8 and 64.4 kcal mol$^{-1}$ for singlet and triplet states, respectively (the difference appears due to the variations of geometry compared to that optimized using def2-TZVPP basis set), while the energy of the final system $^1N_2$ + $^3O$ appeared to be only slightly higher (35.6 kcal mol$^{-1}$) to that obtained at the full B3LYP/def2-TZVPP level (Fig. 81). From these data the B3LYP/def2-SVP//def2-TZVPP level was used for all further calculation, expect of the def2-TZVP basis set applied for copper atoms for geometries and frequencies.

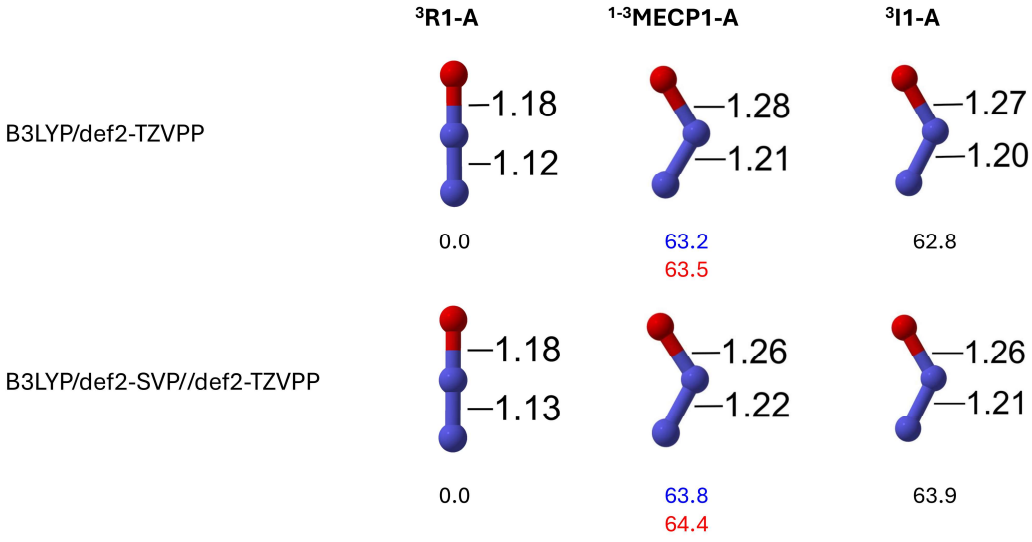


Figure 81 Geometries, N–O distances (Å) and relative free Gibbs energies (kcal mol$^{-1}$) of the singlet-state reactant, MECP state and triplet-state intermediate of $N_2O$ dissociation mechanism calculated at the stated levels. Blue (top) and red (bottom) energies for the MECP point designate those calculated at the singlet and triplet state for a given MECP geometry.

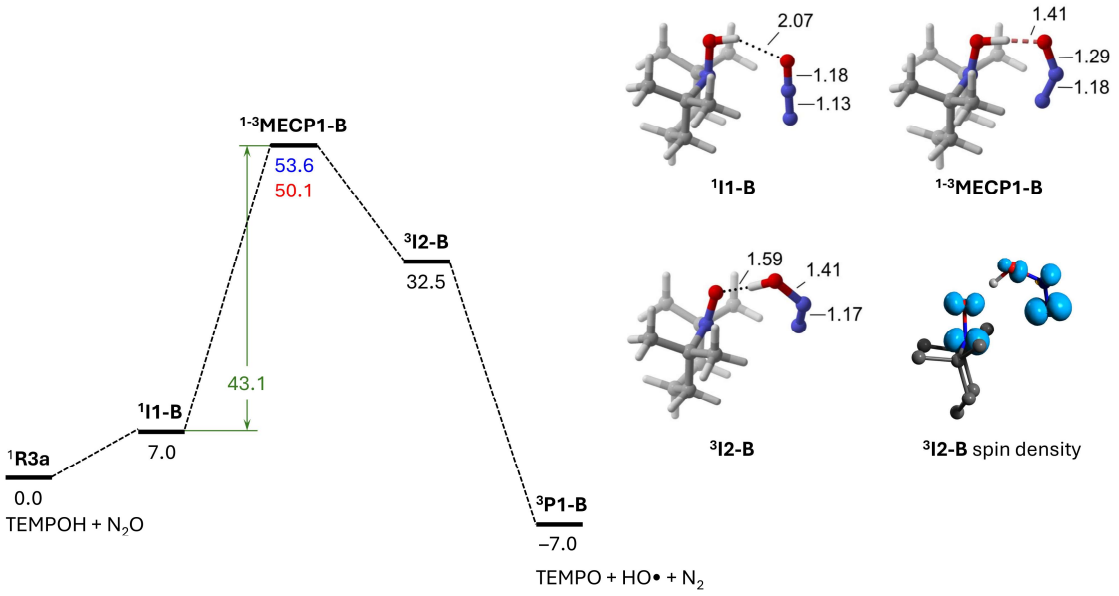


Figure 82 . Molecular structures, key interatomic distances (Å) and relative free Gibbs energies (kcal $mol^{-1}$) of the reaction profile between protonated reduced TEMPO radical (TEMPOH) and $N_2O$. Blue (top) and red (bottom) energies for the MECP point designate those calculated at the singlet and triplet state for a given MECP geometry. The spin density isosurface is shown at 0.02 a.u. level.

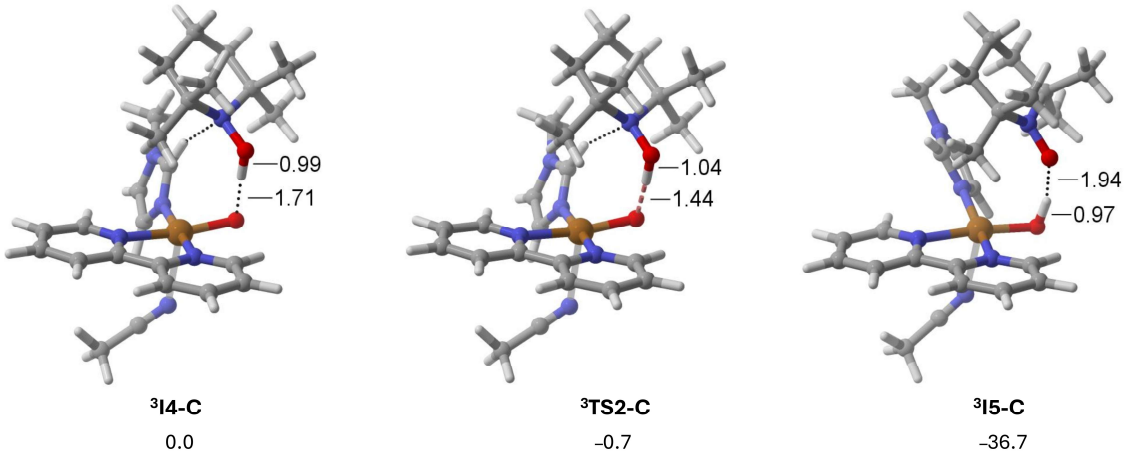


Figure 83 Molecular structures, key interatomic distances (Å) and relative free Gibbs energies (kcal $mol^{-1}$) of the reaction between protonated reduced TEMPO radical (TEMPOH) and copper-oxyl species $[(bipy)Cu\text{-}O•(NMI)(MeCN)]^+$.

# 7. References


1. M. C. Pichardo, G. Tavakoli, J. E. Armstrong, T. Wilczek, B. E. Thomas and M. H. G. Prechtl, *Chemsuschem*, 2020, **13**, 882-887.
2. F. Neese, *Wiley Interdisciplinary Reviews-Computational Molecular Science*, 2022, **12**, e1606.
3. P. J. Stephens, F. J. Devlin, C. F. Chabalowski and M. J. Frisch, *Journal of Physical Chemistry*, 1994, **98**, 11623-11627.
4. R. H. Hertwig and W. Koch, *Chemical Physics Letters*, 1997, **268**, 345-351.
5. F. Weigend and R. Ahlrichs, *Phys Chem Chem Phys*, 2005, **7**, 3297-3305.
6. E. Caldeweyher, C. Bannwarth and S. Grimme, *Journal of Chemical Physics*, 2017, **147**, 034112.
7. G. L. Stoychev, A. A. Auer and F. Neese, *Journal of Chemical Theory and Computation*, 2017, **13**, 554-562.
8. V. Asgeirsson, B. O. Birgisson, R. Bjornsson, U. Becker, F. Neese, C. Riplinger and H. Jonsson, *Journal of Chemical Theory and Computation*, 2021, **17**, 4929-4945.
9. J. N. Harvey, M. Aschi, H. Schwarz and W. Koch, *Theoretical Chemistry Accounts*, 1998, **99**, 95-99.
10. V. Barone and M. Cossi, *Journal of Physical Chemistry A*, 1998, **102**, 1995-2001.
11. A. V. Marenich, C. J. Cramer and D. G. Truhlar, *Journal of Physical Chemistry B*, 2009, **113**, 6378-6396.
12. CYLview20; Legault, C. Y., Université de Sherbrooke, 2020 (http://www.cylview.org)
13. M. D. Hanwell, D. E. Curtis, D. C. Lonie, T. Vandermeersch, E. Zurek and G. R. Hutchison, *J. Cheminformatics*, 2012, **4**, 17.
14. J. N. Harvey, *Phys Chem Chem Phys*, 2007, **9**, 331-343.